



Selección e ingeniería de nano-anticuerpos específicos por antígenos tumorales

Tesis para optar por el título de:

Doctor en Ciencias en Modelación y Computación Científica

Autor: Lic. Yunier Serrano Rivero

Directores: Dr. Ernesto Moreno Frías

Dr. Alain Antonio González Pose

Dr. Frank Camacho Casanova

UNIVERSIDAD DE MEDELLÍN
FACULTAD DE CIENCIAS BÁSICAS
2023



**MINISTERIO DE CIENCIA,
TECNOLOGÍA E INNOVACIÓN**



**COLOMBIA
CIENTÍFICA**
Conocimiento Global para el Desarrollo



**PROGRAMA
NanoBioCáncer**

Tabla de contenido	
Capítulo 1 Introducción	3
Hipótesis	26
Objetivo general y objetivos específicos	26
Listado de artículos incluidos en la tesis	27
Capítulo 2 Design and construction of a synthetic nanobody library: testing its potential. with a single selection round strategy	28
Capítulo 3 Selecting nanobodies specific for the epidermal growth factor from a synthetic nanobody library	30
Capítulo 4 Engineered synthetic nanobody-based biosensors for electrochemical detection of epidermal growth factor receptor	32
Capítulo 5 Discusión general	34
Capítulo 6 Conclusiones	36
Capítulo 7 Recomendaciones	38
Capítulo 8 Referencias bibliográficas	40
Anexos. Asociados a los capítulos 1, 2 y 3	44

Capítulo 1

INTRODUCCION

1. Panorámica mundial del cáncer e importancia económica y en la medicina de los anticuerpos

Los cánceres son una de las patologías humanas más devastadoras que presentan una gama versátil de características clínicas distintivas que han provocado millones de muertes cada año en todo el mundo. Este grupo de enfermedades constituyen más de cien condiciones genéticamente diversas que comparten varios puntos en común en los mecanismos moleculares y alteraciones metabólicas entre sí. Esta patología constituye el resultado de la alteración de la señalización y el metabolismo celular, lo cual provoca la división y supervivencia descontroladas de las células transformadas. Una gran cantidad de moléculas, factores y condiciones han sido designadas como causas subyacentes para el inicio y la progresión de la enfermedad (Upadhyay 2021). Según reportes de la Agencia Internacional para la Investigación del Cáncer y la Organización Mundial de la Salud (OMS) en el 2020 ocurrieron 19,3 millones de nuevos casos de cáncer (18,1 millones excluyendo el cáncer de piel no melanoma) y casi 10,0 millones de muertes por cáncer (9,9 millones excluyendo el cáncer de piel no melanoma) ocurrieron en todo el mundo. El cáncer de mama en la mujer superó al cáncer de pulmón como el cáncer diagnosticado con más frecuencia con un estimado de 2,3 millones de nuevos casos (11,7 %), seguido del cáncer de pulmón (11,4 %), colorrectal (10,0 %), próstata (7,3 %) y estómago (5,6 %). El cáncer de pulmón continúa siendo la causa principal de muerte con un estimado de 1,8 millones de muertes (18 %), seguido del cáncer colorrectal (9,4 %), hígado (8,3 %), estómago (7,7 %) y mama en mujeres (6,9 %) (Sung et al. 2021). Por otro lado; los tratamientos o métodos que se utilizan para la eliminación del cáncer se clasifican en tradicionales (Ej: extracción quirúrgica del tejido tumoral, radioterapia y quimioterapia) y no tradicionales (inmunoterapia). Los métodos tradicionales son agresivos para los pacientes, ya que son inespecíficos (dañan tejidos sanos y tumorales), mientras que la inmunoterapia es mucho menos agresiva debido a que está dirigida específicamente a los tejidos tumorales. En particular; las terapias basadas en anticuerpos monoclonales: “del inglés monoclonal antibodies (mAbs)” ofrecen una alternativa promisoriosa a los métodos tradicionales. Aunque, diversos estudios revelan que la combinación de los métodos tradicionales con la inmunoterapia actúa sinérgicamente en la eliminación del tumor (Li et al. 2023). La popularidad de los mAbs se debe a su alta especificidad y afinidad por su molécula blanco, lo cual los convierte en una herramienta invaluable para la medicina. En este sentido, treinta y un nuevos mAbs han sido aprobados por la Administración de Alimentos y Medicamentos

(FDA) en los EE. UU y la Agencia Europea de Medicamentos en la Unión Europea (UE) hasta el 2013, para constituir un total de 57 mAb utilizados en la clínica hasta finales del 2017. Varios informes financieros revelaron que el mercado de anticuerpos había superado los 98 000 millones de dólares estadounidenses en ventas en diciembre de 2017, con una tasa de crecimiento anual del 18,3 % y una valoración prevista de 137 000 a 200 000 millones de dólares estadounidenses para el 2022. El mercado de anticuerpos está dominado por siete empresas, con el 87% de las ventas totales del mercado de 22 empresas activas lideradas por Genentech, miembro del grupo Roche, con una cuota de mercado del 31% para 11 moléculas de anticuerpos aprobadas. En términos de indicaciones de enfermedades, a diciembre de 2017; 15 de los 57 mAb están aprobados para la terapia del cáncer, y de estos 12 mAb se usan en hematología (Kang y Jung 2019).

1.1 Estructura y función de los anticuerpos

Los anticuerpos, también conocidos como inmunoglobulinas (Igs), son glicoproteínas producidas por las células B durante la respuesta inmune adaptativa. La diversidad de una respuesta de anticuerpos necesaria para reconocer o neutralizar a un amplio rango de antígenos es originada por recombinaciones e hipermutaciones somáticas de un grupo de genes. En mamíferos, la estructura básica de un anticuerpo consiste en dos cadenas pesadas y dos cadenas ligeras, las cuales se pliegan adoptando una estructura en forma de Y. Existen cinco clases o isotipos de anticuerpos (Ej: IgD, IgE, IgG e IgM), cada uno presenta una estructura específica y desempeñan una función determinada en los procesos inmunológicos. Debido a su alta prevalencia en el suero humano, importancia en la respuesta inmune y excelente especificidad. El IgG (150 kDa) constituye el isotipo de preferencia en la inmunoterapia (André et al. 2022). En esta clase de anticuerpo cada cadena pesada se compone de tres dominios constantes (CH1, CH2, y CH3) y uno variable (VH), mientras que la cadena ligera se compone de un dominio constantes CL y otro variable VL (André et al. 2022). A su vez, la molécula de IgG está compuesta por dos fragmentos idénticos de unión al antígeno uno conocidos como fragmentos Fab y una región cristalizable denominada fragmento Fc (Kang y Jung 2019).

Un fragmento Fab se compone por los dominios variables (VH y VL) ubicados hacia el extremo N-terminal del fragmento y dos dominios constantes (CL y CH1) (André et al. 2022). En dicho fragmento los dominios VH y VL se mantienen unidos a través de una interfaz hidrofóbica, mientras que sus dominios constantes CL y CH1 se unen por medio de un puente disulfuro, lo cual le proporciona rigidez y estabilidad al fragmento (Bannas et al. 2017). Una secuencia flexible o bisagra une a los fragmentos Fab con la región Fc. La

integridad y estructura de los anticuerpos es mantenida gracias a la presencia de puentes disulfuros entre los dominios constantes. Por otro lado, los dominios variables son los responsables de la afinidad y especificidad de los anticuerpos hacia el antígeno al cual se une a través de tres lazos hipervariables o regiones determinantes de complementariedad “ del inglés: complementary determining regions (CDRs)”. Los CDRs en los dominios VH y VL resultan en seis lazos hipervariables (H1, H2, H3, L1, L2, y L3) que forman el sitio de unión al antígeno o paratopo (André et al. 2022). Por su parte, la región Fc se compone únicamente de dominios constantes, los cuales median funciones efectoras como la fagocitosis dependiente de anticuerpo FDA (Kang y Jung 2019), la citotoxicidad dependiente de anticuerpo CDA y citotoxicidad dependiente del sistema complemento CDSC (André et al. 2022). Esta región, es además la responsable de prolongar la vida media de los anticuerpos. Las terapias basadas en anticuerpos tienen el propósito de eliminar o neutralizar a los microorganismos o enfermedades. En este sentido, los anticuerpos monoclonales (mAbs) pueden lograrlo mediante unión directa bloqueando la actividad de algunos patógenos como virus y receptores ubicados en la superficie de células tumorales. En otros casos los tratamientos terapéuticos requieren que los anticuerpos desencadenen funciones efectoras como la CDA y/o CDSC. En las respuestas de CDA tras el reconocimiento de un antígeno, el dominio Fc se acopla a los receptores Fc (FcγR) en la superficie de las células efectoras que median la fagocitosis o destrucción del antígeno (Ej. macrófagos y las células asesinas naturales o NK). En cambio, en la respuesta CDSC la región Fc de los anticuerpos promueven directamente la muerte de la célula blanco a través del sistema complemento (André et al. 2022).

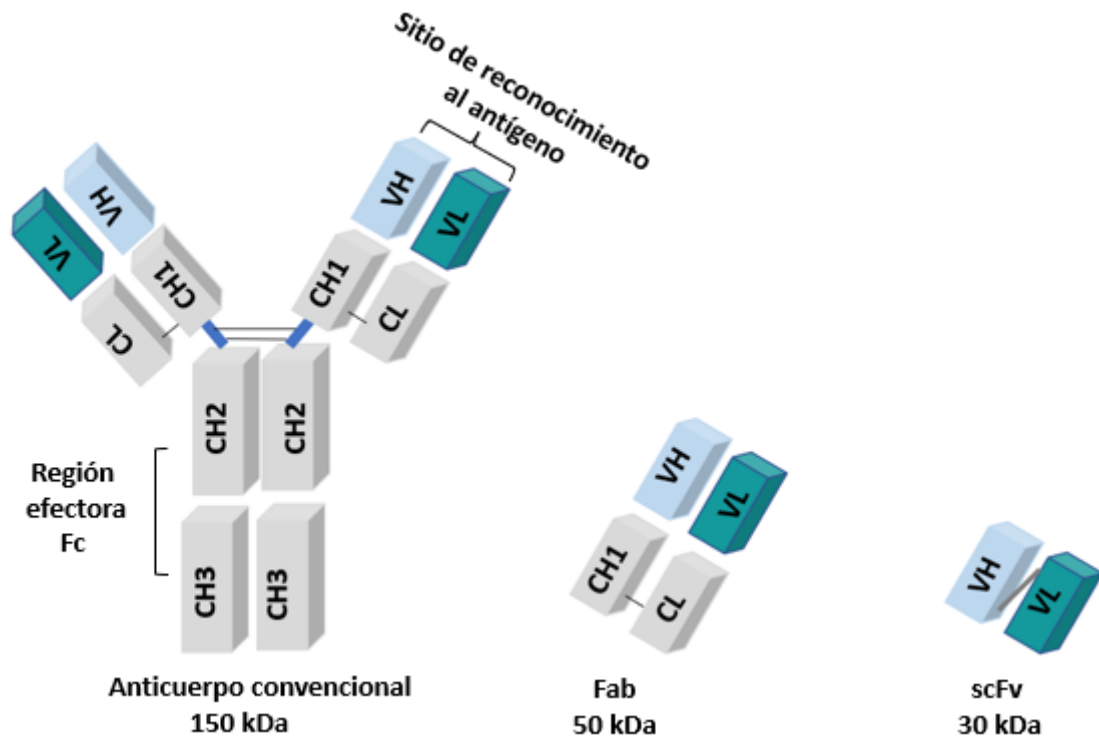


Figura 1. Estructura básica de un anticuerpo monoclonal (IgG1) y sus fragmentos derivados Fab y scFv. La región bisagra se representa en azul, los puentes disulfuros en barras negras, el espaciador o conector en el scFv se representa en gris oscuro.

1.2 Los principales fragmentos de anticuerpos derivados de las IgG

Como se mencionó previamente, los dominios variables Fab (50 kDa) son responsables de la especificidad de unión del anticuerpo y se encuentra formado por dos dominios variables (VH y VL) y dos dominios constantes CH1 y CL. Estos pueden ser obtenidos mediante proteólisis (pepsina, pepsina) o ingeniería genética. Por otro lado, el fragmento variable de simple cadena scFv (30 kDa) es una forma diseñada mediante ingeniería genética de los dominios variables (VH y VL) unidos entre sí por medio de un espaciador o conector flexible. Este fragmento constituye la unidad más pequeña con capacidad de unión al antígeno. La longitud y la composición de aminoácidos de este conector juegan un papel importante en el plegamiento correcto del fragmento, y generalmente tiene una longitud de 10 a 25 aminoácidos. La presencia de los residuos Glu-Lys y Gly-Ser en este espaciador incrementan la solubilidad y flexibilidad del fragmento scFv. A su vez, cada dominio variable se compone de nueve estructuras β que adoptan el plegamiento típico de los dominios variables de las inmunoglobulinas. Los dominios variables (VH y VL) en los fragmentos Fab y scFv se asocian entre sí por medio de una interfase hidrofóbica. Los tres CDRs en estos dominios son complementarios a los epítopos presentes en los antígenos, mientras que el

resto del dominio actúa como andamio (FR1, FR2, FR3 y FR4) para los CDRs y tienen variabilidad insignificante en comparación con los lazos hipervariables (Asaadi et al. 2021). Otras variantes de fragmentos de IgG menos utilizadas también se han obtenidos; ya sea mediante proteólisis (Ej: Fab', F(ab')₂ y (scFv)₂) o ingeniería genética (Ej: diacuerpo y minicuerpo) (Robinson et al. 2004).

1.3 Las potencialidades terapéuticas de los fragmentes de anticuerpos

La mayoría de los anticuerpos disponibles en el mercado se encuentran en formato completo (150 kDa). Estas moléculas poseen una prolongada vida media y la habilidad de inducir las funciones efectoras CDA y CDSC. Sin embargo, su limitada penetración en tumores sólidos debido a su gran tamaño (150 kDa) y sus elevados costos de producción constituyen una barrera para su uso terapéutico. No obstante, mediante la selección de dominios específicos, la vida media, la penetración en los tejidos y la afinidad de algunos fragmentos (Ej: fragmento Fab y el fragmento scFv) puede ser manejada de acorde a la aplicación que se les dará. Estos fragmentos son obtenidos por vía recombinante, y conservan la afinidad y especificidad de los anticuerpos de los que se derivan. A pesar de carecer del dominio efector Fc poseen algunas ventajas respecto a los anticuerpos completos, como: (i): mayor penetración en tumores sólidos, (ii): mayor acceso a epítomos ocultos que podrían no estar disponibles para los anticuerpos completos, y (iii): al ser moléculas menos complejas carentes de glicosilación pueden ser producidos en bacterias, lo cual disminuye sus costos de producción. La aprobación de fragmentos de anticuerpos Abciximab, Ranibizumab, Certolizumab pegol y Idarucizumab en formato Fab, y Blinatumomab y Brolocizumab en formato scFv; por sólo citar algunos, han demostrado las potencialidades terapéuticas de estas moléculas (André et al. 2022).

2. Anticuerpos no convencionales: “anticuerpos de dominios de cadena pesada”.

Los anticuerpos de dominios de cadena pesada; del inglés “heavy chain only antibodies (HCAbs)” son una clase no convencional de anticuerpos que han ganado popularidad como moléculas terapéuticas promisorias. Estos anticuerpos, poseen menor tamaño que los anticuerpos IgG convencionales y fueron descubiertos a partir del suero de camélidos (Hamers-Casterman et al. 1993) y posteriormente en peces de esqueleto cartilaginoso (Greenberg et al. 1995). Estos carecen de las cadenas ligeras y el dominio CH1 (Hamers-Casterman et al. 1993). El porcentaje de los HCAbs y anticuerpos IgG convencionales en el suero de los camélidos es variable. En camellos puede constituir el 50-80 %, mientras que en las especies de camélidos sudamericanos el 10-25 % (Muyldermans 2013). Los

camélidos básicamente producen tres tipos de inmunoglobulinas (IgG1, IgG2 y IgG3). La IgG1 es muy similar a las IgG convencionales, mientras que las IgG 2 y 3 carecen de las cadenas ligeras y los dominios CH1. Pero la región bisagra en la IgG2 es notoriamente más larga que la región bisagra en la IgG3 (Hamers-Casterman et al. 1993). Los fragmentos variables de los anticuerpos de camélidos expresados por vía recombinantes constituyen los denominados nano-anticuerpos (Nbs), VHH o sdAbs (Muyldermans 2013) (Figura 2). Estas moléculas son más pequeñas (15 kDa), solubles, estables, y más fácil de producir en hospederos bacterianos que los fragmentos Fab y scFv derivados de los anticuerpos convencionales (Asaadi et al. 2021).

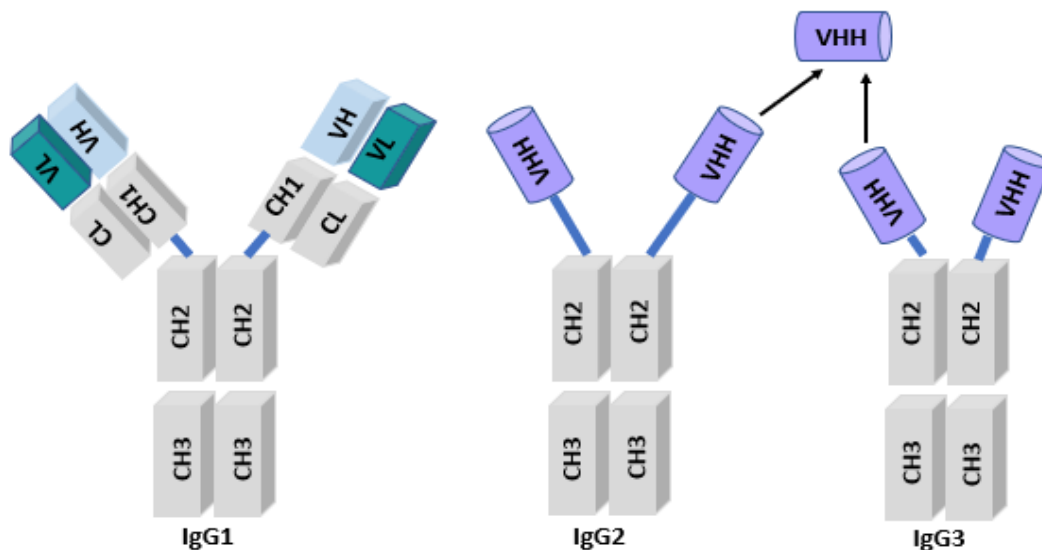


Figura 2. Estructura de los anticuerpos de camélidos y el nano-anticuerpo o dominio variable VHH derivado de estos.

2.1. Características generales de los dominios VHH de camélidos

Los dominios VHH de camélidos y los dominios VH de los anticuerpos convencionales comparten algunos rasgos estructurales. Ambos fragmentos de anticuerpos constan de cuatro regiones marco conservadas (FR1, FR2, FR3 y FR4) y tres regiones determinantes de complementariedad (CDR 1, CDR 2 y CDR3) responsables de determinar su especificidad por el antígeno (Jin et al. 2023). Los dominios VHH y VH poseen nueve estructuras β que adoptan el plegamiento típico de los dominios variables de las inmunoglobulinas. Estas estructuras se organizan en dos laminas β compuestas por 4 y 5 estructuras β , respectivamente, las cuales se conectan por medio de lazos y un puente disulfuro altamente conservado entre las Cys en las posiciones 23 y 94. La ausencia del dominio VL en los dominios VHH provoca diferencias en el FR2 y los CDRs. En los anticuerpos convencionales los tres lazos del VH (H1, H2 y H3) y los tres lazos del VL (L1, L2 y L3) se

yuxtaponen y proporcionan una superficie de contacto con el antígeno de unos 600–900 Å². En general, el paratopo de estos forman una cavidad, un surco o una superficie plana, cuyas arquitecturas se han relacionado con el reconocimiento de moléculas pequeñas, péptidos lineales y antígenos grandes (como las proteínas). En contraste, con la ausencia del dominio VL en los anticuerpos de camélidos los residuos hidrofóbicos son reemplazados por aminoácidos hidrofílicos (Phe37, Glu44, Arg45 y Gly47), lo cual garantiza la estabilidad del dominio VHH y evita la exposición de la región hidrofóbica al solvente (Figura 3). Estas modificaciones sustentan la mayor solubilidad de los dominios VHH en relación con los dominios VH y los fragmentos scFv derivados de los anticuerpos convencionales. En los dominios VHH, los CDRs 1 y 3 poseen mayor longitud que sus contrapartes en los anticuerpos convencionales, siendo el CDR3 de estos notablemente largo. Esta peculiaridad de los CDRs compensa la ausencia de los tres CDRs del dominio VL y la diversidad combinatoria del par VH-VL de los anticuerpos convencionales. La longitud de los CDR1 y 3 en los dominios VHH les proporcionan una superficie de contacto con el antígeno de 600–800 Å² similar a la que ofrecen los seis CDRs del par VH-VL de los anticuerpos convencionales. Además, la mayor longitud del CDR1 acompañada de mutaciones en puntos críticos impresos en la línea germinal VHH compensa la variabilidad del dominio VL de los anticuerpos convencionales, mientras que las mutaciones somáticas en los residuos en las posiciones 28 y 30 se incorporan durante el proceso de maduración de afinidad para participar directamente en la unión al antígeno (Asaadi et al. 2021). La notable longitud del CDR3 en los Nbs sugiere la selección de dominios VHH funcionales después de la recombinación V-D-J. Un CDR3 extendido implica una mayor flexibilidad lo que es entrópicamente contraproducente para su unión al antígeno. Esto se compensa a través del establecimiento de un puente disulfuro adicional entre los CDR 1 y 3, CDR 2 y 3 o CDR 3 y el FR2 (Muyldermans 2013, Asaadi et al. 2021). En este sentido, muchos dominios VHH de camellos contienen un par extra de residuos de Cys en los CDRs 1 y 3, que se sabe que forman un puente disulfuro entre estos restringiendo su flexibilidad en ausencia del antígeno. Sorprendentemente, en los dominios VHH de llamas este puente disulfuro adicional ocurre con menos frecuencia (~10%), lo cual es lo esperado debido a que el CDR3 promedio en estos camélidos es notablemente más corto que en los dominios VHH de dromedarios (Muyldermans 2013). La notable longitud de los CDR3 en los Nbs les proporciona una distinta preferencia por los epítopos de los antígenos. La estructura de los dominios VHH forman un paratope de superficie convexa haciéndolos adecuados para el reconocimiento de cavidades en la superficie del antígeno. Los CDR3 pueden adoptar

estructuras protuberantes o sobresaliente, lo cual es poco usual debido a que en la mayoría de los casos estos se pliegan sobre la región FR2 adoptando una estructura plana. Por otro lado, aunque hay una mayor variabilidad en el CDR3 su implicación en la unión al antígeno es bastante limitada. En contraste, los aminoácidos ubicados hacia el extremo N-terminal del CDR 1 suelen estar muy involucrados en el reconocimiento del antígeno (Muyldermans 2013). En resumen; los CDRs 1 y 3 en el paratope de los dominios VHH pueden adoptar una variedad de estructuras que van desde lazos protuberantes a planos, lo cual les proporciona un mayor acceso superficies planas, cavidades, lazos protuberantes y hendiduras del antígeno (Salvador et al. 2019).

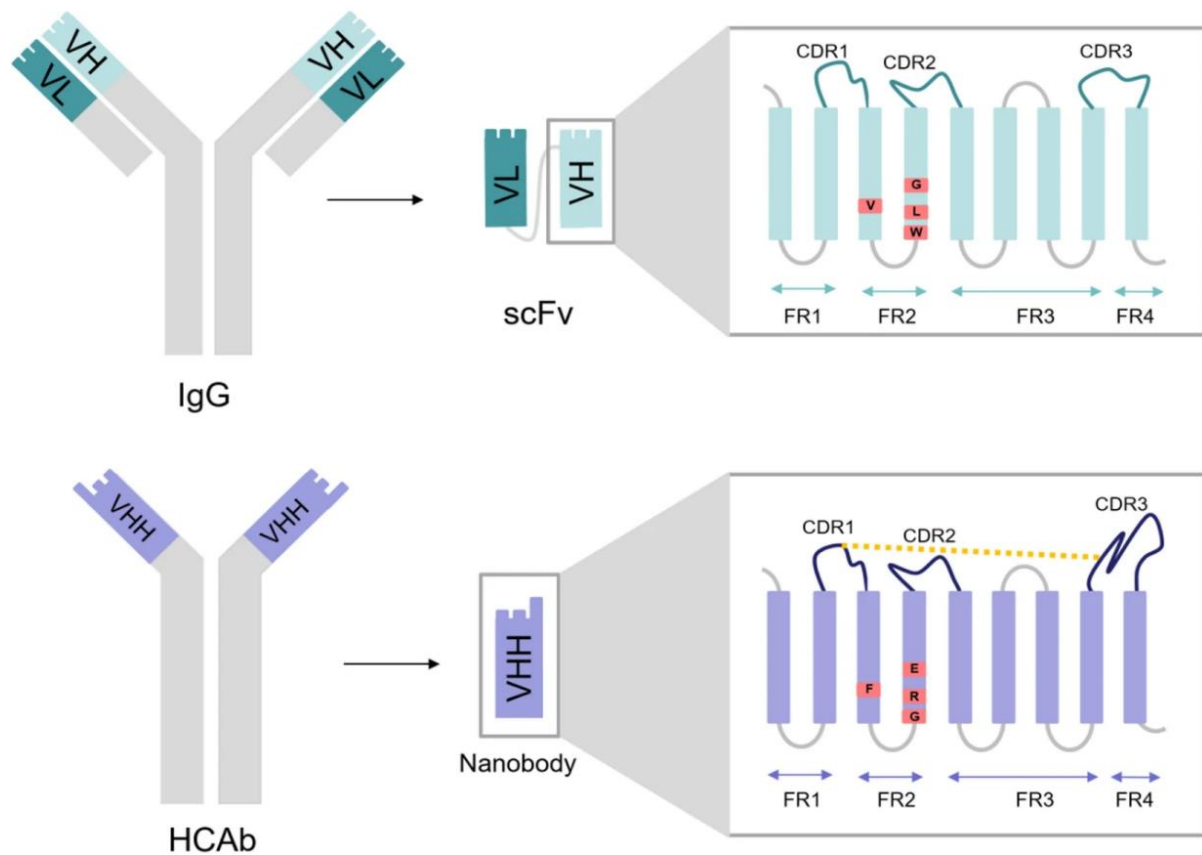


Figura 3. Esquema representativo de las diferencias entre los nano-anticuerpos y los scFv. Estructura de un anticuerpo IgG convencional, un fragmento scFv, un anticuerpo de camélido (HCAb) y un nano-anticuerpo (Asaadi et al. 2021).

2.2. Los nano-anticuerpos como moléculas únicas

Los Nbs muestran algunas ventajas sorprendentes frente a los anticuerpos convencionales (mAb) que son dignas de mención, ya que combinan características deseables de los mAb con algunas de las propiedades beneficiosas de fármacos pequeños:

(i): Pueden unirse a una amplia gama de epítomos mostrando afinidades en el rango nanomolar e incluso picomolar. Siendo comparables o superiores a las de los mAb convencionales. Los CDR 3 de los Nbs es notablemente más largo que el CDR3 de los dominios VH de los anticuerpos convencionales. (ii): Pueden ser producidos en forma de multímeros. Debido al pequeño tamaño y naturaleza monomérica de los Nbs. Estos son fáciles de manipularse genéticamente para obtener moléculas fusionadas con la finalidad de proporcionarles multiespecificidad y versatilidad. Para aplicaciones terapéuticas, los Nbs bivalentes y biespecíficos son un formato muy atractivo. La bivalencia permite que los anticuerpos se unan a antígenos multiméricos con gran avidéz y la biespecificidad consiste en unirse simultáneamente a dos antígenos diferentes. Esta opción es particularmente atractiva para aplicaciones terapéuticas y para extender la vida media de los Nbs. (iii): Los Nbs son moléculas altamente estables y solubles. Presentan propiedades biofísicas y bioquímicas óptimas que incluyen solubilidad, tolerancia térmica y resistencia proteolítica. El plegamiento del CDR 3 y el contenido hidrofílico del FR 2 les otorga una alta solubilidad en soluciones acuosas. Además, imparten alta estabilidad conformacional y térmica. La capacidad de unión de los Nbs al antígeno se mantiene invariable hasta después de 1 semana a 37 °C y su desnaturalización puede ser reversible después de largos períodos de incubación a 90 °C. Además de la resistencia térmica, los Nbs son estables en presencia de proteasas y agentes caotrópicos, así como a pH extremos. Los Nbs también pueden ser diseñados para tolerar la proteólisis intracelular, lo cual, junto a su capacidad para modular la actividad de su molécula blanco los convierte en agentes ideales para bloquear la funcionalidad de antígenos intracelulares. Con este fin se han desarrollado los llamados intrabodies (fragmentos de anticuerpos recombinantes o Nbs que se expresan intracelularmente) que se unen específicamente a proteínas intracelulares. Los intrabodies han sido muy útiles en la neutralización de patógenos intracelulares o en el tratamiento de enfermedades neurodegenerativas. La resistencia proteolítica y la estabilidad bajo condiciones extremas de los Nbs también los hacen adecuados para su uso en vías alternativas de administración (Ej: administración oral). En cuanto al uso de Nbs con fines de diagnóstico, la alta estabilidad de Nbs a altas concentraciones de solventes orgánicos, pH y temperaturas extremas abre una amplia gama de aplicaciones para la detección de moléculas pequeñas o proteínas. Esto se debe al hecho de que estas características físicas permitir el uso de métodos de inmovilización más eficientes con fines de bio-detección, la posibilidad de analizar contaminantes a baja concentración después de un paso de preconcentración e incluso aumentar la cinética de bio-reconocimiento trabajando a altas

temperaturas. (iv): Los Nbs poseen una elevada capacidad para penetrar los tejidos y son rápidamente eliminados de la sangre. Debido a que la tasa de difusión intercelular pasiva dentro de un tejido depende del tamaño molecular y es inversamente proporcional a éste. En este sentido, un Nb monovalente de 15 kDa debe penetrar con mayor facilidad los tejidos en comparación a los mAbs convencionales (150 kDa). Esta característica puede ser muy útil para combatir tumores debido a que los Nbs puede diseñarse con el fin de modificar o neutralizar moléculas oncogénicas, redirigirlos a un compartimento celular específico o expresarlos en la superficie de la célula tumoral para desencadenar una respuesta inmune contra esta (Salvador et al. 2019). La rápida eliminación renal de los Nbs $t(1/2) < 30$ min podría constituir una limitante para su uso terapéutico (Verhaar et al. 2021), ya que la terapia generalmente requiere altas dosis y de la administración frecuente del agente terapéutico, se han desarrollado varios métodos para aumentar la vida media de los Nbs. Estos incluyen la adición de polietilenglicol, conjugación a albúmina, o fusión a un fragmento Fc de un anticuerpo convencional. Sin embargo, vale la pena mencionar que, para algunas aplicaciones, la rápida eliminación renal de los Nbs puede ser ventajosa. Además, el pequeño tamaño de los Nbs les proporciona la capacidad de cruzar la barrera hematoencefálica convirtiéndolos en moléculas atractivas para el tratamiento de enfermedades neurodegenerativas. (v): Los Nbs reconocen epítopos ocultos. Estudios cristalográficos de anticuerpos convencionales han revelado que en la mayoría de los casos la superficie de unión al antígeno es plana o cóncava. Por el contrario, los Nbs a menudo se une a hendiduras y cavidades, lo cual es favorecido por la presencia de un CDR1 extendido y un CDR3 notablemente más alargado y expuesto. Estos cambios estructurales permiten arquitecturas de unión con superficies planas, cavidades, lazos expuestos y hendiduras (Salvador et al. 2019). Así como sitios catalíticos de enzimas y a receptores (Ledsgaard et al. 2022). Por lo tanto, esta característica de los Nbs y su pequeño tamaño promueven su interacción con nuevos epítopos que son inaccesibles para los pares VH-VL de los anticuerpos convencionales, y también explican la capacidad de Nb para unirse y neutralizar blancos que son notoriamente difíciles de alcanzar con los anticuerpos convencionales. (vi): Los Nbs poseen escasa o ninguna inmunogenicidad para el hombre. Esto se debe a que los dominios VHH de camélidos presentan un alto grado de similitud con los dominios VH de los anticuerpos humanos, lo que significa que hasta la fecha no han mostrado ninguna reacción de inmunogenicidad inesperada. Sin embargo, para los tratamientos terapéuticos prolongados se prefiere la humanización de la región RF2 de los Nbs con el fin de disponer de una secuencia de aminoácidos que muestre un alto grado de

homología con respecto a las VH humanas (vii): Los costos de producción de los Nbs son relativamente bajos. Los mAbs son grandes proteínas multiméricas que suelen sufrir modificaciones postraduccionales. Por eso, su producción se limita a los costosos cultivos de células de mamíferos. En cambio, los Nbs pueden ser producidos fácilmente en a partir de hospederos más económicos, (Ej: bacterias, levaduras, hongos) (Salvador et al. 2019).

2.3. Aplicaciones médicas de los nano-anticuerpos

Los Nbs poseen un grupo de ventajas que los convierte en moléculas únicas que pueden ser utilizadas en la investigación, la detección y el tratamiento de enfermedades. En particular en el diagnóstico y tratamiento terapéutico del cáncer, lo cual se debe a su alta capacidad para penetrar tumores sólidos, su resistencia a condiciones extremas de pH, de temperatura y solventes orgánicos (Salvador et al. 2019). Además, la avidéz de estas moléculas puede ser incrementada por medio de la ingeniería con el fin de obtenerlos en forma de multímeros (dos o más Nbs específicos por epítopos iguales o a diferentes) (Bannas et al. 2017). Esto ha sido demostrado en estudios con Nbs bivalentes anti EGFR (Roovers et al. 2011) y anti TNF (Beirnaert et al. 2017). Adicionalmente, los Nbs mantienen su estabilidad después de ser acoplados a compuestos inorgánicos, orgánicos y a otras proteínas (Ej: radioisótopos, fluoróforos, biotina, trazadores enzimáticos, drogas, etc.) lo que incrementa su gama de usos (Salvador et al. 2019). Los Nbs también han sido exitosamente acoplados a biosensores con el fin de ser usados en la detección de antígenos marcadores de cáncer de próstata (Hosseindokht et al. 2021), la proteína espiga del coronavirus (Katz 2021), al antígeno carcinoembrionario (Rao et al. 2022), entre otros. Por otro lado, entre las innumerables aplicaciones de los Nbs para el tratamiento del cáncer destaca la generación de Nbs específicos por el receptor del factor de crecimiento epidérmico (del inglés EGFR), el cual se produce a altos niveles en la superficie de las células de algunos tejidos tumorales (Salvador et al. 2019). En las células tumorales, el EFR se activa luego de la unión del factor de crecimiento epidérmico (del inglés: EGF) y desencadena una cascada de señalización que trae como resultado el desarrollo del tumor. Los Nbs 9G8 y 7D12 se unen específicamente al dominio extracelular del EGFR, y ensayos *in vitro* han mostrado que estos son eficientes en inhibir el desarrollo de tumoral. Las células tumorales pueden incrementar simultáneamente los niveles del EGFR y su ligando (EGF) (Roovers et al. 2011, Schelch et al. 2021), lo cual favorece la ocurrencia de metástasis. En este contexto, ya ha sido desarrollada una vacuna terapéutica (CIMAvox-EGF) contra el EGF circulante con demostrada eficacia frente al cáncer de pulmón avanzado (Evans et al. 2022). Sin embargo, hasta la fecha no se ha reportado el desarrollo de anticuerpos

específicos por el EGF. Esto posiblemente se deba a que para esta pequeña (6 kDa) y globular molécula, no se han descrito cavidades definidas, lo cual dificulta la generación de fármacos y anticuerpos contra ella (Guardiola et al. 2018). En un reciente trabajo reportado por el grupo de Guardiola se obtuvieron Nbs específicos por el EGF de una biblioteca inmune originada a partir de una alpaca (Guardiola et al. 2018) y posteriormente demostraron la capacidad de estos para inhibir la activación del EGFR (Guardiola et al. 2022). Otros antígenos blancos para el tratamiento del cáncer lo constituyen el factor de necrosis tumoral y factor de crecimiento vascular-endotelial: del inglés tumour necrosis factor alpha (TNF α) y vascular endothelial growth factor (VEGF), respectivamente. Se ha documentado el efecto promotor de ambas moléculas en el crecimiento y progresión de los tumores (Coşkun et al. 2018) y estudios *in vitro* han demostrado que la administración de Nbs específicos por estas son eficaces en disminuir su desarrollo (Verhaar et al. 2021).

3. La tecnología de producción de péptidos/proteínas/fragmentos de anticuerpos en la superficie de fagos (del inglés: Phage display)

Aunque la tecnología de hibridomas fue pionera en el tiempo y todavía se usa comúnmente en la producción anticuerpos monoclonales. Los mAbs derivados de murinos tienen una eficacia terapéutica limitada. Se ha visto en pacientes tratados con mAbs derivados de murinos desarrollan una respuesta inmunológica frente a estos anticuerpos o respuesta humana anti-IgG de ratón (HAMA). Dicha respuesta acelera la eliminación de estos anticuerpos y podría dar lugar a las indeseables respuestas alérgicas tras repetidas administraciones de estos. Las técnicas de ingeniería de anticuerpos se utilizaron posteriormente en la creación de anticuerpos quiméricos o humanizados mediante la combinación de los CDRs de anticuerpos murinos con las regiones constantes de los anticuerpos humanos. Actualmente, la tecnología de la hibridoma se ha desarrollado hasta lograr generar anticuerpos completamente humanos a partir de ratones transgénicos (Ej: HuMabMouse y Xenomouse). En estos ratones el loci que codifica para las inmunoglobulinas murinas ha sido reemplazado por el loci que codifica para las inmunoglobulinas humanas. Sin embargo, la tecnología de phage display ha surgido como una alternativa a la tecnología de la hibridoma (Alfaleh et al. 2020). Esta tecnología fue introducida por primera vez por Smith en 1985 a partir de fagos filamentosos (Smith 1985). Seguidamente, Parmley y Smith describieron un proceso de selección y enriquecimiento por afinidad conocido como que permitió el aislamiento de fagos recombinantes en función de su afinidad por su molécula blanco (Parmley y Smith 1988). Luego, el grupo de McCafferty fueron pioneros al utilizar esta tecnología en la expresión y selección de

fragmentos de anticuerpos (McCafferty et al. 1990). La tecnología de phage display es un método *in vitro* que se utiliza con el fin de seleccionar un péptido/proteína/fragmento de anticuerpo expresado en la superficie de bacteriófagos. Las bibliotecas de fagos de péptidos (fagos recombinantes) contienen miles de millones de variantes, y se seleccionan a partir de su afinidad por su molécula blanco. Usualmente, los péptidos que se unen con mayor fortaleza a su blanco se enriquecen después de 3 a 5 rondas de selección, es decir, selección por afinidad de péptido específico de un gran repertorio de clones (fagos recombinantes). La tecnología de phage display se puede utilizar para identificar diferentes entidades biológicas, como proteínas, toxinas, virus, bacterias, células cancerosas e incluso sustancias no orgánicas, como metales, aleaciones, semiconductores y superficies plásticas. La información detallada sobre los genomas de los fagos filamentosos ha sido la clave del éxito para las aplicaciones generalizadas de esta tecnología. Con el cursar del tiempo las metodologías de phage display se han refinado y avanzado para permitir el descubrimiento de anticuerpos contra blancos complejos y anticuerpos con características de unión peculiares (Anand et al. 2021).

3.1. Basamento de la tecnología de phage display

La tecnología de phage display es una técnica molecular basada en una modificación genética del ADN del fago para permitir la expresión de una molécula de interés (péptidos/proteínas/ fragmentos de anticuerpos) en la superficie del fago al producirla fusionada a una de las proteínas de su cápside. El gen que codifica para la molécula de interés se inserta fusionado al gen que codifica para una de las proteínas de la cápside del virus, ya sea en el genoma del virus o en un fagemido (Anand et al. 2021). En el segundo caso, se requiere de un fago auxiliador que complemente las proteínas de la cápside y garantice la producción de fagos recombinantes, lo cual es esencial para posteriores procesos de selección (Anand et al. 2021). Cuando las partículas virales son producidas por el huésped, estas poseen la o las moléculas de interés fusionados a una o varias proteínas de su cápside (presentan a la molécula de interés en su superficie). El poder de la tecnología de phage display se fundamenta en su capacidad para formar una conexión física entre la molécula expresada (fenotipo) y una secuencia de ADN que codifica la molécula de interés (genotipo). Tal enlace fenotipo-genotipo permite la selección, la identificación y la determinación de la secuencia de aminoácidos de los clones específicos por un determinado blanco mediante la secuenciación del genoma del fago o del fagemido al que se le insertó el gen codificante para la molécula de interés (Jaroszewicz et al. 2022).

Existen varias etapas claves que son necesarias tener en cuenta a la hora de implementar la tecnología de phage display, y el primero es el diseño de la biblioteca, que puede incluir varios millones o más de clones de ADN que contienen los genes que codifican para la molécula (péptidos/proteínas/fragmentos de anticuerpos) que se producirán en la superficie del fago. Seguidamente, la biblioteca se clona en el genoma del fago (ya sea un vector clásico o un sistema fagémido), y se valida que la molécula de interés se produzca funcionalmente en la superficie del fago. El procedimiento de selección permite una identificación fácil del fago recombinante específico por una molécula blanco. Esta tecnología ofrece las ventajas de identificar regiones interactivas de péptidos, proteínas o fragmentos de anticuerpos sin conocimiento previo sobre el tipo y la naturaleza de la interacción con su blanco. Así como la posibilidad de seleccionar clones específicos por un blanco a partir de un amplio repertorio de clones de fagos recombinantes (hasta 10^{14} partículas virales por mL) (Jaroszewicz et al. 2022). A su vez, los fragmentos de anticuerpos que usualmente son expresados usando esta tecnología, son los scFv, los Nbs, y en menor medida los fragmentos Fab (Ledsgaard et al. 2022).

3.2. Características del fago del fago filamentoso M13

El desarrollo de la tecnología de phage display fue posible solo después de una comprensión detallada de la biología de los bacteriófagos, y especialmente de los fagos filamentosos. Los virus que infectan células bacterianas se utilizaron durante años como modelos en microbiología y biología molecular, aunque su uso práctico siguió siendo bastante ilusorio durante mucho tiempo. Sin embargo, la acumulación de conocimientos sobre la estructura y las funciones de los bacteriófagos hizo posible emplearlos en el desarrollo de herramientas sofisticadas en ingeniería genética y sistemas biológicos que permitieron la detección de un gran número de moléculas para seleccionar aquellas con fines específicos y deseados (Jaroszewicz et al. 2022).

Los fagos Ff son un grupo de virus filamentosos capaces de infectar bacterias Gramnegativas, como *Escherichia coli* (*E. coli*), que portan el plásmido F. Estos virus pertenecen a la familia *Inoviridae* y al género *Inovirus*. El fago filamentoso M13, constituye el miembro de esta familia más utilizado en la tecnología de phage display. Otros miembros de la familia como el fd y f1, también han sido utilizados. Por otro lado, el fago filamentoso M13 es un virus de ADN circular monocatenario de aproximadamente 6.4 kb. Estos virus filamentosos poseen 6,5 nm de diámetro y 930 nm de longitud, y su genoma está compuesto por 11 genes que codifican para las proteínas de cápside (pIII, pVI, pVII, pVIII y pIX) (Figura1), para las proteínas que participan en la replicación viral (pII, pV y pX) y para

las proteínas involucradas en su ensamblaje (pI, pIV y pXI). Las proteínas pIII (3 a 5 copias) y pVI se ubican en un extremo de la partícula viral, mientras que en el otro extremo se disponen las proteínas pVII y pIX. La proteína pVIII constituye la proteína más abundante (hasta 2700 copias) (Figura 4, y ocupa casi toda la superficie de la partícula viral (Jaroszewicz et al. 2022). La infección por fagos filamentosos evoca un tipo específico de estado lisogénico en el que las bacterias infectadas se ensamblan y secretan fagos al medio de cultivo (cuando se cultivan en condiciones de laboratorio). En la etapa inicial del ciclo de vida del fago, la infección se inicia a partir de la unión de la proteína pIII del fago al pilus F de *E. coli*. Durante esta fase, el DNA monocatenario del fago es transferido a la célula huésped donde es transformado en una forma replicativa de doble cadena por la maquinaria de replicación del hospedero. Seguidamente, la forma replicativa del genoma viral es replicado, y a partir de este se generan múltiples copias de ADN monocatenario. Durante esta fase también se sintetizan las proteínas virales (de la cápside, involucradas en su replicación y ensamblaje). El ensamblaje de las nuevas partículas virales se desencadena cuando se alcanza una concentración adecuada de la proteína pV del fago, y luego estas son secretadas al medio de cultivo (Jaroszewicz et al. 2022).

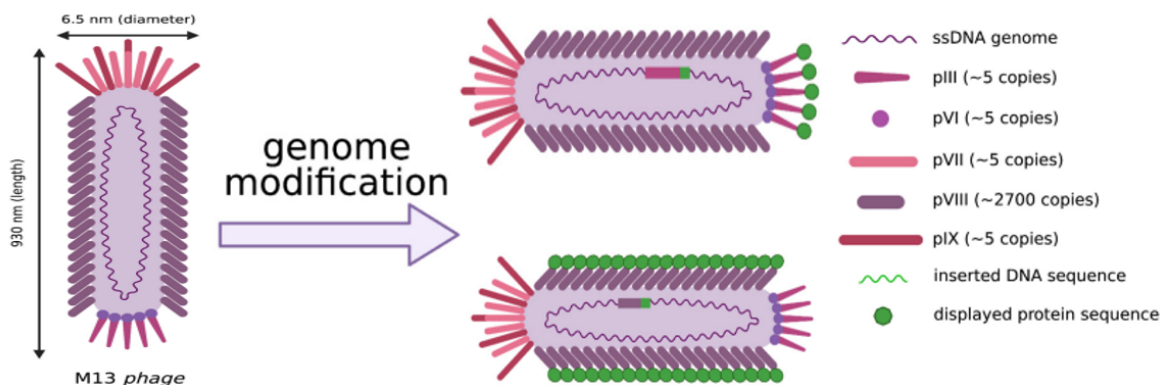


Figura 4. Estructura del fago filamentosos M13, y principios del phage display. El fago M13 pertenece a la familia de los fagos filamentosos. Tiene un genoma de ADN monocatenario (ssDNA) y su cápside está formada por cinco proteínas diferentes. El "cásico phage display" se basa en la modificación del genoma del fago que consiste en una inserción del gen codificante para la molécula de interés en el marco de lectura de una de las proteínas de la cápside (pIII o pVIII). Como resultado, la partícula del virión del fago presenta a la molécula de interés en su superficie (displayed protein sequence) (Jaroszewicz et al. 2022).

3.3. Sistemas de phage display basados en proteínas de la cápside del fago M13

Como se mencionó anteriormente, la molécula de interés (péptidos/proteínas/fragmentos de anticuerpos) son producidas fusionadas al menos a una de las proteínas de la cápside

del virus. La información para dicha fusión se encuentra en el genoma del fago o en el fagemido, según sea el caso (Figura 5). En este sentido, las proteínas pIII y pVIII constituyen las opciones de preferencia (Alfaleh et al. 2020), siendo la proteína pVIII adecuada para péptidos y proteínas pequeñas, mientras que para péptidos y proteínas grandes se prefiere la utilización de la proteína pIII. La distinción clave en el uso de una de las dos proteínas de la cápside como plataforma de phage display depende del número de copias que se desee obtener de la molécula de interés (Figura 5). A partir de la plataforma pIII-molécula de interés se puede obtener de 1 a 5 copias de la molécula de interés. En cambio, a partir de la plataforma pVIII-molécula de interés se pueden obtener cientos o miles de copias de la molécula de interés (Figura 4). Para experimentos como el aislamiento de anticuerpos de alta afinidad, el uso de la fusión a pIII es más adecuado porque se prefiere una valencia reducida. Por otro lado, la fusión pVIII da como resultado una selección de alta avidéz, pero probablemente una unión de baja afinidad. Además de las proteínas pIII y pVIII, también se han utilizado como plataformas a las proteínas pVI, pVII y pIX. Los vectores de fagos fueron las primeras plataformas utilizadas en los primeros experimentos de phage display y, en general es más fácil trabajar con ellos. Sin embargo, algunos inconvenientes están asociados con este tipo de vectores, como la pérdida de infectividad de pIII debido a la fusión de péptidos extraños. Además, la presentación polivalente resultante conlleva un mayor riesgo de seleccionar fagos recombinantes con baja afinidad por su molécula blanco. Por lo cual se desarrollaron los fagemidos (híbridos de fago y vector de plásmido), que permiten la presentación monovalente de la molécula de interés en la superficie del fago. Los sistemas basados en fagemidos tienen dos copias del gen pIII o pVIII ubicados en replicones distintos. La forma recombinante del gen pIII o pVIII fusionado al gen que codifica para la molécula de interés se encuentra en el fagemido, mientras que el gen codificante para pIII o pVIII de tipo salvaje (sin fusión) se encuentra en el genoma del fago (fago auxiliar). Los fagemidos están diseñados para contener el origen de replicación tanto del fago M13 como del plásmido para su propagación en *E. coli*. Estos poseen al gen codificante para la proteína pIII o pVIII, un gen marcador (resistencia a antibiótico) y sitios de clonación múltiple. Sin embargo, no contienen ninguno de los otros genes estructurales o no estructurales necesarios para la multiplicación y ensamblaje de un fago funcional. Los fagemidos se pueden usar como plásmidos, lo que permite el uso de herramientas de biología molecular para su manipulación. Los fagemidos también pueden empaquetarse en un fago M13 usando al fago auxiliar, el cual contiene un origen de replicación defectuoso y proporciona las proteínas estructurales necesarias para el ensamblaje de una partícula

viral funcional. Por otro lado, "fago auxiliador de tipo salvaje" se refiere a un fago M13 que codifica todas las proteínas del virión. Este fago generalmente tiene un origen de replicación Ff que es resistente a la interferencia y/o una señal de empaquetamiento defectuosa y un origen de replicación adicional (derivado de plásmido para la propagación de su genoma en *E. coli*) que permite la replicación selectiva y el empaquetamiento del fagemido. Esta característica garantiza que ~90% de las nuevas partículas virales contengan al fagemido en su interior en lugar del genoma viral. Una de las ventajas que ofrecen los vectores basados en fagemidos, consiste en la producción monovalente de la molécula de interés en la superficie del fago recombinante evitando los efectos negativos de la avidéz debido a la expresión de muchas copias de esta (Jaroszewicz et al. 2022). La presencia de un codón de parada ámbar entre el Nb y el gen que codifica para la proteína pIII en el sistema de selección basados en fagemidos, ofrece la ventaja de evitar los efectos de la avidéz durante los procesos de selección. Sin embargo, las bacterias secretan una gran cantidad de fagos (sin la molécula de interés fusionada a la proteína pIII), lo cual reduce la eficiencia del enriquecimiento de viriones que presentan la molécula de interés en su superficie (Muyldermans2021).

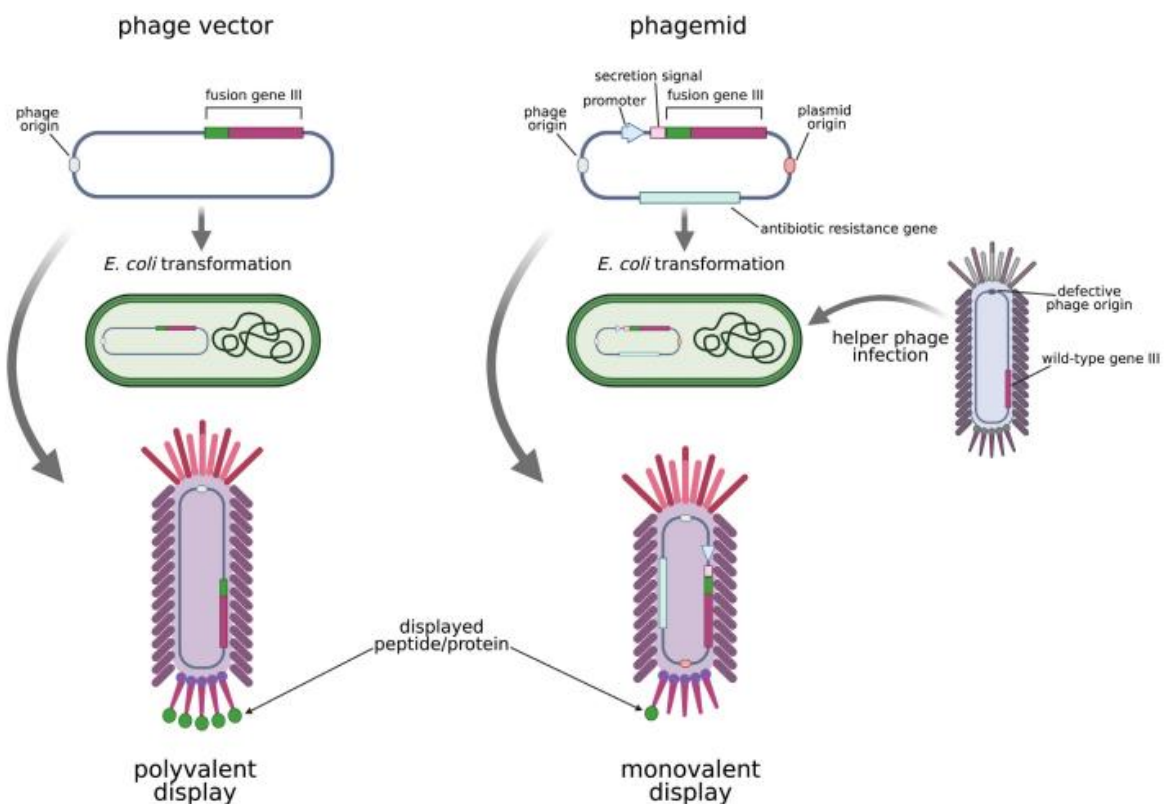


Figura 5. Comparación de un vector basado en fagos y un vector basado fagemido. La principal diferencia entre el vector de fago y el fagemido es la valencia de la molécula de interés resultante expresada en su superficie.

Si el vector de fago contiene solo una copia de un gen recombinante que codifica la proteína de la cápside que presenta, la presentación de fago resultante siempre es polivalente. El uso de un fagemido, a su vez, genera la presentación de una valencia más baja (en el caso de pIII mayoritariamente monovalente) ya que el fago auxiliar proporciona la copia de tipo salvaje de la proteína de la cápside que suele expresarse de manera más eficiente que la recombinante.

3.4. Las bibliotecas de fagos recombinantes

Una biblioteca de fagos recombinantes es una población diversificada de clones de fagos en la que cada clon contiene un inserto de ADN (gen codificante para la molécula de interés) y su correspondiente producto expresado en su superficie fusionado a una o varias de las proteínas de su cápside. La principal ventaja que ofrecen las bibliotecas de fagos recombinantes consiste en la posibilidad de analizar simultáneamente un gran número de clones de fagos. Otros de los beneficios de las bibliotecas de fagos incluyen bajos costos de propagación y facilidad de manejo debido a la gran cantidad de kits comerciales disponibles para realizar tareas ordinarias de biología molecular. Además, una sola biblioteca de fagos suele ser suficiente para múltiples ciclos de selección, ya que una vez producida puede ser almacenada durante largos periodos de tiempo. Algunas limitaciones de las bibliotecas de fagos pueden incluir errores potenciales en el procedimiento de selección debido a los niveles de expresión variables de la molécula de interés en *E. coli*. Además, las amplificaciones consecutivas de la biblioteca pueden reducir la diversidad de la población de fagos. Sin embargo, a pesar de estas limitaciones las bibliotecas de fagos recombinantes se utilizan ampliamente en el descubrimiento de anticuerpos con fines terapéuticos y de diagnóstico. Hasta la fecha se han publicado diversos artículos relacionados con el desarrollo e implementación de esta tecnología (Jaroszewicz et al. 2022).

3.5 Clasificación de las bibliotecas de fagos recombinantes

Las bibliotecas pueden ser divididas en bibliotecas de péptidos y bibliotecas de anticuerpos (incluidas las bibliotecas de Nbs) y estas últimas a su vez se clasifican en bibliotecas inmunes, bibliotecas naïve y bibliotecas sintéticas (Jaroszewicz et al. 2022).

La construcción de bibliotecas inmunes de Nbs comienza con la toma de sangre de camélidos inmunizados (camello, dromedario, llama o alpaca). Una diversidad de 10^6 - 10^8 es suficiente para seleccionar Nbs con alta afinidad y especificidad por su blanco. Estas bibliotecas poseen los inconvenientes de largos y tediosos protocolos de inmunización. Así como de la construcción de una nueva biblioteca para la selección de Nbs específicos para cada antígeno. En contraste las bibliotecas de Nbs naïve y sintéticas son consideradas bibliotecas universales y no requieren de la inmunización de los animales, ni de la

construcción de una nueva biblioteca para la selección de Nbs específicos para nuevos antígenos. Además, ofrecen la ventaja de generar Nbs específicos por blancos no inmunogénicos como el ARN o el ADN, moléculas que puedan ser tóxicas, contagiosas o dañinas para los animales o el medio ambiente. Sin embargo, las bibliotecas naïve y sintéticas requieren de una diversidad mayor que las bibliotecas inmunes para la obtención de Nbs específicos por todos los posibles antígenos o moléculas blancos frente a los cuales serán sometidas. Además, los Nbs seleccionados a partir de estas bibliotecas podrían necesitar maduración de su afinidad. En particular, las bibliotecas naïve requieren de la toma de grandes volúmenes de sangre (>10L) para poder obtener una diversidad de 10^9 - 10^{11} . Similarmente, las bibliotecas sintéticas requieren de una mayor diversidad de alrededor de 10^9 - 10^{15} que las bibliotecas inmunes (Muyldermans 2021). Pero estas ofrecen la ventaja de no requerir de animales como es el caso de las bibliotecas inmunes y naïves. En general, para el diseño de una biblioteca sintética se debe seleccionar cuidadosamente la estructura marco en la cual estarán ubicados los CDRs. Esta podría corresponder a un Nb cuya estructura cristalográfica sea conocida o a un consenso de múltiples estructuras marco. Además, la región marco debe de ser fácil de producir en células (altos o moderados niveles), termoestable, soluble y capaz de tolerar diferentes CDRs sin afectar la estabilidad de la biblioteca resultante. Los CDR 1 y 2 en la mayoría de los casos se mantienen con una longitud fija, y su variabilidad se establece en base al repertorio natural del Nb usado como molde para el diseño y construcción de la biblioteca. En cambio, el CDR3 es completamente aleatorizado teniendo cuidado de no introducir residuos de Cys que pudieran comprometer su plegamiento (Valdés-Tresanco et al. 2022).

4. Selección de Nbs a partir de bibliotecas de fagos recombinantes

El paso posterior a la obtención de una biblioteca de fagos recombinantes constituye la selección de clones específicos por la molécula blanco. Dicho proceso se basa en la afinidad de los fagos recombinantes por su molécula blanco y básicamente consta de 6 etapas. Etapa 1: Preparación de una biblioteca primaria de fagos o amplificación de una biblioteca ya existente. Etapa 2: Adición de la biblioteca de fagos a una molécula blanco-inmovilizada frente a la cual se desea seleccionar ligandos específicos. La molécula blanca se puede adherir a una superficie sólida (como nitrocelulosa, matrices de columna, microplacas, perlas magnéticas o tubos de poliestireno) o alternativamente, la selección se puede realizar en solución (pero debe ir seguida de un paso de captura por afinidad para aislar los complejos blanco-fago). Etapa 3: Lavado con el fin de eliminar los fagos no unidos

o débilmente unidos a la molécula blanco. Etapa 4: Elución y colección de los fagos unidos a la molécula blanco (Ej: tripsina o cambios en el pH, agregando un ligando competitivo o agentes desnaturalizantes). 5: Amplificación de los fagos colectados mediante la infección de *E. coli* para obtener una nueva biblioteca para la siguiente ronda de selección por afinidad. La repetición de 3 a 5 veces los pasos de unión, elución y amplificación aumentan significativamente la proporción de fagos específicos por la molécula blanco. Un parámetro de selección de afinidad crucial es la astringencia (presión de selección), que refleja el grado en que las partículas de fago con alta afinidad por la molécula blanco se ven favorecidas en relación con los fagos que poseen baja afinidad por la molécula blanco. La astringencia durante las rondas de selección es crucial para coleccionar los fagos de mayor afinidad por la molécula blanco y puede intensificarse mediante un aumento gradual en el número o la duración del paso de lavado. Etapa 6: Después de la última ronda de selección, los clones de fagos se analizan en términos de especificidad utilizando una variedad de métodos para validar la especificidad de los fagos por la molécula blanco, inmunoabsorción ligado a enzimas (ELISA) utilizando anticuerpos anti-Fagos, técnicas de inmunocitoquímica, ensayos como la resonancia de plasmones superficiales (SPR). Después del procedimiento de selección, la secuenciación de ADN por el método de Sanger se usa comúnmente para analizar los clones de fagos (Figura 6). Sin embargo, en las últimas dos décadas se han desarrollado y adaptado metodologías de alto rendimiento, denominadas Secuenciaciones de Nueva Generación (NGS), para secuenciar bibliotecas de presentación de fagos a gran escala. La tecnología NGS permite la identificación de clones extremadamente raros y también proporcionan un espectro completo de sus secuencias a través del análisis de todo el grupo de fagos después de cada ronda o última ronda de selección (Jaroszewicz et al.

2022).

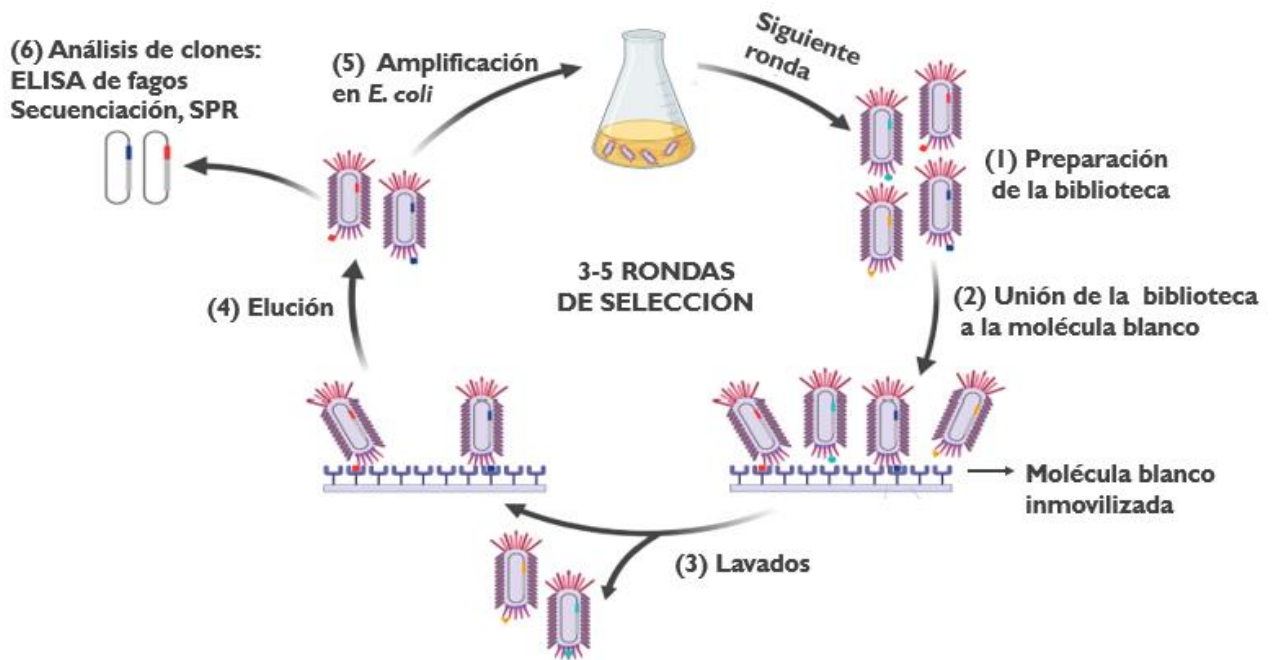


Figura 6. Selección basada en la afinidad de nano-anticuerpos específicos por la molécula blanco. La biblioteca se enfrenta a la molécula blanco previamente. La amplificación de los fagos colectados de la elución se realiza mediante la infección de *E. coli*. El ciclo completo se repite varias veces (generalmente de 3 a 5) para seleccionar los fagos que se unen a la molécula blanco con mayor especificidad. Después de rondas consecutivas de selección se analiza la funcionalidad de las moléculas de interés (Jaroszewicz et al. 2022).

En el trabajo de tesis se diseñó y construyó una biblioteca de nano-anticuerpos expresada sobre bacteriófagos. La funcionalidad de esta se verificó frente al factor de necrosis tumoral, el factor de crecimiento del endotelio vascular y el complejo glicoprotéico del virus Andes utilizando lavados astringentes en combinación con una ronda de selección. Seguidamente uno de los Nb seleccionados se diseñó y construyó como molécula quimérica con el dominio de unión a albúmina (ABD) de la proteína G de *Streptococcus spp* que debe de disminuir su tasa de eliminación renal. Esta biblioteca también se utilizó con el fin de seleccionar Nbs específicos por el factor de crecimiento epidérmico humano utilizando una estrategia de cuatro eluciones secuenciales con trietilamina, glicina-HCl, ultrasonido e infección con *E. coli* TG1. Otra de las tareas abordadas en el trabajo de tesis consistió en la modificación mediante ingeniería de proteínas del Nb 9G8 para su funcionalización a nanosensor. Para esto se procedió a reemplazar los residuos de lisinas por residuos de argininas en el cuerpo

del Nb y su incorporación en su extremo C-terminal. Esta estrategia de optimización no ha sido abordada previamente para el Nb 9G8 y podría ser aplicada para otros Nbs en sistemas de detección para diferentes enfermedades. En particular, en la detección de diferentes marcadores tumorales. Tanto la selección de los Nbs utilizando una ronda de selección, la fusión de uno de estos al ABD, la estrategia de selección de Nbs específicos por el EGF a partir de una biblioteca sintética y la optimización del Nb 9G8 para su funcionalización no ha sido previamente reportado, lo cual muestra la robustez de la biblioteca para la selección de moléculas específicas por diferentes moléculas blanco y la novedad del trabajo realizado.

HIPÓTESIS DE INVESTIGACIÓN

La biblioteca sintética de nano-anticuerpos expresada sobre bacteriófagos posibilita la obtención de moléculas específicas por diferentes antígenos. Así como la modificación mediante ingeniería de proteínas de nano-anticuerpos con estructuras cristalográficas y secuencia de aminoácidos disponibles en la literatura pueden ser optimizados para diferentes aplicaciones.

OBJETIVO GENERAL

Obtener nano-anticuerpos específicos por antígenos tumorales a partir de una biblioteca sintética de fagos recombinantes y mediante el diseño e ingeniería de proteínas de moléculas cuya estructura cristalográfica y secuencia de aminoácidos se encuentren disponibles en la literatura.

OBJETIVOS ESPECÍFICOS

1. Diseñar y producir un nano-anticuerpo específico por el factor de necrosis tumoral (TNF), obtenido de una biblioteca sintética diseñada en nuestro grupo de investigación, como proteína de fusión con el dominio de unión a albúmina de la proteína G de *Streptococcus spp.*
2. Obtener nano-anticuerpos específicos por el factor de crecimiento epidérmico (EGF) humano a partir de la biblioteca sintética de nano-anticuerpos expresada sobre bacteriófagos.
3. Rediseñar y producir un nano-anticuerpo específico por el receptor del factor de crecimiento epidérmico (EGFR), para la funcionalización de un nanosensor.

Listado de artículos incluidos en el presente trabajo de tesis:

- Contreras, M. A., Serrano-Rivero, Y., González, A., Salazar-Urbe, J., Rubio-Carrasquilla, M., Soares-Alves, M., Parra, N. C., Camacho, F., Sánchez, O., & Moreno, E. (2023). Design and Construction of a Synthetic Nanobody Library: Testing Its Potential with a Single Selection Round Strategy. *Molecules*, 28(9), 3708. <https://doi.org/10.3390/molecules28093708> (Aceptado y publicado).
- Serrano-Rivero, Y., Salazar-Urbe, J., Rubio-Carrasquilla, M., Camacho-Casanova, F., Sánchez-Ramos, O., González-Pose, A., & Moreno, E. (2023). Selecting Nanobodies Specific for the Epidermal Growth Factor from a Synthetic Nanobody Library. *Molecules* 2023, 28(10), 4043; <https://doi.org/10.3390/molecules28104043> (Aceptado y publicado).
- Cruz-Pacheco, A. F., Monsalve, Y., Serrano-Rivero, Y., Salazar-Urbe, J., Moreno, E., & Orozco, J. (2023). Engineered synthetic nanobody-based biosensors for electrochemical detection of epidermal growth factor receptor. *Chemical Engineering Journal*, 465, 142941. <https://doi.org/10.1016/j.cej.2023.142941> (Aceptado y publicado)

CAPITULO 2

Design and construction of a synthetic nanobody library: testing its potential with a single selection round strategy

Resumen

Los nano-cuerpos (Nbs) son los dominios variables de los anticuerpos de cadena pesada de los camélidos. Estas moléculas poseen un grupo de ventajas que las hace únicas y útiles en el área de la investigación, el diagnóstico, el tratamiento terapéutico de diferentes enfermedades, entre otras. Estas aplicaciones se deben en gran medida a su pequeño tamaño, su elevada solubilidad, bajos costos de producción, estabilidad en presencia de condiciones extremas de pH, temperatura y agentes caotrópicos. Sin embargo, una de las desventajas de los Nbs consiste en su rápida eliminación renal cuando se desean utilizar con fines terapéuticos. Una de las principales estrategias seguidas con el fin de dar solución a este problema, consiste en su fusión un dominio de unión a albumina. Por otro lado, las bibliotecas sintéticas de fagos recombinantes han surgido como una alternativa a la inmunización animal. En el presente trabajo se reporta el diseño, construcción y validación de una biblioteca de fagos recombinantes, lo cual se realizó en colaboración con un grupo liderado por Oliberto Sánchez Ramos (Universidad de Concepción, Chile). El diseño de esta se siguió un enfoque basado en la estructura en la que los tres lazos hipervariables se sometieron a un esquema de aleatorización, los CDRs 1 y 2, se mantuvieron a una longitud constante de 7 residuos de aminoácidos, mientras que el CDR3 se fijó a una longitud de 10 residuos de aminoácidos. La diversidad de la biblioteca resultante se validó mediante secuenciación, arrojando una diversidad de 100 000 000 que coincide con el diseño teórico. Nuestros colaboradores de la Universidad de Concepción validaron la funcionalidad de la biblioteca mediante la selección de nano-anticuerpos específicos por el factor de crecimiento endotelial vascular (VEGF), el factor de necrosis tumoral (TNF) y el complejo glicoproteico del virus del Andes. Seguidamente, a partir de un clon específico por TNF (clon B6), diseñamos un Nb fusionado al dominio de unión a albúmina humana (del inglés: ABD) de la proteína G de *Streptococcus sp*, se solicitó a la compañía GenScript. su síntesis y clonación en el vector pET22b con una etiqueta myc. Dicho vector aportaría la etiqueta de histidinas para su posterior purificación una vez producida en *Escherichia coli* BL21(DE3). La proteína de fusión Nb anti TNF-ABD se purificó mediante cromatografía de afinidad a quelatos metálicos (IMAC) con un grado de pureza superior al 90 %, se biotiniló, y se evaluó paralelamente su capacidad para reconocer al TNF y a la albúmina de suero humana mediante ELISA indirecto. El complejo Nb anti TNF-ABD-TNF o Nb anti TNF-ABD-Albúmina se detectó con estreptavidina-HRP (1:200). La afinidad de esta proteína de fusión también se midió utilizando el método de regresión lineal. Los resultados obtenidos revelaron que es posible seleccionar nano-anticuerpos específicos por diferentes antígenos a partir de la biblioteca sintética de fagos recombinantes obtenida utilizando una combinación con lavados astringentes con glicina pH 2.2 y un solo paso de elución por competencia frente al antígeno libre. El Nb anti TNF-ABD se produjo exitosamente con una afinidad $KD = (1.48 \pm 0.35) \times 10^{-7}$ M por el TNF, y el dominio al que fue fusionado conservó la capacidad para reconocer a la albúmina de suero humana, lo cual muestra las potencialidades de la estrategia utilizada para disminuir la eliminación renal de los nano-anticuerpos.

Artículo:

Contreras, M. A., Serrano-Rivero, Y., González, A., Salazar-Urbe, J., Rubio-Carrasquilla, M., Soares-Alves, M., Parra, N. C., Camacho, F., Sánchez, O., & Moreno, E. (2023). Design and Construction of a Synthetic Nanobody Library: Testing Its Potential with a Single Selection Round Strategy. *Molecules*, 28(9), 3708. <https://doi.org/10.3390/molecules28093708> (Aceptado y publicado).

CAPITULO 3

Selecting nanobodies specific for the epidermal growth factor from a synthetic nanobody library

Resumen

El factor de crecimiento epidérmico (del inglés: EGF) es uno de los principales ligandos del receptor del factor de crecimiento epidérmico (del inglés: EGFR). Este receptor es producido a altos niveles en la superficie de células tumorales, y constituye uno de los blancos más atractivos para el tratamiento del cáncer. Las células tumorales además de producir altos niveles del EGFR, también producen altos niveles de su ligando, lo cual estimula el desarrollo y agresividad del tumor. Por otra parte, el pequeño tamaño, la naturaleza globular y la ausencia de cavidades descritas para el EGF, constituyen las principales barreras para la generación de anticuerpos monoclonales o fármacos específicos por ella. Sin embargo, se ha reportado una vacuna (CimaVax-EGF) con demostrada eficacia en pacientes con cáncer de pulmón avanzado. En este caso la respuesta de anticuerpos en los individuos inmunizados es la encargada de bloquear la activación del EGFR mediante la unión de estos al EGF circulante. Por otro lado, los nano-anticuerpos (Nbs) constituyen los fragmentos variables de anticuerpos de cadena pesada aislados de los camélidos. Estos, a diferencia de los anticuerpos convencionales son de pequeño tamaño, son más estables, pueden ser producidos en bacterias y poseen la capacidad de reconocer epítomos inaccesibles para estos. Estas características, los hace particularmente atractivos como moléculas candidatas para bloquear la unión del EGF a su receptor mediante su unión al EGF circulante. En este sentido, el grupo de Guardiola en el 2018 seleccionaron y obtuvieron Nbs específicos por el EGF a partir de una biblioteca inmune de alpacas, y demostraron que estos Nbs inhibían eficientemente la activación del EGFR. Nosotros en contraste; seleccionamos Nbs específicos por el FCE a partir de una biblioteca sintética de fagos recombinantes previamente diseñada y construida por nosotros en colaboración con el grupo liderado por Oliberto Sánchez Ramos (Universidad de Concepción, Chile). Para esto primeramente se solicitó a la compañía GenScript la síntesis y clonación del gen codificante para el EGF en pET22b. La proteína EGF se expresó en *Escherichia coli* BL21(DE3), se purificó mediante cromatografía de afinidad a quelatos metálicos (IMAC) y cromatografía de intercambio (aniónico y catiónico) (CI), arrojando un porcentaje de pureza ≥ 95 %. Luego se demostró su actividad biológica en líneas celular A431, las cuales producen altos niveles del EGFR en su superficie. Una vez demostrada la actividad biológica del EGF, se llevó a cabo la selección de Nbs específicos por esta molécula siguiendo una estrategia de cuatro eluciones secuenciales de los fagos recombinantes con trietilamina, glicina, ultrasonido y finalmente mediante infección con *E. coli* TG1. Como resultado se obtuvo un total de 38 clones anti EGF, 21 se secuenciaron, y 4 de estos fueron diferentes. Los clones diferentes se subclonaron en pET22b, se expresaron en *E. coli* BL21 y se purificaron a partir de esta mediante CI seguido de IMAC con un porcentaje de pureza ≥ 95 %. Seguidamente, se biotinilaron y su capacidad para reconocer al EGF frente al cual fueron seleccionados se corroboró mediante ELISA indirecto. Así mismo la constante de disociación para los clones A8-1 y D6-4 se encontró en el orden de 10^{-7} M. Los resultados obtenidos demostraron las potencialidades nuestra biblioteca sintética para seleccionar Nbs específicos por moléculas pequeñas como el EGF, y la estrategia de elución secuencial utilizada permitió exitosamente obtener Nbs específicos por el EGF.

Artículo:

Serrano-Rivero, Y., Salazar-Urbe, J., Rubio-Carrasquilla, M., Camacho-Casanova, F., Sánchez-Ramos, O., González-Pose, A., & Moreno, E. (2023). Selecting Nanobodies Specific for the Epidermal Growth Factor from a Synthetic Nanobody Library. *Molecules*. *Molecules* 2023, 28(10), 4043; <https://doi.org/10.3390/molecules28104043> (Aceptado y publicado).

CAPITULO 4

Engineered synthetic nanobody-based biosensors for electrochemical detection of epidermal growth factor receptor.

Resumen

Los sensores convencionales, es decir, inmunoabsorbentes ligados a enzimas (ELISA) y cromatografía líquida de alta resolución (HPLC), tienen desventajas inherentes, incluida la limitada sensibilidad, instrumentación costosa, procedimientos prolongados, y etapas complicadas de marcaje. Afortunadamente, La nanotecnología ha proporcionado a los biosensores una sensibilidad sin precedentes para el diagnóstico y seguimiento del cáncer. Por otro lado, los nano-anticuerpos (Nbs) constituyen los fragmentos variables de anticuerpos de cadena pesada aislados de los camélidos. Estos, a diferencia de los anticuerpos convencionales son de pequeño tamaño, son más estables, toleran valores extremos de pH, temperatura y pueden ser producidos en bacterias. Además, estas moléculas brindan la posibilidad de ser acopladas tanto a sustancias orgánicas como inorgánicas sin comprometer su estabilidad y capacidad para reconocer a su molécula blanco. Aprovechando estas ventajas, los Nbs han sido eficientemente acoplados a biosensores, lo cual muestra sus potencialidades para el diagnóstico del cáncer. En este sentido, el receptor del factor de crecimiento epidérmico (EGFR) constituye uno de los principales blancos terapéuticos para el tratamiento del cáncer. Esta molécula se produce a elevados niveles en la superficie de algunas células tumorales, convirtiéndolo en un marcador tumoral. En las células tumorales, la unión de su ligando promueve el desarrollo y agresividad del tumor. Por otro lado, el Nb 9G8 ha sido generado específicamente para esta molécula, y ensayos in vitro han demostrado que la unión del Nb 9G8 a su dominio extracelular inhiben su activación. En nuestro estudio, el Nb 9G8 se diseñó y modificó mediante ingeniería. Dichas modificaciones consistieron en el reemplazo de los residuos de lisinas por residuos de argininas presentes en el Nb, mientras que se le introdujo una lisina al inicio de la etiqueta SV5 y dos entre el espaciador entre esta y la etiqueta de histidinas. La síntesis y clonación del gen codificante para el Nb 9G8 en el vector pET22b se solicitó a la compañía de GenScript. Una vez producido el Nb 9G8 en *Escherichia coli* BL21(DE3), se purificó mediante cromatografía de intercambio (aniónica y catiónica) y cromatografía de afinidad a quelatos metálicos con un porcentaje de pureza ≥ 95 %. Seguidamente, se acopló a biosensor a un soporte de óxido de níquel a través de la etiqueta de histidinas y a un soporte de PTAA o poli (ácido tiofeno acético) a través de las lisinas. Una vez acoplado; se corroboró su capacidad para reconocer al EGFR presente en la superficie de líneas células productoras de diferentes niveles de este receptor. Los resultados obtenidos mostraron que los cambios introducidos al Nb 9G8 no comprometieron su capacidad para reconocer al EGFR, y que el acoplamiento a biosensores podría ser una estrategia rápida y eficaz para la detección del EGFR en diferentes líneas celulares, lo cual muestra sus potencialidades para el establecimiento de un sistema de detección a partir de este Nb.

Artículo:

Cruz-Pacheco, A. F., Monsalve, Y., Serrano-Rivero, Y., Salazar-Uribe, J., Moreno, E., & Orozco, J. (2023). Engineered synthetic nanobody-based biosensors for electrochemical detection of epidermal growth factor receptor. *Chemical Engineering Journal*, 465, 142941. <https://doi.org/10.1016/j.cej.2023.142941> (Aceptado y publicado)

CAPITULO 5

DISCUSIÓN GENERAL

La biblioteca sintética de nano-anticuerpos expresados en la superficie de bacteriófagos se diseñó y construyó exitosamente con una diversidad de 100 millones de fagos. La misma fue funcional en sólo una ronda de selección frente a los antígenos factor de necrosis tumoral, factor de crecimiento vascular endotelial y el complejo glicoprotéico del virus Andes, lo cual permitió la identificación de secuencias únicas en casi la totalidad de los clones secuenciados. Adicionalmente, la proteína de fusión con el dominio de unión a albúmina de la proteína G de *Streptococcus spp* diseñada y construida a partir de uno de los nano-anticuerpo específico por el TNF α previamente obtenido a partir de una ronda de selección fue capaz de reconocer al TNF α y a la albumina de suero humana. Este resultado muestra las potencialidades de uso de esta biblioteca para la selección de moléculas con secuencias diferentes utilizando un procedimiento sencillo y rápido basado en una ronda de selección. Además, de generar moléculas cuya vida media puede ser extendida mediante el diseño y construcción de moléculas de fusión con el dominio de unión a albumina. La biblioteca también se utilizó en la selección de nano-anticuerpos específicos por el EGF. Para lo cual se siguió una estrategia de cuatro eluciones secuenciales con trietilamina, glicina- HCl, ultrasonido e infección con *E. coli* TG1 con el fin de colectar la mayor cantidad de moléculas específicas por la molécula blanco. Dicha estrategia permitió identificar 4 secuencias únicas a partir de 21 clones anti EGF secuenciados. De los cuales los clones A8-1 y D6-4 presentaron una constante de disociación en el orden de $10^{-7}M$ similar a las obtenidas por el grupo de Guardiola y colaboradores en el 2018, quienes obtuvieron nano-anticuerpos específicos por es esta molécula a partir de una biblioteca inmune de alpacas. Por otro lado, el desarrollo de métodos de detección eficientes basados en nano-anticuerpos constituye una de las estrategias enfocadas en prevenir las muertes asociadas a cáncer. En este sentido, los métodos basados en biosensores se han convertido en alternativas más económicas, rápidas y sensibles en relación con los métodos clásicos de detección (Ej: ELISA). En vistas a mostrar una de las aplicaciones de los Nbs, se decidió optimizar al Nb 9G8 para su funcionalización a nanosensor. Este Nb es específico por el EGFR, y su estructura cristalográfica y secuencia de aminoácidos se encuentran disponibles en la literatura. La optimización del nano-anticuerpo se basó en el reemplazo de los residuos de lisinas por residuos de argininas en el cuerpo del Nb y su incorporación en su extremo C-terminal. Tanto, las lisinas incorporadas como la etiqueta de histidinas posibilitaron el acople de esta molécula a nanosensores permitiendo la detección del EGFR libre y expresado en la superficie de diferentes líneas celulares.

CAPITULO 6
CONCLUSIONES

1. La biblioteca sintética de nano-anticuerpos se diseñó y construyó exitosamente con una diversidad de 10^8 de moléculas diferentes. A partir de la misma se obtuvieron moléculas específicas por el factor de necrosis tumoral, factor de crecimiento vascular endotelial y el complejo glicoprotéico del virus Andes utilizando una ronda de selección, lo cual permitió verificar la funcionalidad de la biblioteca y obtener más del 95 % de los clones con secuencias de aminoácidos diferentes.
2. La fusión de uno de estos nano-anticuerpos a un dominio de unión a albúmina permitió obtener una molécula quimérica que debe disminuir su eliminación renal. Esta estrategia podría ser aplicable para diferentes nano-anticuerpos con el fin de disminuir su eliminación renal.
3. La biblioteca sintética de nano-anticuerpos permitió la obtención de varios clones específicos por el factor de crecimiento epidérmico (EGF) mostrando las potencialidades de esta para seleccionar moléculas específicas por diferentes antígenos.
4. El rediseño del nano-anticuerpo anti-EGFR 9G8 permitió una óptima funcionalización de un biosensor, que mostró una alta capacidad de discriminar entre células con diferentes niveles de expresión del receptor del factor de crecimiento epidérmico, lo cual muestra sus potencialidades para su utilización en sistemas de diagnóstico y abre las posibilidades de aplicación a otros nano-anticuerpos específicos por otros antígenos de importancia clínica.

CAPITULO 7
RECOMENDACIONES

1. Determinar la afinidad de la proteína de fusión TNF-ABD para la albúmina de suero humana y para la albúmina de suero de ratón.
2. Determinar el tiempo de vida media de la proteína de fusión TNF-ABD en ratones.
3. Evaluar la actividad biológica de los anono-anticuerpos anti EGF en líneas celulares de A431
4. Determinar la afinidad del nano-anticuerpo 9G8 optimizado por el EGFR.

CAPITULO 7
REFERENCIAS BIBLIOGRÁFICAS

- Alfaleh, M. A., Alsaab, H. O., Mahmoud, A. B., Alkayyal, A. A., Jones, M. L., Mahler, S. M., & Hashem, A. M. (2020). Phage Display Derived Monoclonal Antibodies: From Bench to Bedside. *Frontiers in Immunology*, *11*. <https://doi.org/10.3389/fimmu.2020.01986>
- Anand, T., Virmani, N., Bera, B., Vaid, R. K., Vashisth, M., Bardajaty, P., Kumar, A., & Tripathi, B. N. (2021). Phage Display Technique as a Tool for Diagnosis and Antibody Selection for Coronaviruses. *Current Microbiology*, *78*(4), 1124-1134. <https://doi.org/10.1007/s00284-021-02398-9>
- André, A., Moutinho, I., Dias, J., & Da Silva, F. A. (2022). In vivo Phage Display: A promising selection strategy for the improvement of antibody targeting and drug delivery properties. *Frontiers in Microbiology*, *13*. <https://doi.org/10.3389/fmicb.2022.962124>
- Asaadi, Y., Jouneghani, F. F., Janani, S., & Rahbarizadeh, F. (2021). A comprehensive comparison between camelid nanobodies and single chain variable fragments. *Biomark Res.*, *9*(1). <https://doi.org/10.1186/s40364-021-00332-6>
- Bannas, P., Hambach, J., & Koch-Nolte, F. (2017). Nanobodies and Nanobody-Based Human Heavy Chain Antibodies As Antitumor Therapeutics. *Frontiers in Immunology*, *8*. <https://doi.org/10.3389/fimmu.2017.01603>
- Beirnaert, E., Desmyter, A., Spinelli, S., Lauwereys, M., Aarden, L. A., Dreier, T., Loris, R., Silence, K., Pollet, C., Cambillau, C., & De Haard, H. (2017). Bivalent Llama Single-Domain Antibody Fragments against Tumor Necrosis Factor Have Picomolar Potencies due to Intramolecular Interactions. *Frontiers in Immunology*, *8*. <https://doi.org/10.3389/fimmu.2017.00867>
- Coskun, O., Doganlar, O., & Özkan, Ö. F. (2017). Determination of IL-6, TNF- α and VEGF levels in the serums of patients with colorectal cancer. *Cellular and Molecular Biology*, *63*(5), 97-101. <https://doi.org/10.14715/cmb/2017.63.5.18>
- Evans, R. C., Lee, K. H., Wallace, P. K., Reid, M. E., Muhitch, J. B., Dozier, A., Mesa, C., Luaces, P. L., Santos-Morales, O., Groman, A., Cedeno, C., Cinquino, A., Fisher, D. S., Puzanov, I., Opyrchal, M., Fountzilias, C., Dai, T., Ernstoff, M. S., Attwood, K., . (2022). Augmenting antibody response to EGF-depleting immunotherapy: Findings from a phase I trial of CIMAvax-EGF in combination with nivolumab in advanced stage NSCLC. *Frontiers in Oncology*, *12*. <https://doi.org/10.3389/fonc.2022.958043>
- Greenberg, A. S., Avila, D., Hughes, M. S., Hughes, A. D., McKinney, E. C., & Flajnik, M. F. (1995). A new antigen receptor gene family that undergoes rearrangement and extensive somatic diversification in sharks. *Nature*, *374*(6518), 168-173. <https://doi.org/10.1038/374168a0>
- Guardiola, S., Varese, M., Sánchez-Navarro, M., Vincke, C., Teixidó, M., García, J., Muyltermans, S., & Giralt, E. (2018). Blocking EGFR Activation with Anti-EGF Nanobodies via Two Distinct Molecular Recognition Mechanisms. *Angewandte Chemie*, *57*(42), 13843-13847. <https://doi.org/10.1002/anie.201807736>
- Guardiola, S., Sánchez-Navarro, M., Rosell, R., Giralt, E., & Codony-Servat, J. (2022). Anti-EGF nanobodies enhance the antitumoral effect of osimertinib and overcome resistance in non-small cell lung cancer (NSCLC) cellular models. *Medical Oncology*, *39*(12). <https://doi.org/10.1007/s12032-022-01800-1>


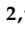

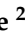

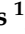
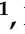



- Hamers-Casterman, C., Atarhouch, T., Muyldermans, S., Robinson, G. W., Hamers, C., Eb, S., Bendahman, N., & Hamers, R. (1993). Naturally occurring antibodies devoid of light chains. *Nature*, *363*(6428), 446-448. <https://doi.org/10.1038/363446a0>
- Hosseindokht, M., Bakherad, H., & Zare, H. (2021). Nanobodies: a tool to open new horizons in diagnosis and treatment of prostate cancer. *Cancer Cell International*, *21*(1). <https://doi.org/10.1186/s12935-021-02285-0>
- Jaroszewicz, W., Morcinek-Orłowska, J., Pierzynowska, K., Gaffke, L., & Węgrzyn, G. (2022). Phage display and other peptide display technologies. *Fems Microbiology Reviews*, *46*(2). <https://doi.org/10.1093/femsre/fuab052>
- Jin, B., Odongo, S., Radwanska, M., & Magez, S. (2023). Nanobodies: A Review of Generation, Diagnostics and Therapeutics. *International Journal of Molecular Sciences*, *24*(6), 5994. <https://doi.org/10.3390/ijms24065994>
- Kang, T. W., & Jung, S. H. (2019). Boosting therapeutic potency of antibodies by taming Fc domain functions. *Experimental and Molecular Medicine*, *51*(11), 1-9. <https://doi.org/10.1038/s12276-019-0345-9>
- Katz, H. E. (2021). Antigen sensing via nanobody-coated transistors. *Nature Biomedical Engineering*, *5*(7), 639-640. <https://doi.org/10.1038/s41551-021-00765-2>
- Ledsgaard, L., Ljungars, A., Rimbault, C., Sørensen, C. K., Tulika, T., Wade, J., Wouters, Y., McCafferty, J., & Gutiérrez, J. M. (2022). Advances in antibody phage display technology. *Drug Discovery Today*, *27*(8), 2151-2169. <https://doi.org/10.1016/j.drudis.2022.05.002>
- Li, Q., Lei, X., Zhu, J., Zhong, Y., Yang, J., Wang, J., & Tan, H. (2023b). Radiotherapy/Chemotherapy-Immunotherapy for Cancer Management: From Mechanisms to Clinical Implications. *Oxidative Medicine and Cellular Longevity*, *2023*, 1-9. <https://doi.org/10.1155/2023/7530794>
- McCafferty, J., Griffiths, A. D., Winter, G., & Chiswell, D. J. (1990). Phage antibodies: filamentous phage displaying antibody variable domains. *Nature*, *348*(6301), 552-554. <https://doi.org/10.1038/348552a0>
- Muyldermans, S. (2021). A guide to: generation and design of nanobodies. *FEBS Journal*, *288*(7), 2084-2102. <https://doi.org/10.1111/febs.15515>
- Parmley, S. F., & Smith, G. D. (1988). Antibody-selectable filamentous fd phage vectors: affinity purification of target genes. *Gene*, *73*(2), 305-318. [https://doi.org/10.1016/0378-1119\(88\)90495-7](https://doi.org/10.1016/0378-1119(88)90495-7)
- Rao, D., Mei, K., Yan, T., Wang, Y., Wu, W., Chen, Y., Wang, J., Zhang, Q., & Wu, S. (2021). Nanomechanical sensor for rapid and ultrasensitive detection of tumor markers in serum using nanobody. *Nano Research*, *15*(2), 1003-1012. <https://doi.org/10.1007/s12274-021-3588-4>
- Robinson, M. S., Weiner, L. M., & Adams, G. S. (2004). Improving monoclonal antibodies for cancer therapy. *Drug Development Research*, *61*(3), 172-187. <https://doi.org/10.1002/ddr.10345>
- Roovers, R. C., Vosjan, M. J., Laeremans, T., Khoulati, R. E., De Bruin, R. C., Ferguson, K. M., Verkley, A. J., Van Dongen, G. A., & Van Bergen En Henegouwen, P. M. (2011). A biparatopic anti-EGFR nanobody efficiently inhibits solid tumour growth. *International Journal of Cancer*, *129*(8), 2013-2024. <https://doi.org/10.1002/ijc.26145>

- Salvador, J. P., Vilaplana, L., & Marco, M. (2019). Nanobody: outstanding features for diagnostic and therapeutic applications. *Analytical and Bioanalytical Chemistry*, 411(9), 1703-1713. <https://doi.org/10.1007/s00216-019-01633-4>
- Schelch, K., Vogel, L. K., Schneller, A., Brankovic, J., Mohr, T., Mayer, R. L., Slany, A., Gerner, C., & Grusch, M. (2021). EGF Induces Migration Independent of EMT or Invasion in A549 Lung Adenocarcinoma Cells. *Frontiers in Cell and Developmental Biology*, 9. <https://doi.org/10.3389/fcell.2021.634371>
- Smith, G. D. (1985). Filamentous Fusion Phage: Novel Expression Vectors That Display Cloned Antigens on the Virion Surface. *Science*, 228(4705), 1315-1317. <https://doi.org/10.1126/science.4001944>
- Sung, H., Ferlay, J., Siegel, R. L., Laversanne, M., Soerjomataram, I., Jemal, A., & Bray, F. (2021). Global Cancer Statistics 2020: GLOBOCAN Estimates of Incidence and Mortality Worldwide for 36 Cancers in 185 Countries. *CA: A Cancer Journal for Clinicians*, 71(3), 209-249. <https://doi.org/10.3322/caac.21660>
- Upadhyay, A. (2021). Cancer: An unknown territory; rethinking before going ahead. *Genes and Diseases*, 8(5), 655-661. <https://doi.org/10.1016/j.gendis.2020.09.002>
- Valdés-Tresanco, M. E., Molina-Zapata, A., González, A., & Moreno, E. (2022). Structural Insights into the Design of Synthetic Nanobody Libraries. *Molecules*, 27(7), 2198. <https://doi.org/10.3390/molecules27072198>
- Verhaar, E. R., Woodham, A. W., & Ploegh, H. L. (2021). Nanobodies in cancer. *Seminars in Immunology*, 52, 101425. <https://doi.org/10.1016/j.smim.2020.101425>
- Yang, Y., & Cao, Y. (2022). The impact of VEGF on cancer metastasis and systemic disease. *Seminars in Cancer Biology*, 86, 251-261. <https://doi.org/10.1016/j.semcancer.2022.03.011>

ANEXOS

Article

Design and Construction of a Synthetic Nanobody Library: Testing Its Potential with a Single Selection Round Strategy

María Angélica Contreras ^{1,†}, Yulier Serrano-Rivero ^{2,†}, Alain González-Pose ², Julieta Salazar-Uribe ²,
Marcela Rubio-Carrasquilla ², Matheus Soares-Alves ¹, Natalie C. Parra ¹, Frank Camacho-Casanova ¹,
Oliberto Sánchez-Ramos ^{1,*} and Ernesto Moreno ^{2,*}

¹ Pharmacology Department, School of Biological Sciences, University of Concepcion, Concepcion 4070386, Chile; mcontrerasv@udec.cl (M.A.C.); malves@udec.cl (M.S.-A.); natparra@udec.cl (N.C.P.); fcamacho@udec.cl (F.C.-C.)

² Faculty of Basic Sciences, University of Medellin, Medellin 050026, Colombia; 0905yunierserrano@gmail.com (Y.S.-R.); agonzalezp@udemellin.edu.co (A.G.-P.); julieta.salazaru@gmail.com (J.S.-U.); marcelaru@yahoo.com (M.R.-C.)

* Correspondence: osanchez@udec.cl (O.S.-R.); emoreno@udemellin.edu.co (E.M.)

† These authors contributed equally to this work.

Abstract: Nanobodies (Nbs) are single domain antibody fragments derived from heavy-chain antibodies found in members of the Camelidae family. They have become a relevant class of biomolecules for many different applications because of several important advantages such as their small size, high solubility and stability, and low production costs. On the other hand, synthetic Nb libraries are emerging as an attractive alternative to animal immunization for the selection of antigen-specific Nbs. Here, we present the design and construction of a new synthetic nanobody library using the phage display technology, following a structure-based approach in which the three hypervariable loops were subjected to position-specific randomization schemes. The constructed library has a clonal diversity of 10^8 and an amino acid variability that matches the codon distribution set by design at each randomized position. We have explored the capabilities of the new library by selecting nanobodies specific for three antigens: vascular endothelial growth factor (VEGF), tumor necrosis factor (TNF) and the glycoprotein complex (GnGc) of Andes virus. To test the potential of the library to yield a variety of antigen-specific Nbs, we introduced a biopanning strategy consisting of a single selection round using stringent conditions. Using this approach, we obtained several binders for each of the target antigens. The constructed library represents a promising nanobody source for different applications.

Keywords: nanobody; synthetic library; phage display; CDR randomization; biopanning; tumor necrosis factor; vascular endothelial growth factor; Andes virus



Citation: Contreras, M.A.; Serrano-Rivero, Y.; González-Pose, A.; Salazar-Uribe, J.; Rubio-Carrasquilla, M.; Soares-Alves, M.; Parra, N.C.; Camacho-Casanova, F.; Sánchez-Ramos, O.; Moreno, E. Design and Construction of a Synthetic Nanobody Library: Testing Its Potential with a Single Selection Round Strategy. *Molecules* **2023**, *28*, 3708. <https://doi.org/10.3390/molecules28093708>

Academic Editor: Jahir Orozco Holguín

Received: 20 March 2023

Revised: 18 April 2023

Accepted: 18 April 2023

Published: 25 April 2023



Copyright: © 2023 by the authors. Licensee MDPI, Basel, Switzerland. This article is an open access article distributed under the terms and conditions of the Creative Commons Attribution (CC BY) license (<https://creativecommons.org/licenses/by/4.0/>).

1. Introduction

Nanobodies (Nbs) are single domain antibody fragments derived from heavy-chain antibodies, lacking the light chain present in classical immunoglobulins [1]. These special antibodies are found in members of the Camelidae family, which includes camels, dromedaries, llamas and alpacas. Nbs have several important advantages as compared to antibodies and their fragments, such as their small size (~15 kDa) and high thermal stability (median melting temperature (T_m) ~67 °C [2]). These tiny proteins have found multiple applications in many different areas, from basic research—for example, as affinity capture reagents and crystallization chaperones [3]—to the clinics, with more than 40 clinical trials reported for different Nb-based products in the ClinicalTrials.gov web repository maintained by the National Institutes of Health (<https://clinicaltrials.gov>) and two Nbs approved for clinical use: one in the United States [4] and another one in Japan [5]. Such application versatility is due in large part to the single-domain structure of Nbs, which

makes them easy to engineer and integrate into many different constructs. Notably, Nbs can achieve high affinities in spite of their smaller binding region displaying only three hypervariable loops [6].

Nbs are obtained mostly from immune libraries generated by animal immunization [6]. During the last few years, however, synthetic libraries with different designs are gaining ground as reliable Nb sources, offering important advantages in terms of cost and speed [7]. Two key features define a synthetic Nb library: framework selection and the design of the complementarity-determining regions (CDRs). A few recent works have relied on both sequence and structural data to define the CDR positions to be randomized, as well as the sets of amino acids (aa) to be introduced at those positions [8–14], including a recent report by our group [15].

A first, comprehensive work in designing and validating a synthetic Nb library was reported in 2016 by Moutel and coworkers [8] using as scaffold an in-house developed framework. They kept CDRs 1 and 2 with a constant length (7 aa each), randomizing each position in a way that resembles the natural diversity observed for these two CDRs. For CDR3, four different CDR3 lengths were introduced (9, 12, 15 and 18 aa) and all the positions were randomized, allowing all amino acids except cysteine. Two years later, McMahon and coworkers [9] reported the structure-based design and construction of a yeast-displayed library in which the amino acid variability in CDRs 1 (7 aa) and 2 (5 aa) recapitulates the natural diversity observed in a set of over 90 Nb crystal structures available at that time. CDR3 was constructed with different lengths (7, 11 and 15 aa), fully randomizing every position. That same year (2018), Zimmermann et al. [10] reported the design and construction of a ribosome-displayed library composed of three sub-libraries with different CDR3 lengths, using two different frameworks. Their design was based on a structure-based analysis of Nb crystal structures, finding that Nbs with a short CDR3 (6 aa) show a concave shape, those with an intermediate length (12 aa) show a protrusion, and those with a longer loop (16 aa) display a convex surface. CDR randomization focused on achieving an optimal balance between charged, polar, aromatic, and non-polar amino acids to keep a moderate hydrophobicity on the binding site surface. In a more recent (2021) report, Chen et al. [14] constructed a ribosome-displayed library using four CDR3 lengths (6, 9, 10 and 13 aa) and fully randomizing each CDR position. Several other synthetic nanobody libraries have been reported during the last few years following similar design strategies, as recently reviewed [7]. Library sizes range from 10^8 – 10^{10} for phage-displayed libraries, and up to 10^{12} when using ribosome display [7].

An important issue to consider in Nb library design is the length of CDR3. It has been shown that nanobodies can recognize clefts and cryptic epitopes in proteins that are less accessible to conventional antibodies [16–18]. This important capability is due to the compact prolate shape of Nbs together with their usually long CDR3 loop that folds over the framework region, generating a convex paratope. In several cases, this effect may be enhanced by a protruding loop structure. Such convex–concave Nb–antigen interface provides an interaction surface as large as that of a two-domain antibody paratope, while interacting with a smaller section of the antigen [16]. As observed by Zimmermann and coworkers [10] from the analysis of a large number of nanobody crystal structures, medium length CDR3 loops (10–12 aa) adopt an extended, protruding conformation that can be inserted into a receptor cavity.

Here, we describe the design and construction of a new synthetic nanobody library with a 10 amino acid-long CDR3, in which the three hypervariable loops were subjected to position-specific randomization schemes. The design follows a structure-based approach that seeks to maintain the high stability shown by the original framework-donor nanobody and increase the number of functional variants within the combinatorial space of mutations. As scaffold, we used the framework region from the camelid nanobody cAbBCII10 [19]. This “universal” framework has been shown to be highly stable ($T_m = 68$ °C [20]), capable of accepting many different CDRs [21], and has been used for the construction of several Nb libraries [15,22–24]. The capabilities of the new library were explored by selecting

nanobodies specific for three therapeutically relevant antigens: tumor necrosis factor (TNF), vascular endothelial growth factor (VEGF) and the glycoprotein complex (GnGc) of Andes virus. To test the potential of the library to yield a variety of antigen-specific Nbs, we introduced a biopanning strategy consisting of a single selection round using stringent conditions, aiming to wash out the weaker binders. By applying this strategy, we obtained several binders for each of the target antigens. For one of the obtained anti-TNF clones, we constructed a recombinant fusion protein that incorporates an albumin binding domain and confirmed the functionality of the two binding modules.

2. Results

2.1. Structure-Based Library Design

The design of this library follows a rationale similar to the approach described in a previous work by our group [15]. The amino acid sequence of the framework region was taken from the camelid nanobody cAbBCII10 [19]—a universal scaffold used for the construction of several Nb libraries [15,22–24]. The design of the CDRs relied on the analysis of the crystal structure of the parent cAbBCII10 nanobody (entry 3DWT in the Protein Data Bank [25]), focusing on the structural role played by individual residues in defining CDR conformation or exposing their side chains for antigen binding. The principles followed in the design of CDRs 1 and 2 are explained in detail in [15]. Briefly, the lengths of these two CDRs were kept as in the original cAbBCII10. Furthermore, the amino acids whose sidechains are packaged against framework residues in the 3D structure, as well as those found to be highly conserved in nanobody sequences, were kept as in the parent nanobody. This way we intended to preserve as much as possible the structural stability of the library mutants. CDR residues with surface-exposed side chains were subjected to tailored randomization by introducing degenerate codons in the gene sequence [26]. The allowed codons did not include cysteines and were carefully chosen to restrict the presence of hydrophobic amino acids at these solvent-exposed positions.

For this library, we chose a 10-long CDR3, which for most of the resulting nanobody variants should create a “concave” binding site topology with an “upright”-oriented and protruding CDR3 loop. This represents an important difference as compared with our previously constructed library, carrying a 14 aa-long CDR3 that bends over the framework flank, creating a “convex” topology [15]. Codons VRN and WMY were introduced at several positions to favor the presence of polar/charged amino acids, while the relatively high probability of Gly in the VRN codon may favor a conformational diversity. The highly variable VNN codon was also used. For the C-terminal part of CDR3 (the last two residues), we took into account the amino acid frequencies observed at these positions in the crystal structures of nanobodies with short CDR3 loops, which show that Ser and Tyr are the most frequent aa at the C-terminal end (position “n”), while polar residues are frequent at position “n – 1” (our own data). For the framework region, codon usage was optimized for bacterial expression. Figure 1 shows the library design at the amino acid, nucleotide and structural levels, as well as the amino acid repertoire corresponding to each of the degenerate codons employed in the design.

A total of 22 sequence positions were randomized. The theoretical variability resulting from this tailored design (calculated by multiplying the numbers of the different amino acids coded at each randomized position) is in the order of 10^{18} . This huge number, however, is in practice drastically reduced in the next two construction steps: firstly, by the actual number of genes that are synthesized and, secondly, by the number of bacteria that become transformed in the process of library construction, as explained below.

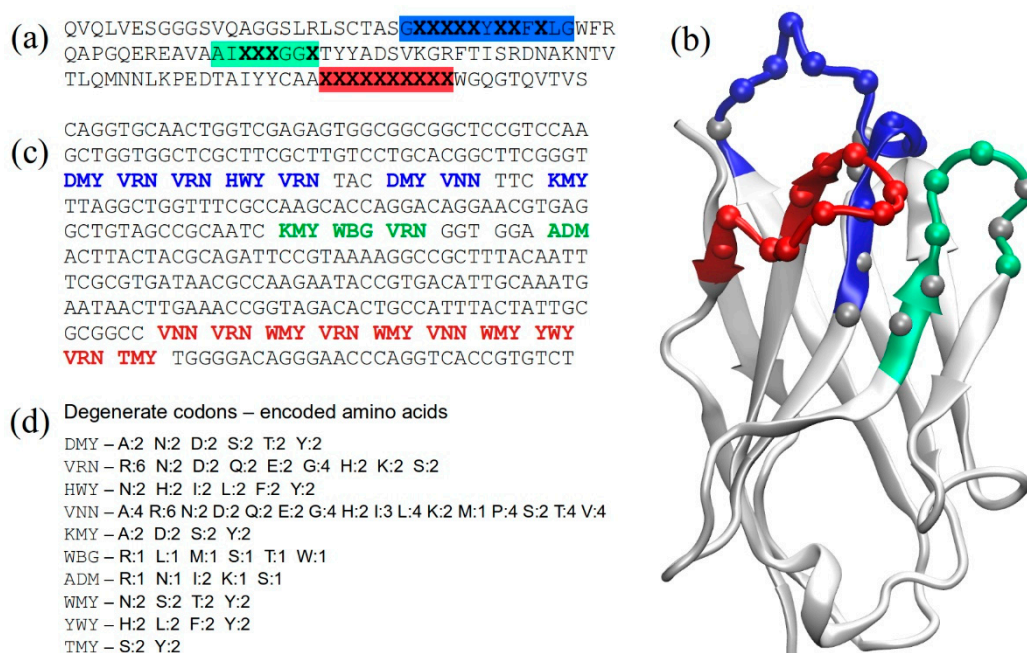


Figure 1. Library design. (a) Sequence design at the amino acid level. Positions chosen for randomization are shown as “X” in bold. The CDR sequences are highlighted in colors (blue, green and red for CDRs 1, 2 and 3, respectively), while the framework region is shown in light gray; (b) 3D model of a representative library nanobody based on the cAbBCII10 crystal structure (PDB: 3DWT). CDRs are colored following the same code as in panel (a). The colored spheres at the alpha carbons in CDRs represent the randomized positions, while gray spheres represent CDR positions that were kept fixed. (c) Nucleotide sequence with degenerate codons, colored by CDR; (d) degenerate codons used in library design and their encoded amino acids, showing also the numbers of resulting codons for each amino acid type.

2.2. Library Construction

The randomized genes were synthesized by GenScript (Piscataway, NJ, USA) and cloned as described in Methods into our ad hoc-designed pMAC phagemid vector [15] (see Figure S1). The amount of synthetic genes used for cloning (4 µg) corresponds roughly to 10^{13} individual molecules, that is, five orders of magnitude lower than the theoretical library variability. The pMAC vector employed for cloning includes a pelB leader containing a *NcoI* restriction site at its 3' end, followed by three other unique restriction sites (*EcoRI*, *BamHI* and *NotI*, in this order). To avoid unnecessary N-terminal and/or C-terminal additions to the recombinant nanobodies, we used the outer *NcoI* and *NotI* sites for cloning. Then, the phagemid codes a short linker (SGGGG), a 6xHis tag, an amber stop codon and, finally, the M13 PIII protein. The amber codon allows the expression of recombinant nanobodies directly from recombinant library plasmids using a non-amber suppressor *E. coli* strain [27], and the obtained nanobodies can then be purified by affinity chromatography using the His tag. The library of recombinant phagemids was transformed by electroporation into SS320 *E. coli* cells as described in Methods.

The library size, which corresponds to its diversity, since with a very high probability each transformed bacterium acquired a unique nanobody gene, was assessed by colony-forming units (CFU) counting. The estimated size was 1.5×10^8 . Phage titration by CFU counting yielded a phage concentration of 3.6×10^{10} cfu/µL.

2.3. Assessing Library Quality and Diversity

One hundred randomly picked library clones were sequenced to evaluate the quality of the constructed library and its diversity, as compared to the theoretical design. From these clones, 76 contained a correct nanobody sequence, 15 showed a reading frame shift,

5 clones contained nanobody sequences with no CDR3, 3 clones yielded arbitrary unknown sequences and 1 clone contained an empty phagemid vector. From these results we obtain an estimate of 76% correct clones in the library, which keeps its actual size in the same order of magnitude previously determined (10^8).

Figure 2 shows a sequence logo obtained from the alignment of the 76 correct nanobody sequences. All the randomized positions show an amino acid variability in correspondence with the gene library design, as illustrated in the figure for three CDR positions. Furthermore, and in spite of the relatively limited number of sequenced clones, even the highly variable positions (e.g., for codons VNN and VRN) show a large diversity, matching the expected repertoire of amino acids. For example, between 14 and 16 different residues, out of 16 possible amino acids, are found at the three positions (34, 102 and 107) coded with the VNN triplet.

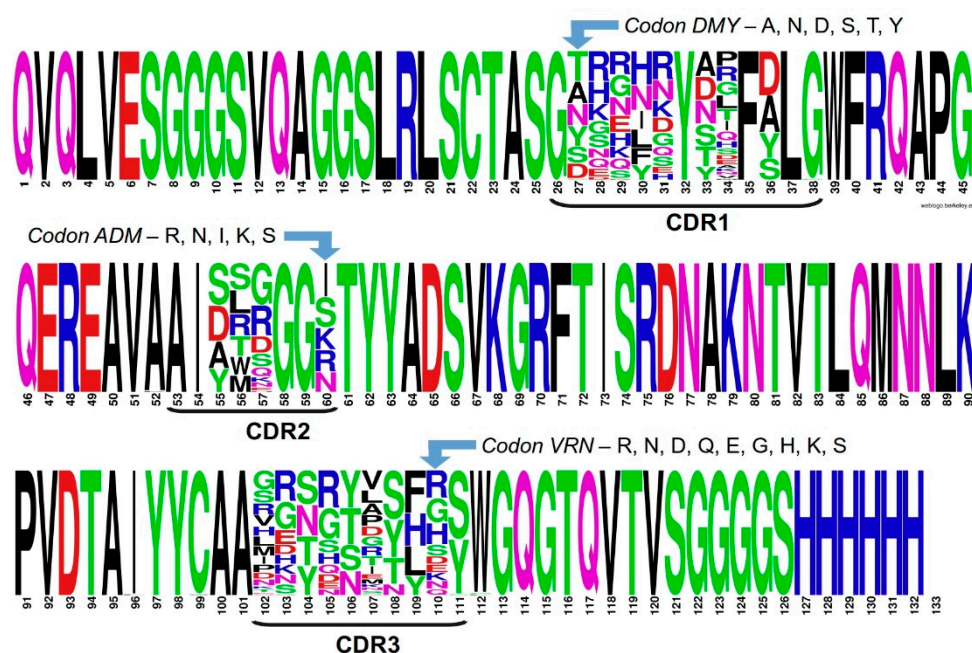


Figure 2. Amino acid distribution per sequence position for the ensemble of 76 correct nanobody clones, shown as a sequence logo. The framework and fixed CDR positions display their conserved amino acid as a single big letter. The amino acid variability found at each randomized position is represented as a stack of letters, each of them with a size that is proportional to its frequency in the multiple alignment. The close match between the theoretical design and the actual experimental diversity is illustrated for three CDR positions (one for each CDR).

2.4. Library Screening

The capability of the library to yield specific binders was tested for three protein antigens: tumor necrosis factor (TNF), vascular endothelial growth factor (VEGF) and the glycoprotein complex (GnGc) of Andes virus. Both TNF and VEGF, as well as their receptors, are relevant therapeutic targets in cancer and autoimmune diseases, and several monoclonal antibodies targeting these molecules have been used in the clinics for several years [28–30]. Furthermore, several nanobodies specific for VEGF have been reported [31], and very recently (Sept/2022) a trivalent anti-TNF nanobody called ozoralizumab was approved in Japan for the treatment of rheumatoid arthritis [5]. Regarding the viral GnGc antigen, to our knowledge no nanobodies specific for this molecule have been yet reported.

2.4.1. Selection of Antigen-Specific Binders in a Single Round

Here we decided to implement a screening procedure based on a single selection round using stringent conditions, aiming at a quick enrichment of the selected phages with the strongest binders in only one selection step, and also as a way of probing the

capabilities of the newly designed library. Before elution, we applied four serial washes with glycine-HCl pH 2.2, a buffer commonly used for elution in phage display biopannings. No phage collection was carried out in this step since the aim of these stringent washes was to remove a large part of the phages that would bind with weaker affinity. In a subsequent, final step, the wells were incubated with a relatively high concentration of the antigen (10 µg/well, 10-fold the amount used for coating) to recover the bound recombinant phages by binding competition against the coated and soluble antigens.

For each antigen, the whole eluted phage sample was used to infect *E. coli* TG1 bacteria, which were seeded on 2xYT/ampicillin plates. The numbers of obtained colonies were 97, 1404 and 1656 for TNF, VEGF and GnGc, respectively. We then proceeded to select individual clones to produce recombinant phages and analyze their ability to bind to their corresponding antigens. For TNF, we tested all the 97 obtained clones, whereas for both VEGF and GnGc we randomly picked 180 clones. Figure 3 shows the results from the binding experiments. Notably, we obtained a high number of positive clones in only one selection round, for the three antigens, several of them showing high OD signals.

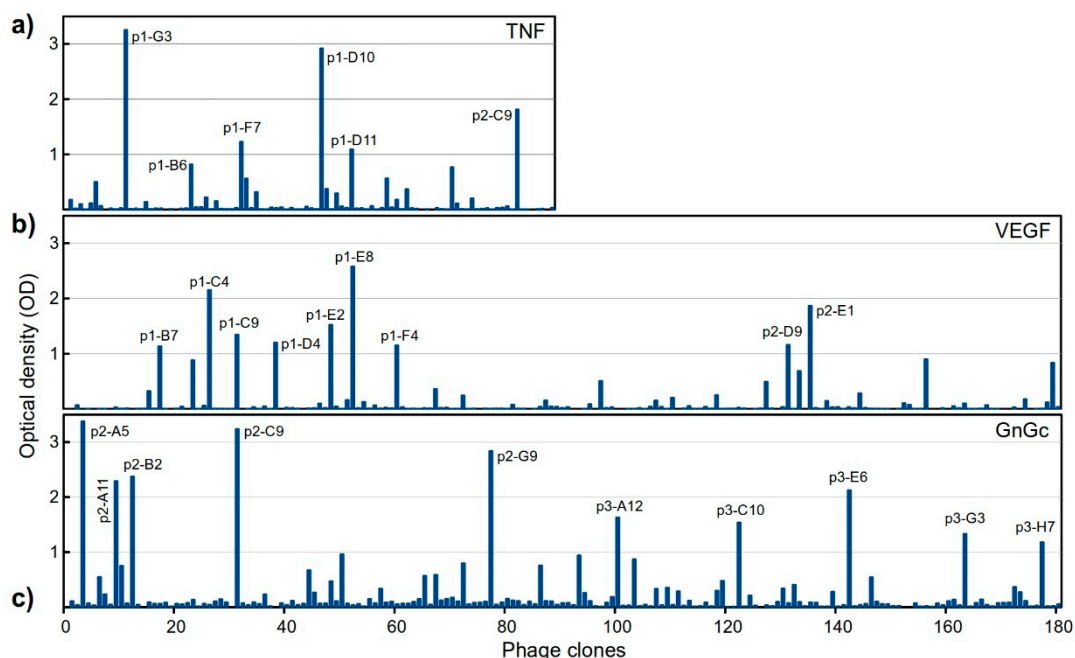


Figure 3. Binding of individual phage clones to their antigens, as measured by ELISA, (a) TNF, (b) VEGF, (c) GnGc. The optical density (OD) values for each clone corresponds to antigen binding with subtracted binding to BSA. For a few clones showing a negative value for this difference, the OD was set to 0 in the graph. The X-axis scale (clone numbers) is common for the three panels. Clones with high binding signal (OD > 1) are labeled, matching their IDs in Figure 4.

2.4.2. Sequencing of Selected Groups of Phage Clones

We decided to sequence all the clones showing OD values above 0.15, for the three antigens, resulting in 28, 24 and 44 clones for TNF, VEGF and GnGc, respectively. In practice, we obtained the sequences for 22, 22 and 34 clones, respectively, since a few of the samples could not be correctly sequenced. Nonetheless, we obtained the sequences for practically all of the best binders shown in Figure 3, with the exception of the anti-TNF clone p1-F7 and the anti-GnGc clone p2-C9.

As shown in Figure 4, for the three antigens we obtained sets of unique different binders (with only one identical pair of anti-TNF clones) as a consequence of performing a single selection round, without further binding clone enrichment. In the three cases, no common sequence motifs are evident from the alignment, for any of the CDRs, which sug-

gests that these clones have different binding modes, likely recognizing different epitopes on the antigen surface.

	Clone	CDR1	CDR2	CDR3
(a) TNF	p1-D11 *	G T N R F S Y T R F A L G	A I A M Q G G R	I Q S S N L T H R Y
	p1-E10
	p2-B5	. Y K . N D . S P W G R Y D Y A Y . D S
	p2-B7	. A . K N R . A L S R R T . T A N Y H S
	p1-D9 H Q N R . D T R G N R T Q . V N . Q S
	p1-B2 N H D L R . A S Y W R R G Y G . R Y L H .
	p2-E2 G . L R . A V . D Y . R V R . G . A S F N .
	p2-B6 A R N N G . N P Y W H T R . K S R S Y G .
	p1-C8 R . L Q . S S R P T H T T N F G .
	p2-B2 E D Y Q . S Y . H P E T N Y . S F G .
	p1-B3 Y R . N K . N T . Y L G P E T N Y . S F G .
	p2-C3 R E N N . D G . D S T R H G Y R R . Y G .
	p1-G6 D Q . I . S S S E G R Y H . V N
	p1-D10 * N Q . R . Y G S S S L R Y N S I
	p1-G3 * A R K . R . Y A S . N T R T R . R S F G .
	p1-B6 * Y G N Y R . N T . S S S S G . K T A S . . S
	p1-E6 D K K Y K . S S L D V R T R S V S L E S
p1-F8 N R E H H . Y A . Y Y S H N R Y N S V S . S	
p2-D4 N O K . R . Y V . Y Y R K L R . . Y N S . K .	
p1-G2 Y Q . H K . N H . Y S R K Q R T E S D N Y . S	
p2-C9 * Y R . N G . . V . D S K N K Y R . P S F K .	
p1-G7 S R N N H . Y T S W G L G Y G V V S Y G .	
(b) VEGF	p1-C1	G A R R H R Y T M F S L G	A I S L R G G K	R G S S Y T T F R S
	p1-E2	. N . K Y L W G R T R . G N . S .
	p1-F4 *	. T . D S R A L . Y . S . S H K .
	p1-E7 D G K N N . T A L . N G S S N H . Y
	p1-B5 D H G N P R D P H . R T A N . H .
	p1-C4 * Y G K L G . Y N R N D . G S R Y H H Y
	p2-D9 * Y G K L G . Y N R N D . G S R Y H H Y
	p1-H7 N N H L S . Y V G L R . R S S N H Q Y
	p2-A9 S G . L A A Y S G K Y G S I N Y . Y
	p2-E1 * S K G D S R Y G S . S . G .
	p2-F10 S G G L G . A R . Y A M K N R . M . H N .
	p1-G4 G N Y K . S R . A S G V R . H S P . Y G .
	p2-H9 Y G Q I K . S A . A S T R . H Y Y K .
	p2-D11 G I N K . Y R L R . R S P Y . N Y
	p1-C9 * T N . N A I . Y A . H R N G . V K Y
	p1-B7 * D G H L K . Y K . A G I Q N R S V N
	p1-E8 * S . G N A R . D H Q R T R S V S H K Y
p2-D5 S . K L G R . Y A . D G . Y A Y L . Y	
p2-C8 N K K . N Y R . Y A S D S R Y . S I Y H G .	
p2-E10 S H K N K . N R . Y A W E V R Y R T G Y L E Y	
p2-B10 D I N . A R A S N G R N H . S S . S .	
p1-D4 * T S . Y N . A I C T Q L R Y R . L Y . K Y	
(c) GnGc	p2-A5 *	G Y R R H N Y Y G F A L G	A I S M R G G N	P R S G S D Y F G Y
	p3-D6	. N . G L E L V G T N Y R T
	p2-F11 D R . N Q . D K S Y V . L
	p3-C7 S N . N S . N S . D W S N N L T L R S
	p3-D8 S G H N R . S H . D T S T . T R N P N L R S
	p2-B2 * S L R . A D G K Y R Y T S . R S
	p3-B7 D H I H V L . N . N . S . R S
	p2-A11 * R . N M . D D W G H S . L S . R S
	p3-C10 * N N H . T K . S D R G H H T S S Y R S
	p3-C12 D E . L R . N H . Y Y W Q S T K Y Q S . E S
	p2-A12 T G S F R . S T . Y A L R G . R Y T N L . S
	p2-E6 T . K F R R . Y T N R G . R . P T L H S
	p2-G2 S . S I Q . S A S Q N T H Y R . H H .
	p2-H6 S . G R . S A T S R H Y S . H H .
	p3-A11 T N Q I R . T R . D R T D Y K . G T Y S .
	p2-G12 D Q G Y G . S L T G Q G . N Y G . L R S
	p3-H7 * A G H Y G . N K . Y D T E Q R Y R S Y .
p2-A9 D S N Y R P . Y Y L G Y H I S . Q .	
p2-F9 N Q D R D R V G . K T N S Y R S	
p3-B3 T K . I G R . D A L Q S . R N I T L E S	
p3-G3 * T K G . G . T P A R Y R H R S	
p3-A5 N . G N R . S A A S G K N N Y R N . R .	
p3-E10 A N H L R . T K Y T S G G Y H N P . Y . S	
p2-D12 S G H N K . S R . S W G R G Y R . G S . K S	
p3-H2 S N S R . D K E N N G S	
p2-D2 S F D A R S N R . G S . N .	
p2-E1 D Y G . A T A W D R S N R . H R .	
p3-E3 N G N K . T P A . G G G Y R . I S . Q .	
p2-G4 S G Q . R . A Y L H R . N K Y R T L K S	
p3-H3 S D . Y H . D K . D D W L Q Y . Y A T L R .	
p2-G9 * H H I D R . Y Y R G K . Y Q T T N . R S	
p3-B9 T G Q Y R . T R . S R G V N Y . T Q S Y D S	
p3-E6 * S . G N S R S	
p3-A12 * H I R . S R . D A S I	
			 G G Y . Y G S . D S

Figure 4. Alignments of CDR sequences obtained for groups of clones selected from the biopannings against the following: (a) TNF (22 clones); (b) VEGF (22 clones) and (c) GnGc (34 clones). Dots indicate the presence of the same amino acid as in the first sequence in the alignment. Red stars denote a high binding signal by ELISA (OD > 1), matching their labels in Figure 3.

2.5. Design and Expression of a Recombinant Fusion Protein with an Anti-TNF Nb

A known drawback for the therapeutic use of nanobodies is their short half-life in serum due their small size. Several strategies can be followed to prolong the Nb half-life, one of them being the genetic fusion or chemical conjugation to a molecule capable of binding to serum albumin [32]. Here, we decided to construct a fusion protein (NbB6-ABD) composed of an anti-TNF Nb and an albumin binding domain (ABD) from the *Streptococcus* sp. G protein, which shows high specificity and affinity for human serum albumin (HSA), with a dissociation constant (KD) in the nanomolar order [33,34] (Figure 5a). The anti-TNF clone p1-B6 was selected for this purpose. Although this clone is not among the strongest binders (OD = 0.9), it was chosen because of its very low background signal to BSA and skim milk (data not shown). In addition to the 46 aa constituting the ABD domain, six additional aa (AVDANS) of the protein were included at the N-terminal end since they are packed with the ABD domain in its crystal structure. A c-Myc tag was included between the nanobody and ABD, separated by short linkers. An *EcoRI* restriction site inserted right after the Nb sequence allows switching the Nb binder to target any antigen of interest. The gene coding for the fusion protein was cloned into the pET22b plasmid, which adds a C-terminal His tag, as shown in Figure 5a.

For binding assays, the fusion protein was biotinylated as described in Methods. Figure 5b shows the ELISA results for the binding to TNF and HSA. The ABD domain kept its binding capability to HSA (Figure 5b, right panel). For the binding of the nanobody domain to TNF, a titration ELISA [35] was performed in order to estimate the dissociation constant, obtaining a $KD = (1.48 \pm 0.35) \times 10^{-7}$ M. This is quite an encouraging result, taking into account that this was an initial test for this fusion protein design, using one of

the obtained anti-TNF clones, which was not among the strongest binders in the phage-based ELISAs.

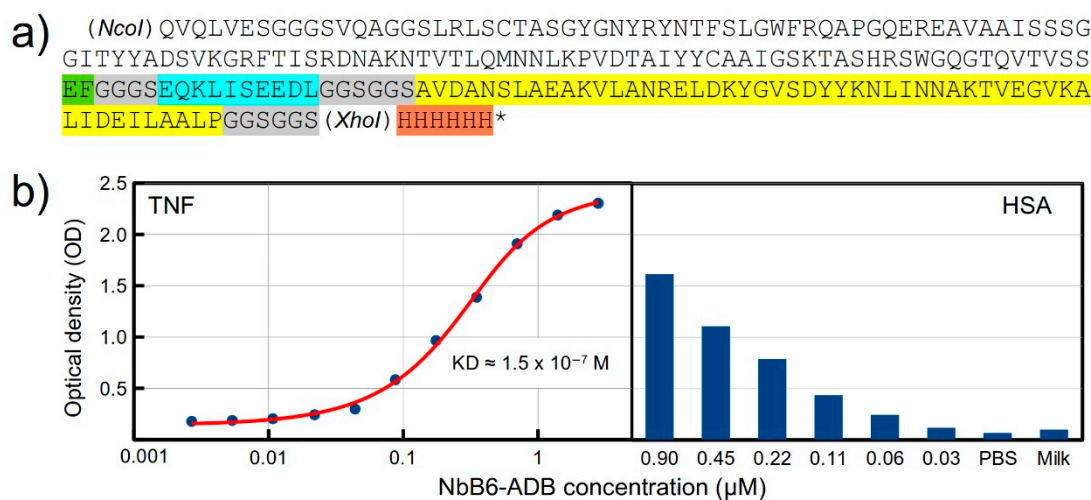


Figure 5. (a) Amino acid (aa) sequence of the NbB6-ABD fusion protein. Legend: White background—anti-TNF nanobody clone p1-B6; green—the two aa coded by an inserted *EcoRI* restriction site; gray—spacers (linkers); cyan—c-Myc tag; yellow—albumin binding domain; orange—6xHis tag. The *NcoI* and *XhoI* restriction sites were used for cloning into the pET22b vector, which adds the C-terminal histidine tag. (b) Binding of NbB6-ABD to TNF (left chart) and to HSA (right chart) as measured by ELISA. (Left chart): Negative control (not shown)—BSA coating: OD = 0.11. The red fitting curve for TNF binding was used for K_D estimation. (Right chart): The Y-axis scale is the same as for the left chart; negative controls—PBS (instead of NbB6-ABD) and skim milk. For both antigens, we used the maximum tested NbB6-ABD concentration for the BSA/milk negative control. Experiments were performed in duplicates.

3. Discussion

We have constructed a new synthetic nanobody library following a tailored, structure-based design. Synthetic libraries are nonspecific and therefore seek to recreate a large clonal variability to increase the probability of obtaining good binders. For this reason, synthetic libraries must be large, at least 10^8 in size, preferably larger [6,7]. Most of the reported synthetic, phage-displayed nanobody libraries have sizes in the order of 10^9 , as recently reviewed [7]. The clonal diversity of our library is in the order of 10^8 , that is, at the lower limit of the accepted range. This level of diversity, however, proved to be enough to produce a high rate of specific clones against three different, relevant therapeutic targets. In this regard, we believe that the library's CDR design creates a high-quality repertoire of binding paratopes that may, to a certain extent, counteract the relatively smaller size of the library.

As scaffold for the library, we chose a well-proven framework—from the cAbBCII10 Nb—that has been shown to support CDR loops of different lengths [21]. This is an important base point in the design to ensure that most of the inserted CDR sequences yield functional nanobodies. As a basis for the CDR design, firstly we carefully analyzed the structural role played by each aa in CDRs 1 and 2 in the parental cAbBCII10 Nb. A first rule applied here was to keep fixed every aa whose sidechain is buried in the structure, as well as those aa found to be highly or relatively conserved in nanobody sequences, or thought to be important in holding CDR conformation in cAbBCII10. This approach differs from the all-position randomization strategies followed in many reported libraries [7], e.g., in [8,11,13,14].

A few recent reports, however, incorporate structure-based strategies to select the positions in CDRs 1 and 2 to be randomized. For example, McMahan and coworkers [9] selected four positions in CDR1 and one in CDR2, based on their large variability in a set of

analyzed Nb sequences. All these positions were fully randomized (avoiding Cys and Met). Zimmerman et al. [10] selected five residues in CDR1 and also in CDR2 for randomization, using three different mixtures of nucleotide triplets. The most used mixture coded for 18 aa (excluding Cys and Pro). CDR residues contributing to the Nb hydrophobic core were kept fixed, as in our library. By difference with these designs, here we used 10 different degenerate codons instead of triplets, tailoring the use of these codons at a position level. The amino acid repertoires resulting from these codons vary from 2 to 16 aa, with most of the sets having only 4 or 6 aa. Even so, the theoretical diversity is huge, in the order of 10^{18} .

Although the cAbBCII10 Nb has been shown to accept CDR1 loops of different lengths [21], in this library we kept the full length of the parental CDR1, randomizing 8 out of its 13 positions. In contrast, only 4 positions were randomized in CDR2. Therefore, most of the variability in the library comes from CDR1 and CDR3, which in a modeled structure (Figure 1) form a shallow concave surface between them. We speculate that this shape would be likely fitting for binding to relatively small globular proteins and slightly concave surface patches on proteins in general. Furthermore, the protruding CDR3 might bind to protein cavities.

The new library was tested against three protein antigens of therapeutic relevance: TNF, VEGF and GnGc (a viral antigen). To evaluate its capabilities, we decided to apply a selection strategy consisting in applying stringent washing conditions, followed by competitive elution, aiming to retrieve mostly strong binders in a single screening step. For stringent washing (repeated four times) we used glycine-HCl pH 2.2—a commonly used elution buffer in phage display biopannings [36]. This way, many phages that otherwise would be collected for a second biopanning round were discarded. Subsequently, the wells were incubated with a relatively high concentration of antigen (100 $\mu\text{g}/\text{mL}$) to recover bound recombinant phages by binding competition against the coated antigens. Such competitive phage elution is also a common procedure used to collect phages with high affinity for their target molecule [6,37].

Stringent washes are very often used before the elution step, but in general, such stringency consists in increasing the washing time, number of washes and/or Tween 20 concentration [6,37–39], as well as decreasing the antigen concentration in each subsequent selection round [6,40,41]. There are few reports, however, in which a glycine-HCl solution was used as a wash buffer. Lunder et al. [42], for example, implemented several protocols that included four glycine-HCl (0.2 M, pH 2.2) washings and then eluted the phages that remained bound to the antigen by direct infection with *E. coli*, ultrasound or competition. On the other hand, although using several selection-amplification rounds enriches the library in clones specific for the target molecule, it may also have a negative effect by reducing the diversity of the finally obtained clones [37].

Here, applying stringent washes and without further enrichment rounds, we were able to obtain a significant number of clones with high, specific binding signals by ELISA, with a positivity of 13–29%. For TNF, we obtained 97 clones, all of which were tested individually. For VEGF and GnGc the number of clones was much higher—around 1400 and 1600, respectively—of which we tested only 180 in each case. Notably, all the positive clones, for the three antigens, corresponded to unique sequences (with the only exception of a pair of clones for TNF), with no evident common motifs. Since for VEGF and GnGc we tested only about 12% of the total number of clones, we would expect about a 10-fold higher number of positive clones for these two antigens, most of them most likely with unique sequences.

Finally, we tested the functionality of one of the obtained anti-TNF nanobodies, in a format of a recombinant fusion protein that incorporates an albumin binding domain—a strategy used to prolong the half-life in serum of therapeutic Nbs [32]. A similar solution was employed in the design of the anti-TNF nanobody trimer ozoralizumab (approved for clinical use in Japan), which consists of two anti-human TNF Nbs and an anti-human serum albumin Nb [5]. The estimated dissociation constant for TNF was in the order of 10^7 M, which is an encouraging result considering that the anti-TNF clone chosen for

this construction showed a moderate OD signal in the phage ELISA. This design can be also extended to multimeric Nb constructions, using Nbs targeting the same antigen in a non-competitive manner to synergistically increase the affinity, as with ozoralizumab.

For future development of this library, we plan to include other CDR3 lengths to enrich its conformational variability. We are also exploring other selection strategies involving different stringent conditions and numbers of selection rounds.

4. Materials and Methods

4.1. *In Silico* Design and Analyses

Several bioinformatics tools were used along the design process and sequence analyses. The program VMD [43] was employed for visualization and analyses of nanobody structures. The Degenerate Codon Designer online tool (<https://www.novoprolabs.com/tools/degenerate-codon-designer>, NovoPro, Shanghai, China, last accessed on 20 January 2023) was used for codon analyses. The CLC Genomics Workbench v.21 (QIAGEN Aarhus, Aarhus, Denmark) was employed for sequence analyses.

4.2. Library Construction

The nanobody gene library was synthesized by GenScript (NJ, USA) following the theoretical design. The genes were flanked with the restriction sites *NotI* and *NcoI* for cloning in the pMAC phagemid vector [15]. After cloning (using 4 µg of both the gene library and pMAC), the recombinant plasmids were transformed by electroporation (voltage 2.5 kV, resistance 200 Ω, capacitance 25 µF) in the *E. coli* strain SS320, previously transduced with the helper phage M13KO7 (New England Biolabs, Ipswich, MA, USA).

Transformed bacteria were recovered in SOC medium for (i) determining library diversity by seeding serial dilutions in plates containing solid 2xYT medium supplemented with 100 µg/mL ampicillin, and (ii) amplifying the recombinant phage library in 2xYT medium containing 100 µg/mL ampicillin, 50 µg/mL kanamycin, 1 mM isopropyl β-D-1-thiogalactopyranoside (IPTG) by incubating 20 h at 30 °C and 185 rpm. Phage library was precipitated from the supernatant with 0.2 volumes of a solution containing PEG/NaCl (20% polyethylene glycol 8000 and 2.5 M NaCl) at 4 °C for two hours, and aliquoted in 10% glycerol until further use [44,45].

4.3. Library Screening

Antigens. Recombinant TNF [46], VEGF [47] and GnGc [48] antigens were produced and purified in-house, at the Pharmacology Department, University of Concepcion, as previously described.

Polystyrene high-binding microtiter plates (Costar) were coated with 100 µL of the antigen (TNF, VEGF or GnGc) at 10 µg/mL (24 wells per antigen for TNF and GnGc, 12 wells for VEGF), and incubated overnight at 4 °C. After two washes with phosphate buffered saline (PBS), wells were blocked with 5% skim milk (Sigma-Aldrich, Burlington, MA, USA) in PBS (300 µL/well) overnight at 4 °C. Wells were washed twice with PBS plus 0.05% Tween 20 and incubated at room temperature (RT) for two hours with 100 µL of library phages (in a quantity 500 times bigger than the library diversity) diluted in 5% skim milk. PBS plus 0.1% Tween 20 was used to perform twenty washes (250 µL/well) of five minutes each. Four additional 5 min washes were made with glycine-HCl (0.2 M, pH 2.2), and subsequently neutralized with PBS pH 7.2 for five minutes. Afterwards, recombinant phages were obtained by competitive elution with 100 µg/mL (100 µL/well) of the antigen of interest (TNF, VEGF or GnGc) for one hour at RT and 300 rpm. The *E. coli* strain TG1 in exponential phase of growing was transduced with the elution and incubated at 37 °C overnight in 2xYT plates supplemented with 100 µg/mL ampicillin and 2% glucose. Deep well plates were used to amplify individual clones in a final volume of 0.5 mL. Individual phage-infected colonies were picked and used to produce phagemid particles in a 96-well plate scale to test their target recognition [49].

4.4. Binding Assays to Detect Positive Phage Clones

Polystyrene high-binding microtiter plates (Costar) were coated with 100 μ L of the antigens (TNF, VEGF or GnGc) at 5 μ g/mL and incubated overnight at 4 $^{\circ}$ C. After washing with PBS, wells were blocked with 3% BSA in PBS (250 μ L/well) for two hours at 37 $^{\circ}$ C. Supernatants of individual clones, previously amplified, were added to the plate (50 μ L of supernatant plus 50 μ L BSA 3%) for one hour at 37 $^{\circ}$ C. After three washes with PBS-0.1% Tween 20, the anti-M13 antibody conjugated to horseradish peroxidase (GE Healthcare, Chicago, IL, USA) diluted 1:5000 in BSA 1% plus PBS-0.05% Tween 20 was added for one hour at 37 $^{\circ}$ C. Plates were washed with PBS 0.1% Tween 20 and the reaction was developed with a solution of o-phenylenediamine dihydrochloride (Sigma-Aldrich) and hydrogen peroxide as substrate, and stopped with 2.5 M sulfuric acid. The absorbance was measured in a Synergy/HTX multi-mode reader (BioTek Instruments, Winooski, VT, USA) at 492 nm.

4.5. Sanger Sequencing

Recombinant phagemids from selected TG1 clones were purified using the GenElute Plasmid Miniprep Kit (Sigma-Aldrich) and sequenced by Macrogen (Seoul, Korea) using the standard M13R primer. Sequences were analyzed using the CLC Genomics Workbench v. 21 (QIAGEN Aarhus, Aarhus, Denmark).

4.6. Production of Recombinant Fusion Protein

The sequence of the ABD from the *Streptococcus* sp. G protein was taken from the PDB structure 1GJS [34]. The gene coding the chimeric protein Nb-TNFB6-ABD was synthesized and cloned into the plasmid pET22b, using the *Nco*I and *Xho*I restriction sites, by GenScript (USA). The production of NbB6-ABD was carried out in two 1L Erlenmeyers containing 500 mL each of SMM9 medium, 0.05% yeast extract (Oxoid, Basingstoke, UK), and 100 μ g/mL ampicillin. After inducing the gene expression with 25 μ M IPTG, the culture was stirred at 100–120 rpm and incubated at 28 $^{\circ}$ C for 18 h in a shaker-incubator (ES-20/80, BOECO, Hamburg, Germany). Next, the culture was centrifuged at 10,000 \times g for 15 min at 4 $^{\circ}$ C, the pellet was re-suspended in half-diluted SMM9, and then subjected to five freeze/thaw rounds.

Soluble NbB6-ABD was obtained in the supernatant after centrifugation at 10,000 \times g for 15 min at 4 $^{\circ}$ C. The presence of the soluble fusion protein was verified by sodium dodecyl sulphate-polyacrylamide gel electrophoresis (SDS-PAGE) and Western blot.

For SDS-PAGE, protein samples were diluted in a buffer with beta-mercaptoethanol and run in 15% polyacrylamide and 3% stacking gels. Western blot assay was performed using a 0.2 μ m PVDF transfer membrane (Thermo Fisher Scientific, Waltham, MA, USA) in a semi-dry transfer system Trans-Blot[®] Turbo[™] (Bio-Rad, USA) at 0.3 A and 25 V for 30 min. After blocking with 5% skim milk in PBS, the membrane was incubated with the HRP anti-6xHis tag rabbit polyclonal antibody (ab1187, Abcam, Boston, MA, USA) diluted 1:5000 in the blocking buffer. The reaction was visualized using a DAB substrate kit (Thermo Fisher Scientific, USA).

Protein purification was performed by immobilized metal affinity chromatography (IMAC) by adding 5 mM imidazole to the equilibrium buffer (150 mM NaCl, 10 mM Na₂HPO₄, pH 7.7) and the initial sample diluted in the same EB. Wash and elution was done in EB by adding 25 mM and 250 mM imidazole, respectively. All fractions were monitored using the purification system BioLogic LP (BioRad, Hercules, CA, USA). Imidazole from the elution sample was removed by diafiltering against PBS (Sigma-Aldrich, Burlington, MA, USA) in 5 kDa Spin-X[®] UF concentrators (Corning, Corning, NY, USA). Samples were analyzed by SDS-PAGE and Western blot as described above. NbB6-ABD purity was estimated using the analytical tool of the iBright 750 Imaging System (Thermo Fisher Scientific, USA), and its concentration was determined using a Pierce BCA Protein Assay Kit (Thermo Fisher Scientific, USA).

For biotinylation of NbB6-ABD, 50 μ L of Na₂CO₃/NaHCO₃ buffer (500 mM, pH 9.6) were mixed with 900 μ L of the fusion protein (1.1 mg/mL). Next, 50 μ L of biotin (H1759,

Sigma-Aldrich, USA) prepared at 10 mg/mL in dimethyl sulfoxide (Merck, Rahway, NJ, USA) was slowly added at a rate of 10 μ L/min and mixed. The amounts used correspond to an 80:1 biotin/NbB6-ABD molar ratio. The reaction was incubated for 6 h at room temperature (RT) under stirring. Free biotin was removed by dialysis (88244, Thermo Fisher Scientific, Waltham, MA, USA) against 4 L of 1X PBS overnight at RT.

4.7. Binding Assay for the Fusion Protein

Binding of biotinylated NbB6-ABD to TNF and HSA was determined by ELISA, using streptavidin-HRP (DY998, Biotechne R&D Systems, USA) for detection. Plate wells (2592, Corning, USA) were coated with 1 μ g of TNF or HSA in carbonate buffer pH 9.6 overnight at 4 °C, then washed three times with 0.3 mL of PBS 1X 0.1% Tween 20 (PBST) and blocked with 3% BSA or 5% milk in 1X PBS for 1 h at room temperature. Wells were then washed three times with 0.3 mL PBST and incubated for 1 h at RT with 100 μ L of different concentrations of the biotinylated protein. Wells were again washed three times with 0.3 mL PBST and incubated for 1 h at RT with 100 μ L streptavidin-HRP (1:200, DY998, Biotechne R&D Systems, USA). They were then washed four times with 0.3 mL PBST, revealed with 100 μ L of 3,3',5,5'-Tetramethylbenzidine (TMB) (DY999, Biotechne R&D Systems, USA), and stopped with 50 μ L of 2N H₂SO₄. Binding signals were read at 450 nm in a plate reader (BOECO, Germany). KD estimation was carried out followed the method and fitting function described in [35]. Linear regression analysis using this function was performed using the MyCurveFit web server (<https://mycurvefit.com/>, last accessed on 20 March 2023).

Supplementary Materials: The following supporting information can be downloaded at: <https://www.mdpi.com/article/10.3390/molecules28093708/s1>, Figure S1: Map of the designed pMAC phagemid vector.

Author Contributions: Conceptualization, O.S.-R. and E.M.; methodology, M.A.C., A.G.-P., Y.S.-R., M.R.-C., F.C.-C., O.S.-R. and E.M.; investigation, M.A.C., Y.S.-R., A.G.-P., J.S.-U., M.R.-C., M.S.-A., N.C.P., F.C.-C., O.S.-R. and E.M.; writing—original draft preparation, M.A.C., A.G.-P., Y.S.-R., J.S.-U., M.S.-A. and E.M.; writing—review and editing, M.A.C., A.G.-P., M.R.-C., N.C.P., F.C.-C., O.S.-R. and E.M.; supervision, project administration and funding acquisition, O.S.-R. and E.M. All authors have read and agreed to the published version of the manuscript.

Funding: This research was funded by MINCIENCIAS, MINEDUCACIÓN, MINCIT and ICETEX through the Program NanoBioCancer (Cod. FP44842-211-2018, project number 58676). M.A.C., F.C.-C. and O.S.-R. thank the University of Concepción for its support. A.G.-P. and E.M. thank the support from the University of Medellín.

Institutional Review Board Statement: Not applicable.

Informed Consent Statement: Not applicable.

Data Availability Statement: The data presented in this study are contained in the article tables and supplementary materials.

Conflicts of Interest: The authors declare no conflict of interest.

Sample Availability: Not applicable. The phagemids and molecules used in this work were either purchased or produced in limited amount only to perform the reported experiments.

References

1. Hamers-Casterman, C.; Atarhouch, T.; Muyldermans, S.; Robinson, G.; Hammers, C.; Songa, E.B.; Bendahman, N.; Hammers, R. Naturally Occurring Antibodies Devoid of Light Chains. *Nature* **1993**, *363*, 446–448. [[CrossRef](#)] [[PubMed](#)]
2. Valdés-Tresanco, M.S.; Valdés-Tresanco, M.E.; Molina-Abad, E.; Moreno, E. NbThermo: A New Thermostability Database for Nanobodies. *Database* **2023**, baad021. [[CrossRef](#)] [[PubMed](#)]
3. Hassanzadeh-Ghassabeh, G.; Devoogdt, N.; De Pauw, P.; Vincke, C.; Muyldermans, S. Nanobodies and Their Potential Applications. *Nanomedicine* **2013**, *8*, 1013–1026. [[CrossRef](#)] [[PubMed](#)]
4. Morrison, C. Nanobody Approval Gives Domain Antibodies a Boost. *Nat. Rev. Drug. Discov.* **2019**, *18*, 485–487. [[CrossRef](#)]
5. Keam, S.J. Ozoralizumab: First Approval. *Drugs*. **2023**, *83*, 87–92. [[CrossRef](#)]

6. Muyldermans, S. A Guide to: Generation and Design of Nanobodies. *FEBS. J.* **2021**, *288*, 2084–2102. [[CrossRef](#)]
7. Valdés-Tresanco, M.S.; Molina-Zapata, A.; Pose, A.G.; Moreno, E. Structural Insights into the Design of Synthetic Nanobody Libraries. *Molecules* **2022**, *27*, 2198. [[CrossRef](#)]
8. Moutel, S.; Bery, N.; Bernard, V.; Keller, L.; Lemesre, E.; de Marco, A.; Ligat, L.; Rain, J.-C.; Favre, G.; Olichon, A.; et al. NaLi-H1: A Universal Synthetic Library of Humanized Nanobodies Providing Highly Functional Antibodies and Intrabodies. *Elife* **2016**, *5*, e16228. [[CrossRef](#)]
9. McMahon, C.; Baier, A.S.; Pascolutti, R.; Wegrecki, M.; Zheng, S.; Ong, J.X.; Erlandson, S.C.; Hilger, D.; Rasmussen, S.G.F.; Ring, A.M.; et al. Yeast Surface Display Platform for Rapid Discovery of Conformationally Selective Nanobodies. *Nat. Struct. Mol. Biol.* **2018**, *25*, 289–296. [[CrossRef](#)]
10. Zimmermann, I.; Egloff, P.; Hutter, C.A.; Arnold, F.M.; Stohler, P.; Bocquet, N.; Hug, M.N.; Huber, S.; Siegrist, M.; Hetemann, L.; et al. Synthetic Single Domain Antibodies for the Conformational Trapping of Membrane Proteins. *Elife* **2018**, *7*, e34317. [[CrossRef](#)]
11. Sevy, A.M.; Chen, M.-T.; Castor, M.; Sylvia, T.; Krishnamurthy, H.; Ishchenko, A.; Hsieh, C.-M. Structure- and Sequence-Based Design of Synthetic Single-Domain Antibody Libraries. *Protein. Eng. Des. Selection.* **2020**, *33*, gzaa028. [[CrossRef](#)]
12. Zimmermann, I.; Egloff, P.; Hutter, C.A.J.; Kuhn, B.T.; Bräuer, P.; Newstead, S.; Dawson, R.J.P.; Geertsma, E.R.; Seeger, M.A. Generation of Synthetic Nanobodies against Delicate Proteins. *Nat. Protoc.* **2020**, *15*, 1707–1741. [[CrossRef](#)]
13. Zhao, Y.; Wang, Y.; Su, W.; Li, S. Construction of Synthetic Nanobody Library in Mammalian Cells by DsDNA-Based Strategies. *Chem. BioChem.* **2021**, *22*, 2957–2965. [[CrossRef](#)]
14. Chen, X.; Gentili, M.; Hacoheh, N.; Regev, A. A Cell-Free Nanobody Engineering Platform Rapidly Generates SARS-CoV-2 Neutralizing Nanobodies. *Nat. Commun.* **2021**, *12*, 5506. [[CrossRef](#)]
15. Moreno, E.; Valdés-Tresanco, M.S.; Molina-Zapata, A.; Sánchez-Ramos, O. Structure-Based Design and Construction of a Synthetic Phage Display Nanobody Library. *BMC. Res. Notes.* **2022**, *15*, 124. [[CrossRef](#)]
16. De Genst, E.; Silence, K.; Decanniere, K.; Conrath, K.; Loris, R.; Kinne, J.; Muyldermans, S.; Wyns, L. Molecular Basis for the Preferential Cleft Recognition by Dromedary Heavy-Chain Antibodies. *Proc. Natl. Acad. Sci. USA* **2006**, *103*, 4586–4591. [[CrossRef](#)]
17. Uchański, T.; Pardon, E.; Steyaert, J. Nanobodies to Study Protein Conformational States. *Curr. Opin. Struct. Biol.* **2020**, *60*, 117–123. [[CrossRef](#)]
18. Shi, Z.; Li, X.; Wang, L.; Sun, Z.; Zhang, H.; Chen, X.; Cui, Q.; Qiao, H.; Lan, Z.; Zhang, X.; et al. Structural Basis of Nanobodies Neutralizing SARS-CoV-2 Variants. *Structure* **2022**, *30*, 707–720.e5. [[CrossRef](#)]
19. Conrath, K.E.; Lauwereys, M.; Galleni, M.; Matagne, A.; Frère, J.-M.; Kinne, J.; Wyns, L.; Muyldermans, S. β -Lactamase Inhibitors Derived from Single-Domain Antibody Fragments Elicited in the *Camelidae*. *Antimicrob. Agents. Chemother.* **2001**, *45*, 2807–2812. [[CrossRef](#)]
20. Dumoulin, M.; Conrath, K.; Van Meirhaeghe, A.; Meersman, F.; Heremans, K.; Frenken, L.G.J.; Muyldermans, S.; Wyns, L.; Matagne, A. Single-Domain Antibody Fragments with High Conformational Stability. *Protein. Sci.* **2002**, *11*, 500–515. [[CrossRef](#)]
21. Saerens, D.; Pellis, M.; Loris, R.; Pardon, E.; Dumoulin, M.; Matagne, A.; Wyns, L.; Muyldermans, S.; Conrath, K. Identification of a Universal VHH Framework to Graft Non-Canonical Antigen-Binding Loops of Camel Single-Domain Antibodies. *J. Mol. Biol.* **2005**, *352*, 597–607. [[CrossRef](#)] [[PubMed](#)]
22. Wei, G.; Meng, W.; Guo, H.; Pan, W.; Liu, J.; Peng, T.; Chen, L.; Chen, C.-Y. Potent Neutralization of Influenza A Virus by a Single-Domain Antibody Blocking M2 Ion Channel Protein. *PLoS ONE* **2011**, *6*, e28309. [[CrossRef](#)] [[PubMed](#)]
23. Yan, J.; Li, G.; Hu, Y.; Ou, W.; Wan, Y. Construction of a Synthetic Phage-Displayed Nanobody Library with CDR3 Regions Randomized by Trinucleotide Cassettes for Diagnostic Applications. *J. Transl. Med.* **2014**, *12*, 343. [[CrossRef](#)] [[PubMed](#)]
24. Chi, X.; Liu, X.; Wang, C.; Zhang, X.; Li, X.; Hou, J.; Ren, L.; Jin, Q.; Wang, J.; Yang, W. Humanized Single Domain Antibodies Neutralize SARS-CoV-2 by Targeting the Spike Receptor Binding Domain. *Nat. Commun.* **2020**, *11*, 4528. [[CrossRef](#)]
25. Vincke, C.; Loris, R.; Saerens, D.; Martinez-Rodriguez, S.; Muyldermans, S.; Conrath, K. General Strategy to Humanize a Camelid Single-Domain Antibody and Identification of a Universal Humanized Nanobody Scaffold. *J. Biol. Chem.* **2009**, *284*, 3273–3284. [[CrossRef](#)]
26. Cornish-Bowden, A. Nomenclature for Incompletely Specified Bases in Nucleic Acid Sequences: Recommendations 1984. *Nucleic Acids Res.* **1985**, *13*, 3021–3030. [[CrossRef](#)]
27. Hoogenboom, H.R.; Griffiths, A.D.; Johnson, K.S.; Chiswell, D.J.; Hudson, P.; Winter, G. Multi-Subunit Proteins on the Surface of Filamentous Phage: Methodologies for Displaying Antibody (Fab) Heavy and Light Chains. *Nucleic Acids Res.* **1991**, *19*, 4133–4137. [[CrossRef](#)]
28. van Loo, G.; Bertrand, M.J.M. Death by TNF: A Road to Inflammation. *Nat. Rev. Immunol.* **2022**, *15*, 1–15. [[CrossRef](#)]
29. Leone, G.M.; Mangano, K.; Petralia, M.C.; Nicoletti, F.; Fagone, P. Past, Present and (Foreseeable) Future of Biological Anti-TNF Alpha Therapy. *J. Clin. Med.* **2023**, *12*, 1630. [[CrossRef](#)]
30. Ghalehbandi, S.; Yuzugulen, J.; Pranjol, M.Z.I.; Pourgholami, M.H. The Role of VEGF in Cancer-Induced Angiogenesis and Research Progress of Drugs Targeting VEGF. *Eur. J. Pharmacol.* **2023**, 175586. [[CrossRef](#)]
31. Arezumand, R.; Alibakhshi, A.; Ranjbari, J.; Ramazani, A.; Muyldermans, S. Nanobodies As Novel Agents for Targeting Angiogenesis in Solid Cancers. *Front. Immunol.* **2017**, *8*, 1746. [[CrossRef](#)]
32. Dennis, M.S.; Zhang, M.; Meng, Y.G.; Kadkhodayan, M.; Kirchhofer, D.; Combs, D.; Damico, L.A. Albumin Binding as a General Strategy for Improving the Pharmacokinetics of Proteins. *J. Biol. Chem.* **2002**, *277*, 35035–35043. [[CrossRef](#)]

33. Jonsson, A.; Dogan, J.; Herne, N.; Abrahmsen, L.; Nygren, P.-A. Engineering of a Femtomolar Affinity Binding Protein to Human Serum Albumin. *Protein Eng. Des. Sel.* **2008**, *21*, 515–527. [[CrossRef](#)]
34. Johansson, M.U.; Frick, I.-M.; Nilsson, H.; Kraulis, P.J.; Hober, S.; Jonasson, P.; Linhult, M.; Nygren, P.-Å.; Uhlén, M.; Björck, L.; et al. Structure, Specificity, and Mode of Interaction for Bacterial Albumin-Binding Modules. *J. Biol. Chem.* **2002**, *277*, 8114–8120. [[CrossRef](#)]
35. Eble, J.A. Titration ELISA as a Method to Determine the Dissociation Constant of Receptor Ligand Interaction. *J. Vis. Exp.* **2018**, *15*, 57334. [[CrossRef](#)]
36. Lakzaei, M.; Rasaee, M.J.; Fazaeli, A.A.; Aminian, M. A Comparison of Three Strategies for Biopanning of Phage-scFv Library against Diphtheria Toxin. *J. Cell. Physiol.* **2019**, *234*, 9486–9494. [[CrossRef](#)]
37. Jaroszewicz, W.; Morcinek-Orłowska, J.; Pierzynowska, K.; Gaffke, L.; Węgrzyn, G. Phage Display and Other Peptide Display Technologies. *FEMS Microbiol. Rev.* **2022**, *46*, fuab052. [[CrossRef](#)]
38. Scarrone, M.; González-Techera, A.; Alvez-Rosado, R.; Delfin-Riela, T.; Modernell, Á.; González-Sapienza, G.; Lassabe, G. Development of Anti-Human IgM Nanobodies as Universal Reagents for General Immunodiagnosics. *New Biotechnol.* **2021**, *64*, 9–16. [[CrossRef](#)]
39. Roshan, R.; Naderi, S.; Behdani, M.; Cohan, R.A.; Ghaderi, H.; Shokrgozar, M.A.; Golkar, M.; Kazemi-Lomedasht, F. Isolation and Characterization of Nanobodies against Epithelial Cell Adhesion Molecule as Novel Theranostic Agents for Cancer Therapy. *Mol. Immunol.* **2021**, *129*, 70–77. [[CrossRef](#)]
40. Kazemi-Lomedasht, F.; Behdani, M.; Bagheri, K.P.; Habibi-Anbouhi, M.; Abolhassani, M.; Arezumand, R.; Shahbazzadeh, D.; Mirzahoseini, H. Inhibition of Angiogenesis in Human Endothelial Cell Using VEGF Specific Nanobody. *Mol. Immunol.* **2015**, *65*, 58–67. [[CrossRef](#)]
41. Wu, M.; Tu, Z.; Huang, F.; He, Q.; Fu, J.; Li, Y. Panning Anti-LPS Nanobody as a Capture Target to Enrich *Vibrio Fluvialis*. *Biochem. Biophys. Res. Commun.* **2019**, *512*, 531–536. [[CrossRef](#)] [[PubMed](#)]
42. Lunder, M.; Bratkovič, T.; Urleb, U.; Kreft, S.; Štrukelj, B. Ultrasound in Phage Display: A New Approach to Nonspecific Elution. *Biotechniques* **2008**, *44*, 893–900. [[CrossRef](#)] [[PubMed](#)]
43. Humphrey, W.; Dalke, A.; Schulten, K. VMD: Visual Molecular Dynamics. *J. Mol. Graph.* **1996**, *14*, 33–38. [[CrossRef](#)] [[PubMed](#)]
44. Tonikian, R.; Zhang, Y.; Boone, C.; Sidhu, S.S. Identifying Specificity Profiles for Peptide Recognition Modules from Phage-Displayed Peptide Libraries. *Nat. Protoc.* **2007**, *2*, 1368–1386. [[CrossRef](#)]
45. Chen, G.; Sidhu, S.S. Design and Generation of Synthetic Antibody Libraries for Phage Display. In *Monoclonal Antibodies: Methods and Protocols*; Ossipow, V., Fischer, N., Eds.; Humana Press: Totowa, NJ, USA, 2014; pp. 113–131.
46. Contreras, M.A.; Macaya, L.; Neira, P.; Camacho, F.; González, A.; Acosta, J.; Montesino, R.; Toledo, J.R.; Sánchez, O. New Insights on the Interaction Mechanism of RhTNF α with Its Antagonists Adalimumab and Etanercept. *Biochem. J.* **2020**, *477*, 3299–3311. [[CrossRef](#)]
47. Parra, N.C.; Mansilla, R.; Aedo, G.; Vispo, N.S.; González-Horta, E.E.; González-Chavarría, I.; Castillo, C.; Camacho, F.; Sánchez, O. Expression and Characterization of Human Vascular Endothelial Growth Factor Produced in SiHa Cells Transduced with Adenoviral Vector. *Protein J.* **2019**, *38*, 693–703. [[CrossRef](#)]
48. Beltrán-Ortiz, C.E.; Starck-Mendez, M.F.; Fernández, Y.; Farnós, O.; González, E.E.; Rivas, C.I.; Camacho, F.; Zuñiga, F.A.; Toledo, J.R.; Sánchez, O. Expression and Purification of the Surface Proteins from Andes Virus. *Protein. Expr. Purif.* **2017**, *139*, 63–70. [[CrossRef](#)]
49. Baek, H.; Suk, K.; Kim, Y.; Cha, S. An Improved Helper Phage System for Efficient Isolation of Specific Antibody Molecules in Phage Display. *Nucleic. Acids. Res.* **2002**, *30*, e18. [[CrossRef](#)]

Disclaimer/Publisher’s Note: The statements, opinions and data contained in all publications are solely those of the individual author(s) and contributor(s) and not of MDPI and/or the editor(s). MDPI and/or the editor(s) disclaim responsibility for any injury to people or property resulting from any ideas, methods, instructions or products referred to in the content.

Article

Selecting Nanobodies Specific for the Epidermal Growth Factor from a Synthetic Nanobody Library

Yunier Serrano-Rivero ^{1,†}, Julieta Salazar-Uribe ^{1,†}, Marcela Rubio-Carrasquilla ¹, Frank Camacho-Casanova ², Oliberto Sánchez-Ramos ², Alain González-Pose ^{1,*} and Ernesto Moreno ^{1,*}

¹ Faculty of Basic Sciences, University of Medellin, Medellin 050026, Colombia; 0905yunierserrano@gmail.com (Y.S.-R.); julieta.salazaru@gmail.com (J.S.-U.); marcelaru@yahoo.com (M.R.-C.)
² Pharmacology Department, School of Biological Sciences, University of Concepcion, Concepcion 4070386, Chile; fcamacho@udec.cl (F.C.-C.); osanchez@udec.cl (O.S.-R.)
* Correspondence: agonzalezp@udemedellin.edu.co (A.G.-P.); emoreno@udemedellin.edu.co (E.M.)
† These authors contributed equally to this work.

Abstract: The epidermal growth factor (EGF) is one of the most critical ligands of the EGF receptor (EGFR), a well-known oncogene frequently overexpressed in cancerous cells and an important therapeutic target in cancer. The EGF is the target of a therapeutic vaccine aimed at inducing an anti-EGF antibody response to sequester this molecule from serum. However, strikingly, very few investigations have focused on EGF immunotargeting. Since the use of nanobodies (Nbs) for EGF neutralization may be an effective therapeutic strategy in several types of cancer, in this study, we decided to generate anti-EGF Nbs from a recently constructed, phage-displaying synthetic nanobody library. To our knowledge, this is the first attempt to obtain anti-EGF Nbs from a synthetic library. By applying a selection strategy that uses four different sequential elution steps along with three rounds of selection, we obtained four different EGF-specific Nb clones, and also tested their binding capabilities as recombinant proteins. The obtained results are very encouraging and demonstrate the feasibility of selecting nanobodies against small antigens, such as the EGF, from synthetic libraries.

Keywords: epidermal growth factor; nanobody; synthetic library; phage display



Citation: Serrano-Rivero, Y.; Salazar-Uribe, J.; Rubio-Carrasquilla, M.; Camacho-Casanova, F.; Sánchez-Ramos, O.; González-Pose, A.; Moreno, E. Selecting Nanobodies Specific for the Epidermal Growth Factor from a Synthetic Nanobody Library. *Molecules* **2023**, *28*, 4043. <https://doi.org/10.3390/molecules28104043>

Academic Editor: Jahir Orozco Holguín

Received: 24 March 2023
Revised: 8 May 2023
Accepted: 9 May 2023
Published: 12 May 2023



Copyright: © 2023 by the authors. Licensee MDPI, Basel, Switzerland. This article is an open access article distributed under the terms and conditions of the Creative Commons Attribution (CC BY) license (<https://creativecommons.org/licenses/by/4.0/>).

1. Introduction

The human epidermal growth factor (EGF) is a small protein of 53 amino acids, whose fold is structured by three disulfide bonds. It demonstrates potent biological activity in vitro and in vivo by stimulating cell and organ proliferation [1]. Furthermore, the EGF is one of the most critical ligands of the EGF receptor (EGFR) [2], a well-known oncogene frequently overexpressed in cancerous cells, causing cell-cycle deregulation, exacerbated angiogenesis, apoptosis blockade, and tumoral cell migration [3]. It was found very early that EGF detection in carcinomas is closely related to high levels of malignancy [4]. Indeed, EGF signaling is essential for tumor-cell growth for several types of cancer [5,6], and it is linked to the epithelial–mesenchymal transition, in which epithelial cells are transformed into fibroblast-like phenotypes with high motility and invasive properties, contributing to cancer metastasis [7,8]. Therefore, along with the EGFR, the EGF is also considered a potential target for cancer therapy.

The prevention of cancer using our own immune system against self-antigens is possible due to the observed natural self-reactivity of immune cells against autologous antigens [9]. In the case of the EGF, a self-antibody response against this molecule would diminish the serum availability of EGF, thus reducing EGFR activation and, in consequence, cancer-cell proliferation. Following this active therapeutic approach, a novel anti-EGF vaccine named CIMAvax-EGF was developed. This vaccine is based on a chemical conjugate of EGF and the protein P64k from *Neisseria meningitidis*, adjuvanted with Montanide ISA

51 VG [10]. The main function of this immunogen is to break the EGF's self-tolerance, inducing an anti-EGF antibody response, which dramatically reduces the EGF concentration in serum [11]. More than 10 clinical trials have been completed with the therapeutic cancer vaccine CIMAvax-EGF, including phase II, III, and IV trials, demonstrating safety, long-term immunogenicity and a significant effect on survival, with several patients achieving long-term survival after vaccination [10].

An alternative, passive-therapy-based approach for sequestering EGF would involve different antibody formats, particularly, nanobodies (Nbs), which are single-domain antibody fragments derived from the heavy chain antibodies found in camelids [12]. Nbs have several advantageous properties over classical antibodies: small size, high stability and solubility, and easy tailoring for multiple applications. Furthermore, they can achieve high affinities despite the fact that their monomeric binding region displays only three hypervariable loops. Nbs have become a relevant class of biomolecules with multiple applications, especially as diagnostic tools and promising therapeutic agents in cancer and other diseases [13]. They are obtained mostly from immune libraries, constructed from animal immunization with the target antigen [14]. In recent years, however, synthetic nanobody libraries have gained ground as alternative Nb sources, offering several advantages, such as lower costs and faster results [15]. As these libraries are not generated for a specific antigen, they can be used for the selection of nanobodies against numerous antigens, including those with high toxicity or low immunogenicity [15].

A successful example of the use of nanobodies to sequester a circulating cytokine is ozoralizumab—a trivalent anti-TNF nanobody, which was recently approved in Japan for the treatment of rheumatoid arthritis [16]. Strikingly, despite the proven potential of EGF as a cancer target, there are very few investigations focused on EGF immunotargeting. A recent work by Guardiola et al. reported the generation of anti-EGF Nbs using an immune library from alpaca, and showed their ability to block EGFR phosphorylation and produce antitumor effects in vitro [17,18]. To our knowledge, these were the only anti-EGF nanobodies reported before the present study.

Since the use of Nbs for EGF neutralization may be an effective therapeutic strategy in several types of cancer, in this study, we decided to generate anti-EGF nanobodies from our recently constructed synthetic nanobody library, based on the phage-display platform [19]. After three selection rounds, each of which used four different serial elution methods, we obtained about forty positive recombinant phage clones. Twenty of these clones were sequenced, resulting in four different amino-acid sequences. These three distinct nanobodies were produced in BL21 (DE3) and purified by ion exchange (IEC) and immobilized metal affinity (IMAC) chromatography, and their ability to bind to EGF was demonstrated.

2. Results and Discussion

2.1. Design and Production of a Recombinant EGF Protein

Firstly, we designed and produced, in-house, a recombinant EGF (rEGF) protein with two tags (SV5 and 6xHis) that confer a more versatile functionality to this molecule (Figure 1a). The rEGF gene was cloned into the bacterial expression vector pET22b (Figure 1b) under the control of strong bacteriophage T7 transcriptional and translational signals, which allow the production of large amounts of recombinant proteins upon induction. The inclusion of the PelB-signal peptide before the rEGF gene allows secretion into the periplasmic compartment, in order to obtain a protein of interest that is soluble after bacterial lysis. The bacterial system (*E. coli* BL21 (DE3)) successfully produced the rEGF, as expected (Figure 1c). After cell lysis, a rEGF fraction remained soluble (Figure 1d), and it was successfully purified by IMAC and IEC (Figure 1e). Although part of the recombinant protein was lost in the different chromatographic steps, we were able to obtain a sufficient amount, with more than 90% purity. The biological activity of the rEGF was assessed in vitro using the human cell line A431, characterized by high EGFR overexpression [20]. The cells were treated with different rEGF concentrations, ranging from 100 pm to 100 nM. Similarly as found in early studies with EGF [21], the lowest applied rEGF concentration

(100 pM) stimulated cell growth in cultures with a low concentration (0.5%) of fetal bovine serum (FBS). This effect vanished with higher rEGF concentrations. On the other hand, the expected inhibitory effect of high rEGF concentrations (10 and 100 nM) [21] was markedly observed in A431 cells cultured with 5% FBS (Figure 1f). Having proven the functionality of the in-house-produced rEGF (hereafter called EGF), we proceeded to select EGF binders from our synthetic nanobody library.

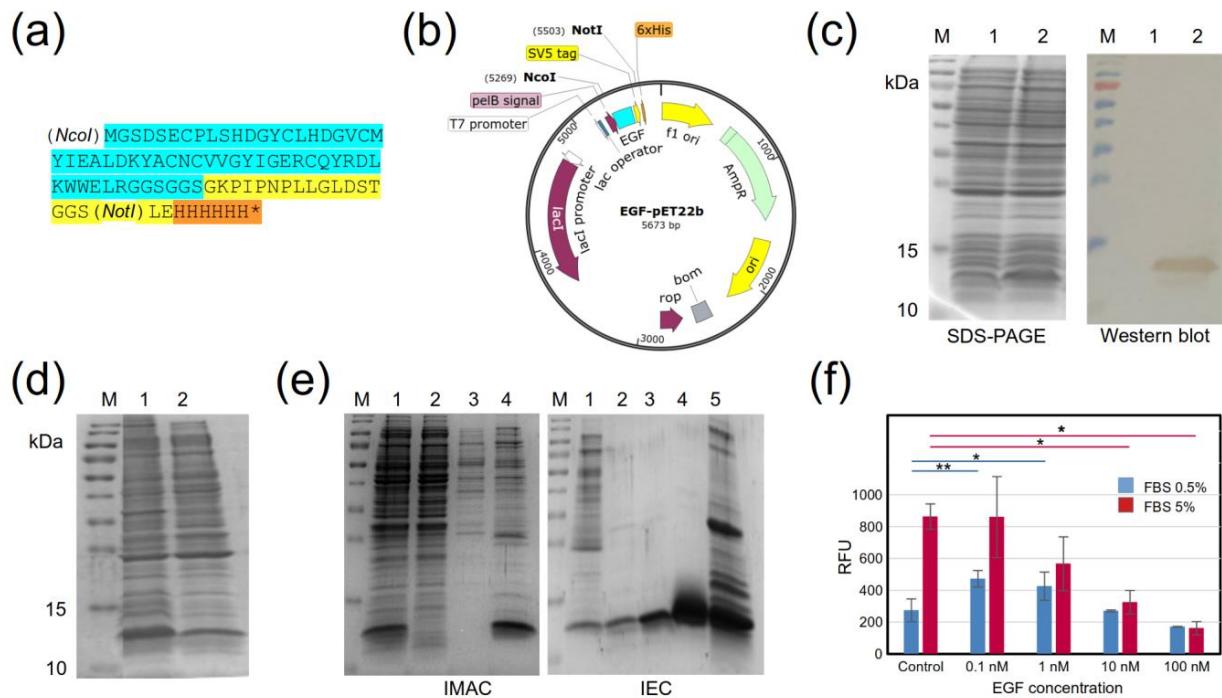


Figure 1. Production of (r)EGF in *E. coli*. (a) Amino-acid sequence of rEGF with C-terminal tags: cyan—EGF, yellow—SV5 tag, orange—6xHis tag. (b) Scheme of the pET22b-rEGF expression vector. (c) SDS-PAGE and Western blot of the production of rEGF in BL21 (DE3). The rEGF was identified using an anti-His tag monoclonal antibody conjugated to HRP. M: molecular-weight marker, Trident Prestained Protein Ladder GTX50875 (GeneTex, USA), 1: untransformed BL21, 2: BL21 transformed with pET22b-rEGF. (d) SDS-PAGE of the rEGF-soluble fraction obtained by cell lysis using several freezing/thawing rounds. M: molecular-weight marker, 1: total fraction of BL21 transformed with pET22b-hEGF, 2: soluble fraction of BL21 transformed with pET22b-hEGF. (e) SDS-PAGE of the rEGF-purification process. Left panel: first purification stage by IMAC. M: molecular-weight marker, 1: initial sample, 2: unbound proteins, 3: wash (40 mM imidazole), 4: elution (250 mM imidazole). Right panel: second purification stage with IEC. M: molecular-weight marker, 1: initial sample from IMAC elutions, 2, 3, and 4: unbound proteins, 5: elution from the anionic exchanger Bio-Scale Mini Macro-Prep High Q Cartridge (BioRad, Hercules, CA, USA). (f) In vitro evaluation of rEGF biological activity in A431 cells. Two FBS concentrations were used: (0.5%—blue bars; and 5%—red bars). Measurements were performed in triplicate. Stars indicate statistically significant differences between experimental conditions (* $p < 0.05$, ** $p < 0.005$).

2.2. Selection of EGF-Binding Phages

As a small protein, EGF presents a relatively small surface area for antibody/nanobody recognition, which presents a challenge in obtaining nanobodies from a synthetic library. We decided to implement a screening procedure based on three selection rounds, each of which was composed of four different types of elution, performed sequentially, using the following: (i) triethylamine (TEA—1), (ii) glycine-HCl (Gly—2), (iii) ultrasound (Uls—3), and (iv) the addition of the TG1 strain to previously washed wells (TG1—4). The aim was to recover binders with different physico-chemical properties that would not be eluted with TEA (a commonly used elution buffer), followed by binders not eluted either with Gly, and

so on. After each round, the phages collected from each elution were pulled together for amplification, except for the final round, in which the phages from the different elutions were amplified separately.

The use of successive rounds of selection against the antigen of interest is intended to increase the proportion of antigen-specific phages [14,22]. As in this study, Guardiola et al. performed three selection rounds to obtain EGF-specific phages from an alpaca immune library [17]. In most cases, the phages bound to the target molecule were collected using a single method, which can either be triethylamine (e.g., [17,23–25]), glycine [26–28], ultrasound (albeit to a lesser extent, such as in [29,30]) and, rarely, infection by the direct addition of cells to the wells [29]. The use of a single elution method may limit phage collection, losing a fraction of phages that remain strongly bound to the immobilized target molecule in the wells. In contrast, in our study, we used four sequential elutions, recovering significant amounts of phages in each of them.

With the aim of optimizing the screening of clones by ELISA for binding to EGF, we first tested groups of selected clones, each of which consisted of four individual clones (all belonging to the same elution). We evaluated 17, 15, 16, and 16 groups from the TEA, Gly, UltS, and TG1 elutions, respectively. A plate blocked with skimmed milk was included to identify mock-phages. Thus, this assay allowed us to select groups with a high EGF binding signal and low background. Figure 2a shows the ELISA results from this screening. Following the criterion defined in the Methods, a total of 24 positive groups were obtained, which were distributed as follows: TEA-14, Gly-5, UltS-1, and TG1-4. Subsequently, the individual clones from these 24 groups were tested in the same way (Figure 2b), with one important addition. As the recombinant EGF molecule has a C-terminal tail containing SV5 and His tags, we added a third plate coated with a non-related protein with the same C-terminal tail, to discard anti-tag phages. Of the 96 individual clones, 38 met the positivity criteria, and they were distributed by elution, as follows: TEA-16, Gly-1, UltS-1, and TG1-11. A few of these clones, mostly from the TG1 elution, also showed strong anti-tag binding (Figure 2b).

2.3. Sequences of Selected Clones

Most of the EGF-positive phage clones (21 clones, discarding only a few weaker binders), as well as several of the C-tail tag binders were sent for sequencing. Figure 3 shows the sequences obtained for the CDRs (the framework is common to all the nanobodies derived from the library). The 21 EGF-positive clones corresponded to only four unique Nb sequences, and 17 of the clones were identical. These results are comparable to those obtained by Guardiola et al., who recovered six different anti-EGF clones from an immune library [17].

The use of four different elutions for binder recovery yielded intriguing results. The group of 17 identical clones was composed of phages from three elutions (TEA-8; Gly-2; TG1-7); the identical A8-1/B3-1 pair of clones and the single C10-1 clone were obtained from the TEA elution, whereas the single clone, D6-4, was recovered from the TG1 elution. The mixed origin of the repeated clones obtained after the third selection round might have been associated with the pulling of the four elutions from rounds 1 and 2 for amplification and subsequent inputs for rounds 2 and 3, respectively. On the other hand, the unique D6-4 clone was the result of the sequential application of the four types of elution; otherwise, it would not have been recovered. The five anti-tag phage clones in fact corresponded to two unique Nb sequences. In future screenings, it would be interesting, and possibly more productive, to keep each elution separately through all the selection rounds.

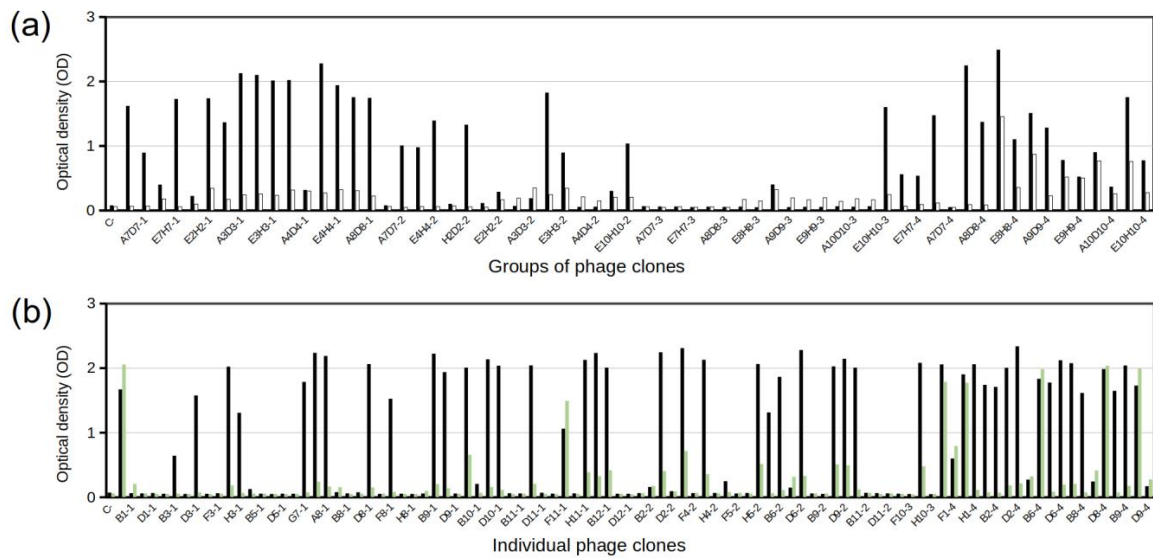


Figure 2. ELISA screening of selected phage clones for binding to EGF. (a) Identification of phage groups that bind to EGF (black bars). White bars correspond to background (milk) signals. (b) Positive phage groups were individualized and re-screened. Green bars correspond to binding to an unrelated nanobody with the same C-terminal tail as the recombinant EGF. Positivity was defined as $OD_{450nm} \geq 0.8$ for EGF binding, and an OD_{450nm} for milk or an unrelated tagged protein three or more times lower than for EGF. The last number in clone names refers to the type of elution: 1—TEA, 2—Gly, 3—UltS—3, 4—TG1.

Clone	CDR1	CDR2	CDR3
A11-2	SGDHNNQYNKFALG	A I S S N G G K	ARRYQYETHRS
A2-4 ★
C9-1
C10-1 ★	. . . R Q Y H . S V T G T Q S G S G Y . . Y
A8-1 ★	. . N S . Y . . P H . D G . . R	. V G S R T R N Y . Y
B3-1 ★	. . N S . Y . . P H . D G . . R	. V G S R T R N Y . Y
D6-4 ★	. . T R R Y K . . V . D T G . . R	. . . T N N A N F . Y
D8-4 Tag	. . N N S Y R . . R . D L R . . R	. M G N R . R N . D .
F11-1 Tag	. . N N S Y R . . R . D L R . . R	. M G N R . R N . D .
A1-1	. . N R K F N . Y N . D D . S . . I	. T . T G S A Y F G Y
B6-4 Tag	. . N R K F N . Y N . D D . S . . I	. T . T G S A Y F G Y
C9-4	. . N R K F N . Y N . D D . S . . I	. T . T G S A Y F G Y

Framework sequence:

QVQLVESGGGSVQAGGSLRLSCTASXXXXXXXXXXXXXXXXWFRQAPGQEREAVAXXXXXXXXXT
 YYADSVKGRFTISRDNKNTVTLQMNNLKPEDTAIYYCAAXXXXXXXXXXWGQGTQVTVS

Figure 3. CDR amino-acid sequences of selected clones. Red stars are for EGF binders, while “Tag” in blue is for tag-positive clones. Dots indicate the presence of the same amino acid as in the first sequence in the alignment. The first group of three clones (A11-2, A2-4, and C9-1), from different elutions, are representative of the group of 17 identical clones. The common framework sequence supporting the library is from the camelid nanobody cAbBCIII0 [31]). CDRs are underlined, with their amino acids represented with “X”.

2.4. Production of the Four Recombinant Anti-EGF Nanobodies

The four anti-EGF Nbs with different sequences (clones A8-1, A11-2, C10-1, and D6-4) were expressed as recombinant proteins by cloning their genes into pET22b and producing

them in *E. coli* BL21 (DE3), which is a commonly used system for nanobody production, with a high level of success [32–34]. The recombinant-protein production behaved similarly for the four nanobodies. Upon the induction with IPTG, a majority protein band of approximately 16 kDa was observed in the four induced cultures, while it was absent in the negative control. A Western blot corroborated the observation that all four bands corresponded to recombinant nanobodies (Figure 4a). The design incorporating the signal-peptide PelB allowed the secretion of the produced proteins into the bacterial periplasm, producing a large amount of soluble protein. After production, the four nanobodies were purified by combining two chromatographic methods: ion-exchange chromatography (IEC) followed by immobilized metal-affinity chromatography (IMAC). Usually, a single IMAC purification step is not sufficient to obtain Nbs with a high degree of purity; therefore, at least one additional molecular exclusion or IEC is also used [35], being the combination of IMAC and molecular exclusion chromatography the most commonly used method for Nb purification [25,34,36]. Here, we decided to first carry out an IEC step, which removed more than 50% of the contaminating proteins, followed by IMAC, which yielded recombinant Nbs with about 90% purity (Figure 4b).

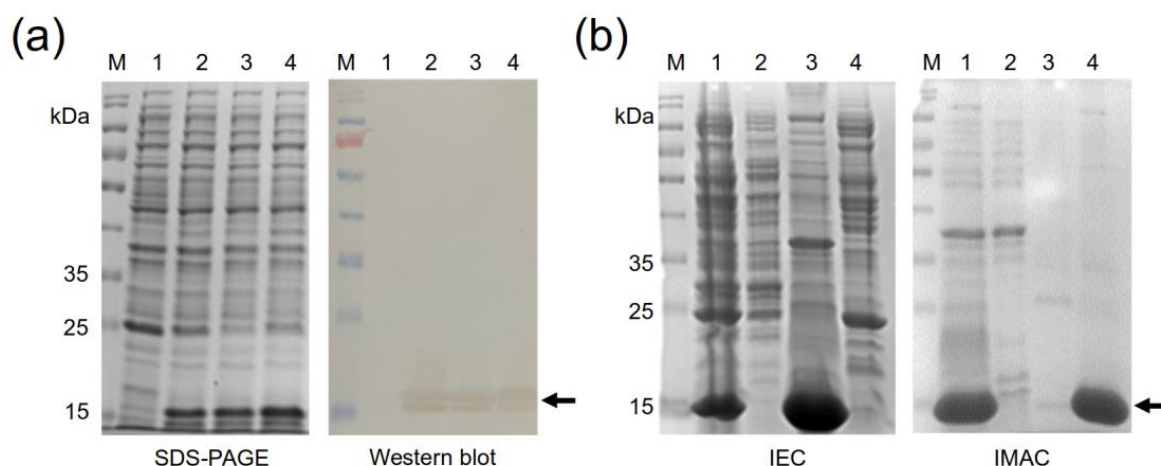


Figure 4. Production and purification of anti-EGF nanobodies. (a) SDS-PAGE and Western blot of nanobody production in BL21 (DE3). M: molecular-weight marker, PageRuler Prestained Protein Ladder (Thermo Fisher Scientific, USA), 1: untransformed BL21; BL21 transformed with (2) pET22b-NbA8-1, (3) pET22b-NbA11-2, and (4) pET22b-NbD6-4. The nanobodies were identified using an anti-His tag monoclonal antibody conjugated to HRP. (b) SDS-PAGE of the nanobody-purification process. Left panel: first purification stage by IEC. M: molecular-weight marker, 1: initial sample, 2: unbound proteins, 3: elution from the anionic exchanger, Bio-Scale Mini Macro-Prep High Q Cartridge (BioRad, USA), 4: elution from the cationic exchanger CM Sepharose Fast Flow (GE Healthcare, USA). Right panel: second purification stage by IMAC. M: molecular-weight marker, 1: initial sample from IEC, 2: unbound proteins, 3: wash (40 mM imidazole), 4: elution (250 mM Imidazole). Arrow heads indicate the protein bands corresponding to nanobodies A8-1, A11-2, and D6-4.

2.5. Binding Assays for Selected Recombinant Anti-EGF Nanobodies

The recognition of the EGF by the recombinant nanobodies was assessed by indirect ELISA. In a first attempt, we intended to use the SV5 tag in the recombinant EGF molecule for detection, by coating the wells with the recombinant nanobodies, adding the recombinant EGF and then an HRP-conjugated anti-SV5 antibody. This approach, however, yielded very weak signals. We speculate that with such a small molecule as a nanobody, adsorption on a plastic surface would reduce the binding-site availability or affect the conformation of the flexible CDR3 loop.

Since no other tag was available for detection (the His tag is common in both nanobodies and the EGF), we decided to biotinylate the recombinant nanobodies, taking advantage of the three lysine residues found in the framework region. With this method, we

successfully detected the expected nanobody–antigen-binding signals, and assessed the dissociation constant (KD) for the two best binders from a titration ELISA [37] (Figure 5). The nanobodies A8-1 and D6-4 showed very similar binding strengths, with KD in the order of 10^{-7} M, while the Nbs A11-2 y C10-1 showed a weaker binding (their KD values could not be assessed).

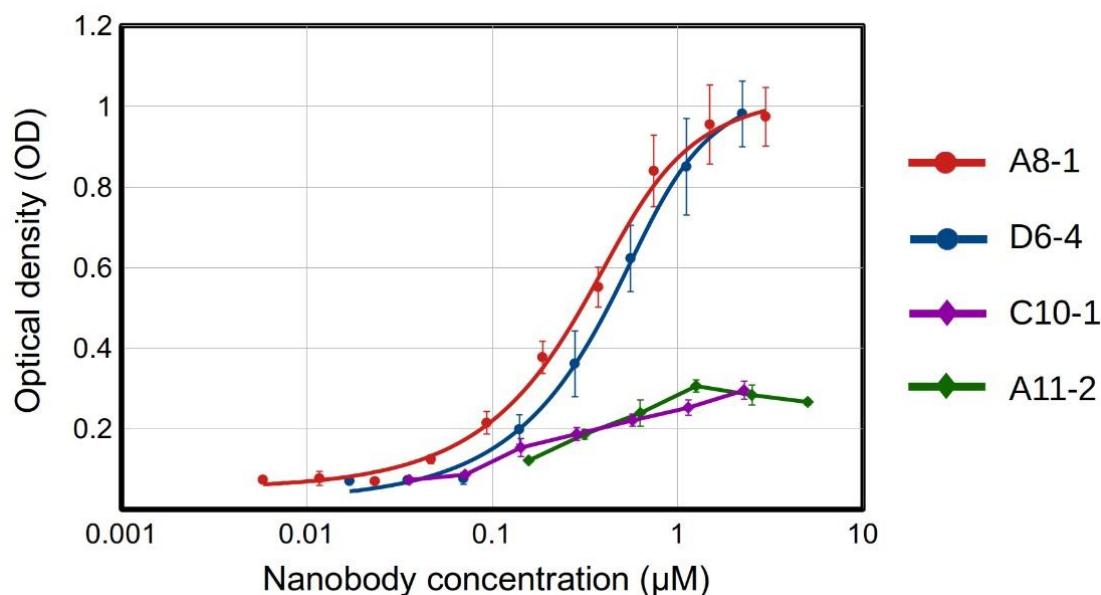


Figure 5. Binding of recombinant nanobodies to EGF by indirect ELISA. Biotinylated nanobodies were detected with streptavidin conjugated to HRP. The red and blue fitting curves were used for KD estimation, for clones A8-1 ($KD = (2.4 \pm 0.7) \times 10^{-7}$ M) and D6-4 ($KD = (3.7 \pm 0.8) \times 10^{-7}$ M), respectively. Negative controls (not shown)—BSA coating: OD = 0.11. For all Nbs, we used the maximum tested concentration for the negative controls. Experiments were performed in triplicates.

It is worth noting that while the clone A8-1 has no lysine in its CDRs, D6-4 shows a lysine in CDR1. This lysine could have been affected in the biotinylation procedure, thus abolishing or diminishing the binding capabilities of a fraction of the nanobody molecules. Therefore, the KD for the clone D6-4 might, in fact, be better. The other two clones also displayed lysine residues in their CDRs (two in A11-2, one in CDRs 1 and 2, and one in C10-1 in CDR2), which may have partially affected their binding to EGF. The impairment of the binding capacity of antibodies after biotinylation has been described, and it might be counteracted by establishing an adequate biotin:antibody ratio [38]. The incorporation of biotin into histidine, serine, threonine, and tyrosine residues has also been observed [39]. At least two of these residues are present in the CDRs of the four anti-EGF Nbs, and their possible biotinylation might have exerted a negative effect on the EGF recognition.

Despite these possible drawbacks, the affinities estimated for the clones A8-1 and D6-4 were similar to those measured by Guardiola et al. for five out of their six anti-EGF nanobodies, which showed KD values in the 10^{-7} molar order, while only one clone yielded a KD in the 10^{-8} M order [17]. That is, the anti-EGF nanobodies selected in this work from a synthetic library were comparable in terms of affinity to those obtained from an immunized alpaca. It is worth noting that these KD values are in the same order as the KD of the EGF–EGFR complex, which, in different studies using surface plasmon resonance (SPR) has been found to be within the range of 100–400 nM [40–42]. Notably, two of the anti-EGF Nbs obtained by Guardiola et al. were capable of inhibiting the binding of EGF to its receptor and EGFR phosphorylation, with IC50 constants in the micromolar order [17]. They also inhibited cell viability in tumor cells resistant to the EGFR-tyrosine-kinase inhibitor, osimertinib [18].

In this study, we applied a sequential stringent elution method for selecting specific anti-EGF Nb clones from the library, in which the triethylamine solution (suffix 1) was the first elution applied and the addition of TG1 cells (suffix 4) was the last. Therefore, it is reasonable to expect that the nanobodies obtained from the last elution should have a higher binding capacity. Paradoxically, our best binder was obtained from the first elution. This interesting outcome suggests that the nature of the molecular interactions governing nanobody–antigen binding determine the type of elution that detaches the nanobody from the immobilized antigen.

2.6. Concluding Remarks

In this study, we obtained four EGF-binding nanobodies from a synthetic library, applying a selection strategy that used four different sequential elution steps along three rounds of selection. To our knowledge, this was the first attempt to obtain anti-EGF nanobodies from a synthetic library. Notably, two of the obtained nanobodies showed KD values similar to those obtained for the Nbs derived from an immune library. It has been shown that it is possible to obtain high-affinity binders from synthetic libraries [15,43]. However, the fact that EGF is a small protein, offering a relatively small surface area for antibody/nanobody recognition, represents a major challenge. Thus, the obtained results are very encouraging. The next step will be to test the neutralizing capabilities of the obtained nanobodies. In future anti-EGF biopannings, as well as in those for other small proteins, we plan to use a different antigen-presentation system, in which the EGF is completely exposed for nanobody recognition, by, for example, using a biotinylated tag for anchoring to a streptavidin base [44]. In this way, we expect to increase the probability of obtaining high-affinity binders from the synthetic library.

3. Materials and Methods

3.1. Synthetic Library Production

The synthetic nanobody library was designed and constructed by our group as described in [19]. In this study, the library previously cloned into the phagemid pMAC and transformed in the *E. coli* strain SS320 was amplified into the amber suppressor, *E. coli* strain TG1. For this purpose, 300 mL of 2xYT medium containing 100 µg/mL ampicillin was inoculated with the TG1 strain and grown at 37 °C, and at 250 rpm, until an OD_{600nm} of 1.5. The phage library previously obtained in SS320 bacteria was used to transduce TG1 cells at a multiplicity of infection (MOI) of 58 at 37 °C for one hour (30 min static and 30 min at 50 rpm). After spinning at 2000 × g for 15 min at 4 °C and discarding supernatant, the pellet was resuspended in 300 mL of 2xYT medium with 100 µg/mL ampicillin and incubated at 28 °C, 100 rpm, overnight. Next, 200 mL of the previous culture was added to a final volume of 800 mL of 2xYT medium with 100 µg/mL ampicillin and cultured at 37 °C, 250 rpm until an OD_{600nm} of 2. The culture was transduced with the helper phage M13K07 at a MOI of 25 at 37 °C for one hour (30 min static and 30 min at 50 rpm), and spined at 2000 × g for 15 min at 4 °C. The pellet was diluted in 500 mL of 2xYT medium containing 100 µg/mL ampicillin, 50 µg/mL kanamycin, and 1 mM isopropyl β-D-1-thiogalactopyranoside (IPTG) for library amplification. After calculating library diversity, recombinant phages were concentrated by precipitation with PEG/NaCl (20% polyethylene glycol 8000 and 2.5 M NaCl) and aliquoted in 10% glycerol.

3.2. Production and Purification of a Recombinant EGF Protein

The gene coding the EGF was synthesized and cloned into the pET22b-expression vector (pET22b-EGF) by GenScript (Piscataway, NJ, USA). After transforming chemically competent BL21 (DE3), two inocula of 5 mL, each grown at 37 °C and at 250 rpm, overnight, in 2xYT medium with 100 µg/mL ampicillin were added to two Erlenmeyers of 1 L containing 500 mL each of Saline Minimal Medium M9 (SMM9) (45 mM Na₂HPO₄ (Sigma-Aldrich, Burlington, MA, USA), 22 mM KH₂HPO₄ (Sigma, Burlington, MA, USA), 19 mM NH₄Cl (Merck, Rahway, NJ, USA), 8.4 mM NaCl (Sigma-Aldrich, Burlington, MA, USA)),

0.05% yeast extract (Oxoid, Basingstoke, UK), and 100 µg/mL ampicillin. After reaching an OD_{600nm} of 0.5, the gene expression was induced with 25 µM IPTG, and cultures were incubated at 28 °C and at 100 rpm, overnight. Next, cultures were centrifuged at $10,000 \times g$ for 15 min at 4 °C, and the pellet was resuspended in buffer A (150 mM NaCl, 15 mM Na_2HPO_4 , pH 7.4) and subjected to five freeze/thaw rounds for cell lysis. Soluble rEGF was obtained in the supernatant after spinning at $10,000 \times g$ for 15 min at 4 °C. The presence of soluble EGF was verified by sodium dodecyl sulphate–polyacrylamide gel electrophoresis (SDS-PAGE) and Western blot.

For SDS-PAGE, protein samples were diluted in a buffer with beta-mercaptoethanol and run in 15% polyacrylamide and 3% stacking gels. Western blot assay was performed in a 0.2-µm PVDF-transfer membrane (Thermo Fisher Scientific, Waltham, MA, USA) and a semi-dry transfer system Trans-Blot[®] Turbo[™] (Bio-Rad, Hercules, CA, USA) at 0.3 A and 25 V for 30 min. After blocking with 5% skimmed milk in PBS, the membrane was incubated with the HRP anti-6X His tag rabbit polyclonal antibody (ab1187, Abcam, Boston, MA, USA) diluted 1:5000 in the blocking buffer. The reaction was visualized using a DAB substrate kit (Thermo Fisher Scientific, Waltham, MA, USA).

The rEGF was purified in two chromatographic stages. (i) The lysis supernatant containing rEGF was purified by immobilized metal-affinity chromatography (IMAC) by adding 5 mM imidazole to buffer A as equilibrium buffer and the initial sample. After loading the sample, the HisPur Ni-NTA Spin Column (Thermo Fisher Scientific, Waltham, MA, USA) was washed with 25 mM imidazole, and protein was eluted with 250 mM imidazole. Samples, washing, and elution were prepared in buffer A. (ii) For ion-exchange chromatography (IEC), a serial connection of two columns was used. One column featured the weak cation-exchanger CM Sepharose Fast Flow (GE Healthcare, Chicago, IL, USA), and the other was a pre-packed column with the anion exchanger, Bio-Scale Mini Macro-Prep High Q Cartridge (BioRad, Hercules, CA, USA). Both were equilibrated with buffer B (50 mM NaCl, 7 mM Na_2HPO_4 (Sigma-Aldrich, Burlington, MA, USA), 83 mM imidazole, pH 8). Samples from IMAC were diluted three times in water and loaded into these columns. After column equilibration with the same buffer B, the anion exchanger was eluted with buffer C (500 mM NaCl, 7 mM Na_2HPO_4 , pH 5), and the cation exchanger was eluted with the same buffer C at pH 10. The pH of buffers for IEC was carefully adjusted according to the theoretical isoelectric point of rEGF, calculated using Prot-Pi (<https://www.protpi.ch/Calculator/ProteinTool> (accessed on 10 March 2023)). All fractions were monitored using the purification system, BioLogic LP (BioRad, Hercules, CA, USA). Samples containing the rEGF were diafiltered against PBS (Sigma, USA) in Spin-X[®] UF concentrators of 5 kDa (Corning, Corning, NY, USA), and analyzed by SDS-PAGE and Western blot, as described above. The rEGF purity was estimated using the analytical software of the iBright 750 Imaging System (Thermo Fisher Scientific, Waltham, MA, USA), and its concentration was determined using the Pierce BCA Protein Assay Kit (Thermo Fisher Scientific, Waltham, MA, USA).

3.3. Biological Activity of Recombinant EGF

The EGF activity was determined by an in vitro assay using the A431 cell line. Ninety-six-well plates (2592, Corning, Corning, NY, USA) were used for seeding 2500 cells/well in DMEM plus 0.5% or 5% fetal bovine serum (FBS), which were treated with different EGF concentrations (0.1 nM, 1 nM, 10 nM, and 100 nM) for four days. No EGF was added to negative control. Cell viability was measured with AlamarBlue Cell Viability Reagent (Invitrogen, Waltham, MA, USA) in a Varioskan LUX Multimode Microplate Reader (Thermo Fisher Scientific, Waltham, MA, USA).

3.4. Selection of EGF-Binding Phages

Polystyrene high-binding microtiter plates (Costar) were coated with 100 µL of the EGF antigen at 10 µg/mL (eight wells) and incubated overnight at 4 °C. After three washes with phosphate-buffered saline (PBS) plus 0.1% Tween 20 (PBST), wells were blocked with

3% skimmed milk (Sigma-Aldrich, Burlington, MA, USA) in PBS (300 μ L/well) for one hour. Wells were washed three times with PBST and incubated at room temperature (RT) for two hours with 100 μ L of five-hundred times the library diversity diluted in 0.7% skimmed milk. The PBST was used to perform twenty washes (300 μ L/well). Two additional washes were conducted with PBS. Recombinant phage collection was undertaken through sequential steps of four types of elution following neutralization. (i) Triethylamine elution: 0.1 M triethylamine, pH 12.0 (100 μ L/well), for 10 min at RT, followed by neutralization with Tris-HCl 1 M pH 7.5 (100 μ L/well) for 5 min at RT. (ii) Glycine elution: 0.2 M glycine, pH 2.0 (100 μ L/well), for 10 min at RT, followed by neutralization with Tris-HCl 1 M pH 9.1 (100 μ L/well) for 5 min at RT. (iii) Ultrasound elution: after adding 100 μ L/well of PBS, wells were subjected to ultrasound (40 MHz of potency for 30 min). During the first three elutions, wells were washed twice with PBST and once with PBS (300 μ L/well each). (iv) TG1 strain elution: addition of the *E. coli* strain, TG1, in exponential phase of growing (100 μ L/well). This elution was performed after the three elutions described above. Simultaneously, the *E. coli* strain, TG1, was transduced with the three elutions and incubated at 37 °C for 30 min. Elutions were seeded in 2xYT plates plus 100 μ g/mL ampicillin and incubated at 37 °C, and at 250 rpm, overnight.

3.5. Enrichment of Positive Phages

Three biopanning rounds were carried out to enrich the phage pull in EGF binders. For the first round, all colonies from plates obtained from the four elutions were gathered in 15 mL of 2xYT medium with 100 μ g/mL ampicillin, and 5 mL was used to inoculate 50 mL of the same medium, which was incubated at 37 °C, and at 250 rpm, overnight. Next, the culture was diluted 10 times (500 mL) and grown until a OD_{600nm} of 2 was reached. Transduction with the helper phage M13KO7 was performed at a multiplicity of infection (MOI) of 20 at 37 °C for one hour (30 min static and 30 min at 50 rpm). Transduced bacteria were spun at 2000 $\times g$ for 15 min and diluted in 500 mL of 2xYT medium with 100 μ g/mL ampicillin, 50 μ g/mL kanamycin, and 1 mM IPTG for the amplification of recombinant phages at 28 °C, and at 250 rpm, overnight. Amplified phages were concentrated as previously described, for further testing against EGF. The second and third biopanning rounds were conducted in the same way, with a small variation in the final culture volume, from 500 mL to 200 mL.

3.6. Indirect ELISA for Detecting Positive Phage Clones

Polystyrene high-binding microtiter plates (Corning, Corning, NY, USA) were coated with 100 μ L of EGF at 5 μ g/mL and incubated overnight at 4 °C. After washing three times with PBS-0.1% Tween 20 (PBST), wells were blocked with 3% skimmed milk in PBS (300 μ L/well) for one hour at RT. Supernatants of individual clones, previously amplified, were added to the plate (200 μ L of supernatant) for two hours at RT. The M13KO7 phage was used as negative control. Three washes with PBST were performed, and the anti-M13 antibody (G8P) diluted 1:5000 in 3% skimmed milk was added for one hour at RT, followed by an anti-mouse antibody conjugated with horseradish peroxidase at the same dilution, time, and temperature. Plates were washed three times with PBST, and the reaction was visualized with a TMB kit solution (Thermo Fisher Scientific, Waltham, MA, USA). The reaction was stopped with 2.5 M sulphuric acid, and the absorbance was measured in a microplate reader (ES-20/80, BOECO, Hamburg, Germany) at 450 nm. Plates coated with a recombinant anti-EGFR antibody [45] (carrying the same SV5 and 6xHis tags as the recombinant EGF) at 10 μ g/mL and with 3% skimmed milk were used to elude the backgrounds of recombinant phages against the SV5 and histidine tags. Positivity was considered for an OD_{450nm} signal ≥ 0.8 for EGF, and for a signal from milk or the non-related protein that was three or more times lower than for EGF.

3.7. Sequencing

The DNA from clones in TG1 were purified using the GenElute Plasmid Miniprep Kit (Sigma-Aldrich, Burlington, MA, USA) and sequenced by Macrogen (Seoul, Korea). Sequences were analyzed using the CLC Genomics Workbench v.21 (QIAGEN Aarhus, Aarhus, Denmark).

3.8. Production of Selected Recombinant Anti-EGF Nanobodies

The genes coding the anti-EGF nanobodies were extracted from the pMAC phagemid with the restriction enzymes *NcoI/NotI* (New England Biolabs, Ipswich, MA, USA) and cloned in the expression vector pET22b with the same enzymes. Nanobody production was carried out as described above, for EGF.

3.9. Nanobody Purification

The anti-EGF nanobodies were also purified in two chromatographic stages. The first was with IEC, using the same serial connection of two columns described above. Both were equilibrated with half-diluted SMM9 medium. After sample loading in the same equilibrium buffer, each column was eluted separately, as explained previously. Buffer pH was also adjusted based on the theoretical isoelectric point of nanobodies, calculated as described above. The elution from the anion exchanger was diluted three times in water and further purified by IMAC, by adding the same amounts of imidazole as previously described. Fraction monitoring, diafiltering, sample analysis, nanobody purity, and concentration were performed as described above.

3.10. Nanobody Biotinylation

Nanobodies were diluted in 25-mM carbonate/bicarbonate buffer at a concentration around 1 mg/mL. Fifty microliters of biotin (H1759, Sigma-Aldrich, Burlington, MA, USA) at 10 mg/mL in DMSO was slowly added to nanobodies. The final molar ratio biotin:nanobody was 40:1. Reaction was stirred for six hours at RT, under protection from light. Free biotin was removed by dialyzing against PBS.

3.11. ELISA for Biotinylated Anti-EGF Nanobodies

Polystyrene high-binding microtiter plates (Corning, Corning, NY, USA) were coated with 100 μ L of rEGF at 5 μ g/mL and incubated overnight at 4 °C. After washing three times with PBS, 0.1% Tween 20 (PBST), wells were blocked with 3% skimmed milk in PBS (300 μ L/well) for 1 h at RT. Biotinylated nanobodies were serially diluted and incubated for one hour at RT. After washing, streptavidin conjugated to HRP (Biotechne R&D Systems, Minneapolis, MN, USA) diluted 1:200 was added for one hour at RT. The reaction was visualized, stopped, and measured, as described above. The KD estimation was carried out by following the method and fitting function described in [37]. A linear regression analysis using this function was performed using the MyCurveFit web server (<https://mycurvefit.com/>, last accessed on 4 May 2023).

Author Contributions: Conceptualization, A.G.-P. and E.M.; methodology, Y.S.-R., F.C.-C., O.S.-R., A.G.-P. and E.M.; investigation, Y.S.-R., J.S.-U., M.R.-C., F.C.-C., O.S.-R., A.G.-P. and E.M.; writing—original draft preparation, Y.S.-R., J.S.-U., M.R.-C., A.G.-P. and E.M.; writing—review and editing, Y.S.-R., F.C.-C., O.S.-R., A.G.-P. and E.M.; supervision, project administration and funding acquisition, E.M. All authors have read and agreed to the published version of the manuscript.

Funding: This research was funded by MINCIENCIAS, MINEDUCACIÓN, MINCIT and ICETEX through the Program NanoBioCancer (cod. FP44842-211-2018, project number 58676). A.G.-P. and E.M. thank the University of Medellin for its support.

Institutional Review Board Statement: Not applicable.

Informed Consent Statement: Not applicable.

Data Availability Statement: The data presented in this study are contained in the article tables.

Conflicts of Interest: The authors declare no conflict of interest.

Sample Availability: Not applicable. The phagemids and molecules used in this work were either purchased or produced in limited amounts to perform the reported experiments only.

References

1. Cohen, S.; Carpenter, G. Human Epidermal Growth Factor: Isolation and Chemical and Biological Properties. *Proc. Natl. Acad. Sci. USA* **1975**, *72*, 1317–1321. [[CrossRef](#)]
2. Singh, B.; Carpenter, G.; Coffey, R.J. EGF Receptor Ligands: Recent Advances. *F1000Research* **2016**, *5*, 2270. [[CrossRef](#)]
3. Mitsudomi, T. Molecular Epidemiology of Lung Cancer and Geographic Variations with Special Reference to EGFR Mutations. *Transl. Lung Cancer Res.* **2014**, *3*, 205–211. [[PubMed](#)]
4. Tahara, E.; Sumiyoshi, H.; Hata, J.; Yasui, W.; Taniyama, K.; Hayashi, T.; Nagae, S.; Sakamoto, S. Human Epidermal Growth Factor in Gastric Carcinoma as a Biologic Marker of High Malignancy. *Jpn. J. Cancer Res.* **1986**, *77*, 145–152. [[PubMed](#)]
5. Liu, T.-C.; Jin, X.; Wang, Y.; Wang, K. Role of Epidermal Growth Factor Receptor in Lung Cancer and Targeted Therapies. *Am. J. Cancer Res.* **2017**, *7*, 187–202. [[PubMed](#)]
6. Cheaito, K.; Bahmad, H.F.; Jalloul, H.; Hadadeh, O.; Msheik, H.; El-Hajj, A.; Mukherji, D.; Al-Sayegh, M.; Abou-Kheir, W. Epidermal Growth Factor Is Essential for the Maintenance of Novel Prostate Epithelial Cells Isolated from Patient-Derived Organoids. *Front. Cell Dev. Biol.* **2020**, *8*, 571677. [[CrossRef](#)]
7. Kalluri, R.; Weinberg, R.A. The Basics of Epithelial-Mesenchymal Transition. *J. Clin. Investig.* **2009**, *119*, 1420–1428. [[CrossRef](#)]
8. Heerboth, S.; Housman, G.; Leary, M.; Longacre, M.; Byler, S.; Lapinska, K.; Willbanks, A.; Sarkar, S. EMT and Tumor Metastasis. *Clin. Transl. Med.* **2015**, *4*, 6. [[CrossRef](#)]
9. Gonzalez, G.; Montero, E.; Leon, K.; Cohen, I.R.; Lage, A. Autoimmunization to Epidermal Growth Factor, a Component of the Immunological Homunculus. *Autoimmun. Rev.* **2002**, *1*, 89–95. [[CrossRef](#)]
10. Saavedra, D.; Crombet, T. CIMAvax-EGF: A New Therapeutic Vaccine for Advanced Non-Small Cell Lung Cancer Patients. *Front. Immunol.* **2017**, *8*, 269. [[CrossRef](#)]
11. García, B.; Neningen, E.; de la Torre, A.; Leonard, I.; Martínez, R.; Viada, C.; González, G.; Mazorra, Z.; Lage, A.; Crombet, T. Effective Inhibition of the Epidermal Growth Factor/Epidermal Growth Factor Receptor Binding by Anti-Epidermal Growth Factor Antibodies Is Related to Better Survival in Advanced Non-Small-Cell Lung Cancer Patients Treated with the Epidermal Growth Factor Cancer Vaccine. *Clin. Cancer Res.* **2008**, *14*, 840–846. [[CrossRef](#)] [[PubMed](#)]
12. Muyldermans, S. Nanobodies: Natural Single-Domain Antibodies. *Annu. Rev. Biochem.* **2013**, *82*, 775–797. [[CrossRef](#)] [[PubMed](#)]
13. Morrison, C. Nanobody Approval Gives Domain Antibodies a Boost. *Nat. Rev. Drug Discov.* **2019**, *18*, 485–487. [[CrossRef](#)]
14. Muyldermans, S. A Guide to: Generation and Design of Nanobodies. *FEBS J.* **2021**, *288*, 2084–2102. [[CrossRef](#)] [[PubMed](#)]
15. Valdés-Tresanco, M.S.; Molina-Zapata, A.; Pose, A.G.; Moreno, E. Structural Insights into the Design of Synthetic Nanobody Libraries. *Molecules* **2022**, *27*, 2198. [[CrossRef](#)] [[PubMed](#)]
16. Keam, S.J. Ozoralizumab: First Approval. *Drugs* **2023**, *83*, 87–92. [[CrossRef](#)] [[PubMed](#)]
17. Guardiola, S.; Varese, M.; Sánchez-Navarro, M.; Vincke, C.; Teixidó, M.; García, J.; Muyldermans, S.; Giralt, E. Blocking EGFR Activation with Anti-EGF Nanobodies via Two Distinct Molecular Recognition Mechanisms. *Angew. Chem. Int. Ed.* **2018**, *57*, 13843–13847. [[CrossRef](#)]
18. Guardiola, S.; Sánchez-Navarro, M.; Rosell, R.; Giralt, E.; Codony-Servat, J. Anti-EGF Nanobodies Enhance the Antitumoral Effect of Osimertinib and Overcome Resistance in Non-Small Cell Lung Cancer (NSCLC) Cellular Models. *Med. Oncol.* **2022**, *39*, 195. [[CrossRef](#)]
19. Contreras, M.A.; Serrano-Rivero, Y.; González-Pose, A.; Salazar-Urbe, J.; Rubio-Carrasquilla, M.; Soares-Alves, M.; Parra, N.C.; Camacho-Casanova, F.; Sánchez-Ramos, O.; Moreno, E. Design and Construction of a Synthetic Nanobody Library: Testing Its Potential with a Single Selection Round Strategy. *Molecules* **2023**, *28*, 3708. [[CrossRef](#)]
20. Haigler, H.; Ash, J.F.; Singer, S.J.; Cohen, S. Visualization by Fluorescence of the Binding and Internalization of Epidermal Growth Factor in Human Carcinoma Cells A-431. *Proc. Natl. Acad. Sci. USA* **1978**, *75*, 3317–3321. [[CrossRef](#)] [[PubMed](#)]
21. Kawamoto, T.; Sato, J.D.; Le, A.; Polikoff, J.; Sato, G.H.; Mendelsohn, J. Growth Stimulation of A431 Cells by Epidermal Growth Factor: Identification of High-Affinity Receptors for Epidermal Growth Factor by an Anti-Receptor Monoclonal Antibody. *Proc. Natl. Acad. Sci. USA* **1983**, *80*, 1337–1341. [[CrossRef](#)] [[PubMed](#)]
22. Anand, T.; Virmani, N.; Bera, B.C.; Vaid, R.K.; Vashisth, M.; Bardajaty, P.; Kumar, A.; Tripathi, B.N. Phage Display Technique as a Tool for Diagnosis and Antibody Selection for Coronaviruses. *Curr. Microbiol.* **2021**, *78*, 1124–1134. [[CrossRef](#)] [[PubMed](#)]
23. Rojas, G.; Pupo, A.; Gómez, S.; Krengel, U.; Moreno, E. Engineering the Binding Site of an Antibody against N-Glycolyl GM3: From Functional Mapping to Novel Anti-Ganglioside Specificities. *ACS Chem. Biol.* **2013**, *8*, 376–386. [[CrossRef](#)]
24. Hu, Y.; Lin, J.; Wang, Y.; Wu, S.; Wu, J.; Lv, H.; Ji, X.; Muyldermans, S.; Zhang, Y.; Wang, S. Identification of Serum Ferritin-Specific Nanobodies and Development towards a Diagnostic Immunoassay. *Biomolecules* **2022**, *12*, 1080. [[CrossRef](#)] [[PubMed](#)]
25. Hu, Y.; Zhang, C.; Lin, J.; Wang, Y.; Wu, S.; Sun, Y.; Zhang, B.; Lv, H.; Ji, X.; Lu, Y.; et al. Selection of Specific Nanobodies against Peanut Allergen through Unbiased Immunization Strategy and the Developed Immuno-Assay. *Food Sci. Hum. Wellness* **2023**, *12*, 745–754. [[CrossRef](#)]

26. Kaczmarek, J.Z.; Skottrup, P.D. Selection and Characterization of Camelid Nanobodies towards Urokinase-Type Plasminogen Activator. *Mol. Immunol.* **2015**, *65*, 384–390. [[CrossRef](#)]
27. Lakzaei, M.; Raseae, M.J.; Fazaeli, A.A.; Aminian, M. A Comparison of Three Strategies for Biopanning of Phage-scFv Library against Diphtheria Toxin. *J. Cell Physiol.* **2019**, *234*, 9486–9494. [[CrossRef](#)]
28. Kulpakko, J.; Juusti, V.; Rannikko, A.; Hänninen, P.E. Detecting Disease Associated Biomarkers by Luminescence Modulating Phages. *Sci. Rep.* **2022**, *12*, 2433. [[CrossRef](#)]
29. Lunder, M.; Bratkovič, T.; Urleb, U.; Kreft, S.; Štrukelj, B. Ultrasound in Phage Display: A New Approach to Nonspecific Elution. *Biotechniques* **2008**, *44*, 893–900. [[CrossRef](#)]
30. Donatan, S.; Yazici, H.; Bermek, H.; Sarikaya, M.; Tamerler, C.; Urgan, M. Physical Elution in Phage Display Selection of Inorganic-Binding Peptides. *Mater. Sci. Eng. C* **2009**, *29*, 14–19. [[CrossRef](#)]
31. Conrath, K.E.; Lauwereys, M.; Galleni, M.; Matagne, A.; Frère, J.-M.; Kinne, J.; Wyns, L.; Muyldermans, S. β -Lactamase Inhibitors Derived from Single-Domain Antibody Fragments Elicited in the *Camelidae*. *Antimicrob. Agents Chemother.* **2001**, *45*, 2807–2812. [[CrossRef](#)] [[PubMed](#)]
32. de Marco, A. Recombinant Expression of Nanobodies and Nanobody-Derived Immunoreagents. *Protein Expr. Purif.* **2020**, *172*, 105645. [[CrossRef](#)] [[PubMed](#)]
33. Amcheslavsky, A.; Wallace, A.L.; Ejemel, M.; Li, Q.; McMahon, C.T.; Stoppato, M.; Giuntini, S.; Schiller, Z.A.; Pondish, J.R.; Toomey, J.R.; et al. Anti-CfaE Nanobodies Provide Broad Cross-Protection against Major Pathogenic Enterotoxigenic Escherichia Coli Strains, with Implications for Vaccine Design. *Sci. Rep.* **2021**, *11*, 2751. [[CrossRef](#)] [[PubMed](#)]
34. Nagy-Fazekas, D.; Stráner, P.; Ecsédi, P.; Taricska, N.; Borbély, A.; Nyitray, L.; Perczel, A. A Novel Fusion Protein System for the Production of Nanobodies and the SARS-CoV-2 Spike RBD in a Bacterial System. *Bioengineering* **2023**, *10*, 389. [[CrossRef](#)] [[PubMed](#)]
35. Salema, V.; Fernández, L.Á. High Yield Purification of Nanobodies from the Periplasm of *E. coli* as Fusions with the Maltose Binding Protein. *Protein Expr. Purif.* **2013**, *91*, 42–48. [[CrossRef](#)]
36. Kariuki, C.K.; Magez, S. Improving the Yield of Recalcitrant Nanobodies® by Simple Modifications to the Standard Protocol. *Protein Expr. Purif.* **2021**, *185*, 105906. [[CrossRef](#)]
37. Eble, J.A. Titration ELISA as a Method to Determine the Dissociation Constant of Receptor Ligand Interaction. *J. Vis. Exp.* **2018**, *2018*, 57334. [[CrossRef](#)]
38. Cohen, L.; Walt, D.R. Evaluation of Antibody Biotinylation Approaches for Enhanced Sensitivity of Single Molecule Array (Simoa) Immunoassays. *Bioconjug Chem.* **2018**, *29*, 3452–3458. [[CrossRef](#)]
39. Haque, M.; Forte, N.; Baker, J.R. Site-Selective Lysine Conjugation Methods and Applications towards Antibody–Drug Conjugates. *Chem. Commun.* **2021**, *57*, 10689–10702. [[CrossRef](#)]
40. Wade, J.D.; Domagala, T.; Rothacker, J.; Catimel, B.; Nice, E. Use of Thiazolidine-Mediated Ligation for Site Specific Biotinylation of Mouse EGF for Biosensor Immobilisation. *Lett. Pept. Sci.* **2001**, *8*, 211–220. [[CrossRef](#)]
41. Ferguson, K.M.; Berger, M.B.; Mendrola, J.M.; Cho, H.-S.; Leahy, D.J.; Lemmon, M.A. EGF Activates Its Receptor by Removing Interactions That Autoinhibit Ectodomain Dimerization. *Mol. Cell* **2003**, *11*, 507–517. [[CrossRef](#)] [[PubMed](#)]
42. Kuo, W.-T.; Lin, W.-C.; Chang, K.-C.; Huang, J.-Y.; Yen, K.-C.; Young, I.-C.; Sun, Y.-J.; Lin, F.-H. Quantitative Analysis of Ligand-EGFR Interactions: A Platform for Screening Targeting Molecules. *PLoS ONE* **2015**, *10*, e0116610. [[CrossRef](#)] [[PubMed](#)]
43. Moutel, S.; Bery, N.; Bernard, V.; Keller, L.; Lemesre, E.; De Marco, A.; Ligat, L.; Rain, J.C.; Favre, G.; Olichon, A.; et al. NaLi-H1: A Universal Synthetic Library of Humanized Nanobodies Providing Highly Functional Antibodies and Intrabodies. *eLife* **2016**, *5*, e16228. [[CrossRef](#)] [[PubMed](#)]
44. Predonzani, A.; Arnoldi, F.; López-Requena, A.; Burrone, O.R. In Vivo Site-Specific Biotinylation of Proteins within the Secretory Pathway Using a Single Vector System. *BMC Biotechnol.* **2008**, *8*, 41. [[CrossRef](#)]
45. Cruz-Pacheco, A.F.; Monsalve, Y.; Serrano-Rivero, Y.; Salazar-Urbe, J.; Moreno, E.; Orozco, J. Engineered Synthetic Nanobody-Based Biosensors for Electrochemical Detection of Epidermal Growth Factor Receptor. *Chem. Eng. J.* **2023**, *465*, 142941. [[CrossRef](#)]

Disclaimer/Publisher’s Note: The statements, opinions and data contained in all publications are solely those of the individual author(s) and contributor(s) and not of MDPI and/or the editor(s). MDPI and/or the editor(s) disclaim responsibility for any injury to people or property resulting from any ideas, methods, instructions or products referred to in the content.



Engineered synthetic nanobody-based biosensors for electrochemical detection of epidermal growth factor receptor

Andrés F. Cruz-Pacheco^a, Yeison Monsalve^a, Yunier Serrano-Rivero^b, Julieta Salazar-Uribe^b, Ernesto Moreno^b, Jahir Orozco^{a,*}

^a Max Planck Tandem Group in Nanobioengineering, Institute of Chemistry, Faculty of Natural and Exact Sciences, University of Antioquia, Complejo Ruta N, Calle 67 No. 52-20, Medellín 050010, Colombia

^b Faculty of Basic Sciences, University of Medellín, Medellín 050026, Colombia

ARTICLE INFO

Keywords:
Nanobody
Biosensor
Electrochemical detection
Screen-printed electrode bioconjugation chemistry
XPS analysis

ABSTRACT

Two engineered synthetic nanobody-based nanobiocomposite platforms were developed for label-free electrochemical detection of the epithelial growth factor receptor (EGFR) biomarker. Screen-printed carbon electrodes (SPCE) were decorated either with NiO nanoparticles (NPs) or poly(thiophene acetic acid) (PTAA) to link the anti-EGFR nanobody (Nb) and form nanobiocomposites for detecting the EGFR biomarker by electrochemical impedance spectroscopy (EIS). The nanoarchitectures were prepared by in situ electrosynthesis of NiO NPs or PTAA layers at SPCEs. A modified version of the 9G8 Nb (Nb9G8m), specific for the EGFR (anti-EGFR), was designed and produced as the nanobiosensor bioreceptor. This Nb was engineered to provide a hexahistidine tag (6xHis-tag) and a lysine (Lys) dual functionality to form a (6xHis-tag)/Ni²⁺ or Lys/PTAA interface. The biosensing interfaces were characterized by field-emission scanning electron microscopy, energy-dispersive X-ray spectroscopy, X-ray photoelectron spectroscopy, cyclic voltammetry, and EIS. The nanobody/nanobiocomposite-based biosensors detected EGFR proteins in a linear range from 0.25 to 50 $\mu\text{g mL}^{-1}$ and 0.5 to 50 $\mu\text{g mL}^{-1}$, with limits of detection of 0.46 $\mu\text{g mL}^{-1}$ and 1.14 $\mu\text{g mL}^{-1}$, for NiO- and PTAA-based platforms, respectively. The biosensing platforms offer high simplicity, specificity, and selectivity to detect EGFR, but Nbs can be readily engineered to detect other (glycol)proteins. Finally, as a proof of concept, the EGFR was detected in several tumor cell lines, differentiating biomarker expression among them.

1. Introduction

In the early 1990s, a distinct type of antibody composed only of a pair of heavy chains was found in members of the camelid family [1]. The single binding domain of these unique camelid antibodies was termed “nanobody” (Nb), in correspondence with its size on the nanometric scale, with around 2.5 nm in diameter and 4 nm in height [2]. Compared with typical antibodies, the single-domain nature of Nbs makes molecular manipulation easy and facilitates the production of a large variety of formats in which the fusion with other protein domains or the chemical conjugation with different molecules finds many different applications [3].

The design and construction of Nbs offer considerable advantages over their naturally occurring antibody counterparts, including high performance in affinity, thermo-, and long term-stability, shorter production time, and production against a myriad of antigens. Remarkably,

on-demand engineered synthetic Nbs eliminate the need for animal immunization [4]. Furthermore, the intrinsic features of the Nb production and applications include the easy expression in bacteria and yeast because of the smaller size of a single immunoglobulin domain and the possibility of binding the target even at extreme pH conditions and high temperatures (80–92 °C) [5]. The high performance of novel Nb fragments can be exploited not only in the highly selective and sensitive biosensing development [6–8] but in prevention and diagnosis [9], enzymatic inhibition [10], as specific target molecules against Haptens [11], micro-organisms [12], T cell chimeric immunoreceptors [13], anti-idiotypic agents [14], antidote agents [15], and as signaling biomarkers and tumor treatment [16] using targeted NPs [17].

Modifying SPCEs with nanomaterials [18,19] and conducting polymers [20,21] to obtain tuned surface area for bioreceptor immobilization and improved electrochemical performance has received considerable attention in biosensing approaches. For example,

* Corresponding author.

E-mail address: grupotandem.nanobioe@udea.edu.co (J. Orozco).

<https://doi.org/10.1016/j.cej.2023.142941>

Received 22 December 2022; Received in revised form 20 March 2023; Accepted 10 April 2023

Available online 12 April 2023

1385-8947/© 2023 Elsevier B.V. All rights reserved.

rationally designed inorganic electrosynthesized metallic oxide NPs may contribute to massive bioreceptors immobilization but with proper orientation [22]. The metal chelate provided by coordination between the imidazole group in 6xHis-tag with the Ni^{2+} species existing in nickel oxide (NiO) nanostructures illustrates the highly oriented capture of bioreceptors, with shorter immobilization time compared to other methodologies. Besides, highly specific capture of the tagged bioreceptors occurs by the low abundance of naturally occurring histidine chains and the minimal interaction of other amino acid residues [23,24]. In contrast, amino-containing bioreceptors, including Nbs, can bind to chemical-activated carboxylic conducting polymer (FCPs) layers such as that from thiophenes through 1-ethyl(dimethylaminopropyl)carbodiimide (EDC)/N-hydroxysuccinimide (NHS) covalently coupling. The amide bond formation is straightforward but may lead to a random nanobody orientation [25]. Yet, several amino acid mutations or designed peptide tails can be added to favor a proper nanobody orientation, in which the binding site is exposed to the target.

EGFR is a transmembrane glycoprotein located at the cell surface, which plays an essential role as a target for antitumor strategies [26]. Abnormal levels can indicate the presence of some tumors of epithelial origin, such as CRC [27]. As the most prominent representative cell-surface receptor, the EGFR is crucial in external transducing signals through the membrane into the cell, controlling proliferation, differentiation, migration, and modulating apoptosis [28]. Different types of cancer have been associated with the hyperproliferation of cells by aberrant EGFR signaling due to overexpression or mutation [29]. Overexpression of EGFR has been associated with depth invasion of the tumor and, to a lesser extent, response to treatment [30]. Therefore, EGFR overexpression is one of the most critical cell events for identifying, initiating, and proliferating CRC [31].

This study used an anti-EGFR nanobody specially engineered for label-free electrochemical detection of the EGFR glycoprotein in two comparative assays based on the specific interaction of the Nbs at SPCE decorated with electrosynthesized NiO NPs or PTAA layers. The modification of SPCE surfaces through electrochemical potentiostatic methodologies made possible the easy and fast preparation of the interfaces to bind the anti-EGFR Nb. The anti-EGFR Nb was bio-conjugated with the Ni^{2+} ions in NiO via a metal chelate-based affinity bond in a highly oriented fashion, and the properties of the resultant nanocomposite-based platform were compared to that from the covalent linkage of the anti-EGFR Nb, engineered to favor proper orientation, to the exposed carboxyl groups of PTAA by the EDC/NHS chemistry. The nanostructured platforms and the anti-EGFR/EGFR binding event were studied in terms of morphology, chemical surface analysis, and electrochemical behavior. EGFR detection was followed by EIS upon different concentrations of EGFR-spiked buffers and several cell lines with variable levels of protein expressions.

2. Experimental procedures

The detailed procedure for obtaining and purifying the anti-EGFR Nb, structural and sequential characterization, and the procedures for the affinity tests with the antigen, are described in the [supporting information](#) (SI). In addition, the reagents and solutions used in all the tests, as well as the electrochemical, morphological, and chemical characterization by cyclic voltammetry (CV), EIS, field-emission scanning electron microscopy (FE-SEM), energy-dispersive X-ray spectroscopy (EDS) and X-ray photoelectron spectroscopy (XPS) of each stage of the platform nanoengineering are in the same section.

3. Results and discussion

3.1. Redesign of an anti-EGFR Nb for optimal nanosensor functionalization

An engineered version of the 9G8 (Nb9G8) nanobody [32], specific

for the EGFR, was designed and produced as a nanobiosensor bioreceptor. First, the amino acid sequence of Nb9G8 was modified to achieve a dual option to link it to the nanosensing platform by complexing a histidine tag to metal chelates covering the SPCE or covalently coupling amino groups in the protein to carboxyl groups from the PTAA interface. In addition, several amino acid mutations were introduced, and a specially designed peptide tail was added to the C-terminus of the nanobody to favor a proper nanobody orientation, in which the binding site is exposed to the target in the solvent ([Scheme. 1](#)).

Three lysine residues, each carrying a positively charged amino group, were introduced in the peptide tail to optimize the functionalization through chemical conjugation. One of these lysines is part of an SV5 tag, which was included to facilitate protein detection using a commercial antibody specific to this tag. Furthermore, to avoid chemical conjugations leading to unfavorable nanobody orientations, we decided to mutate every lysine residue in the nanobody that is not relevant for EGFR binding or structural integrity. The crystal structure of Nb9G8 in complex with the EGFR [33] was used for these structural analyses.

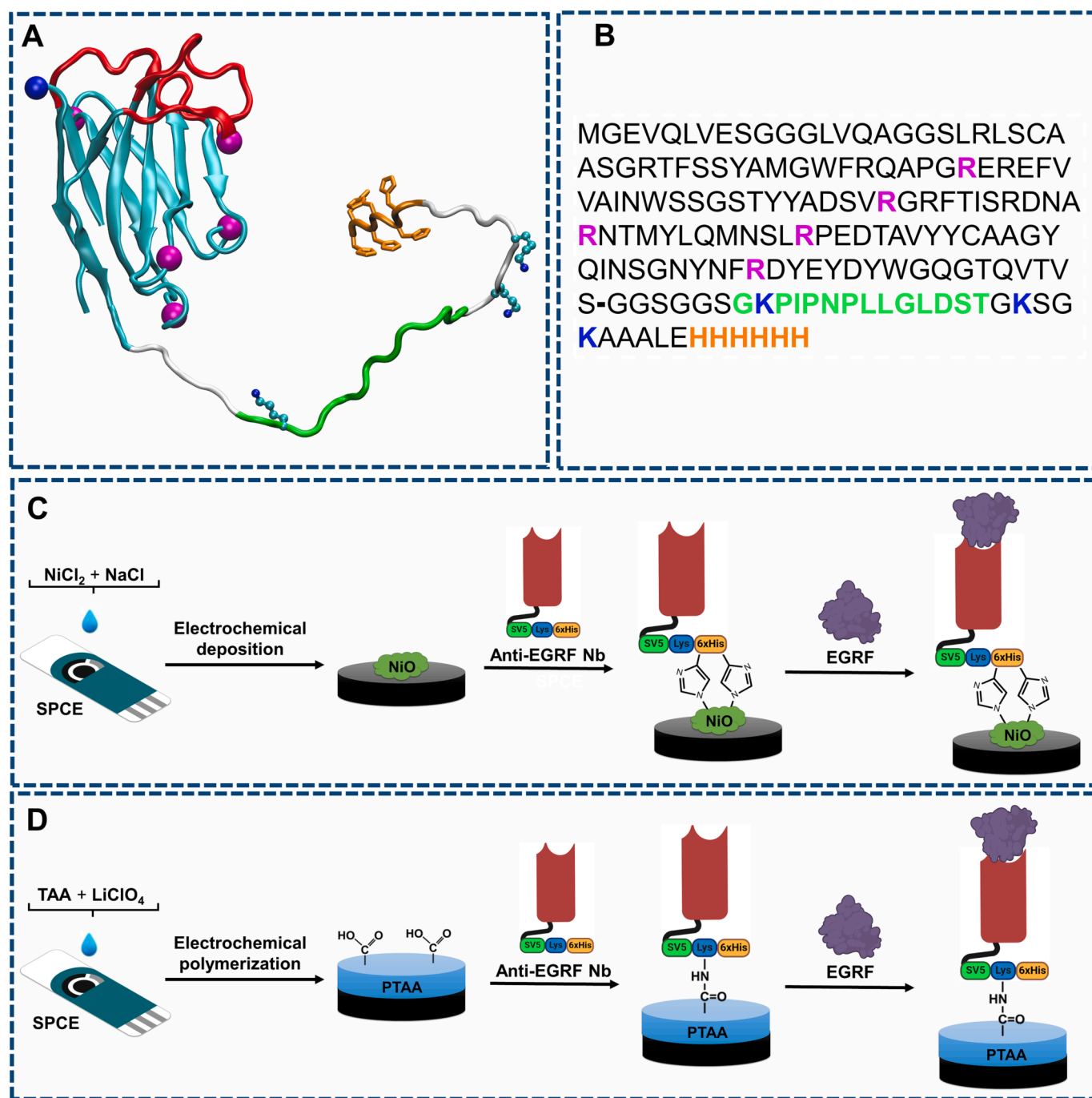
The hypervariable loops (CDRs) of Nb9G8 contain one lysine in CDR3, a loop that plays an important role in antigen binding. Nonetheless, the Nb9G8-EGFR complex structure shows that this lysine neither interacts with the receptor nor has a role in anchoring the CDR3 conformation. Therefore, it can be replaced with a similar residue, like arginine. On the other hand, the framework region shows four lysine residues, all with their side chain pointing to the solvent. The five lysine residues were then mutated to arginine, which has a similar size and carries a guanidino group that retains the positive charge provided by lysine. As a result, the engineered nanobody contains only four amino groups –one at the N-terminal residue (lateral to the binding site) and three in the C-terminal peptide tail.

Finally, the peptide tail was completed with a 6xHis tag encoded in the pET22b(+) expression vector after the Not-I restriction site was used for cloning. The His-tag at the C-terminus served for protein purification by metal ion affinity chromatography (IMAC) and as a linking point at the NiO/SPCE interface.

3.2. Expression and purification of Nb9G8m

Nb9G8m was successfully produced using an expression system composed of the plasmid pET22b-Nb9G8m ([Fig. S1A](#)) and the *E. coli* strain BL21 (DE3) as host. SDS-PAGE and Western-blot showed a protein band of around 17 kDa corresponding to the designed nanobody ([Fig. S1B](#)). The pET22 system, used before to produce recombinant Nbs [34,35], inserts a pelB signaling peptide for protein secretion to the bacterial periplasm, where the Nb disulfide bond can be formed correctly. However, overproduction of the recombinant protein tends to form inclusion bodies that incorporate misfolded molecules. To avoid this undesired effect and improve Nb9G8m solubility, we modified several parameters in the culture conditions, such as culture medium, inductor concentration, temperature, time, and stirring. Also, a physical cell disruption method was implemented based on freeze/thaw cycles to release Nb9G8m to the supernatant. As a result, the recovery of soluble Nb9G8m using the original culture conditions was negligible ([Fig. S1C](#)) compared to the optimized procedure, which yielded a more significant Nb9G8m soluble fraction ([Fig. S1D](#)).

The soluble fraction of Nb9G8m was subjected to a purification process. Initially, only one chromatographic step –IMAC– was performed since this chromatography usually renders the protein of interest with high purity [36]. In this case, however, it was not enough (results not shown). Therefore, Nb9G8m purification was carried out, starting with an IEC chromatographic step, followed by IMAC. This way, the anion exchanger eliminated a significant quantity of contaminant proteins, while Nb9G8m bound to the cation exchanger with fewer contaminants ([Fig. S1E](#)), which were subsequently removed in the IMAC step. This chromatographic procedure yielded the Nb with high purity (>90%), with minor losses in the unbound protein and wash fractions



Scheme 1. Redesign of Nb 9G8 and coupling to the nanobiosensor surface. A) Structural model of the engineered nanobody. The protein backbone is shown in a cyan cartoon representation, with the three CDRs colored red. The N-terminus (carrying an amino group) is marked with a blue sphere, while the five positions mutated from Lys to Arg are marked with spheres in magenta. The C-terminal tail is colored in light gray, with the SV5 and 6xHis tags in green and orange, respectively, and the histidine side chains shown as sticks. The three lysines in the C-terminal tail are represented in balls and sticks. The C-terminal tail is very flexible, so the figure shows one possible conformation arbitrarily chosen among an ensemble of conformations produced by the MODPED server. B) Amino acid sequence of the engineered nanobody. The mutated positions are highlighted in magenta, while the three lysines in the C-terminal tail are marked in bold blue. The SV5 and 6xHis tags are highlighted in green and orange, respectively. C,D) Schematic illustration of the modification of SPCE with C) BSA/anti-EGFR/NiO nanobiocomposite and D) BSA/anti-EGFR/PTAA to detect EGFR protein. NiCl₂, nickel chloride; NaCl, sodium chloride; NiO, nickel oxide; anti-EGFR Nb, epidermal growth factor receptor Nb; SV5Tag, SV5 peptide; Lys, lysine; 6xHis, 6 histidines tag; EGRF, epidermal growth factor receptor; TAA, thiophene acetic acid; LiClO₄, lithium perchlorate; PTAA, poly(thiophene acetic acid).

(Fig. S1F).

3.3. Characterization of nanostructured platforms

The methodologies used to immobilize the anti-EGFR Nb at SPCE

were designed based on the functionalities generated by protein engineering. The electrochemical nanobiosensors developed with the nanostructured SPCEs for detecting the EGFR protein by EIS are shown in Scheme 1. First, Ni NPs were electro synthesized in situ in the presence of NaCl as a supporting electrolyte in the electrochemical reduction of

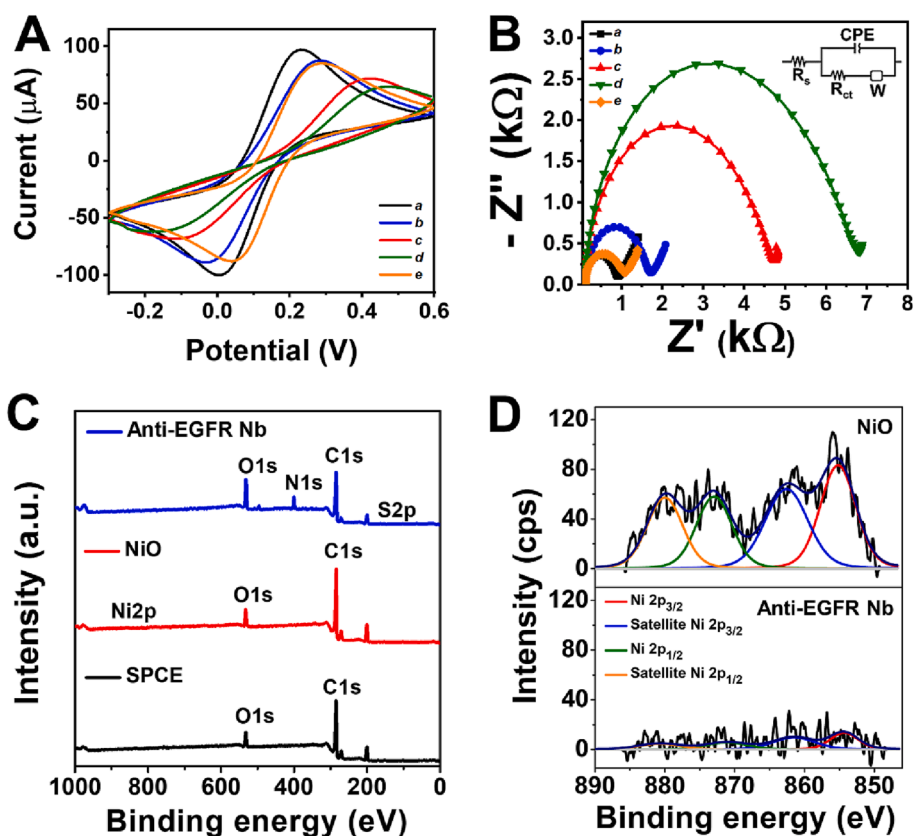


Fig. 1. A) CV and B) EIS response at each step of SPCE modification for NiO-based platform recorded in a 1X PBS pH 7.4 solution containing 5 mM $[\text{Fe}(\text{CN})_6]^{3-/4-}$: a) bare SPCE, b) NiO, c) anti-EGFR Nb, d) BSA and e) EGFR ($50 \mu\text{g mL}^{-1}$). C) Survey spectra for each step of the NiO-platform assembly. D) Corresponding Ni2p core level spectra for NiO bio-conjugation.

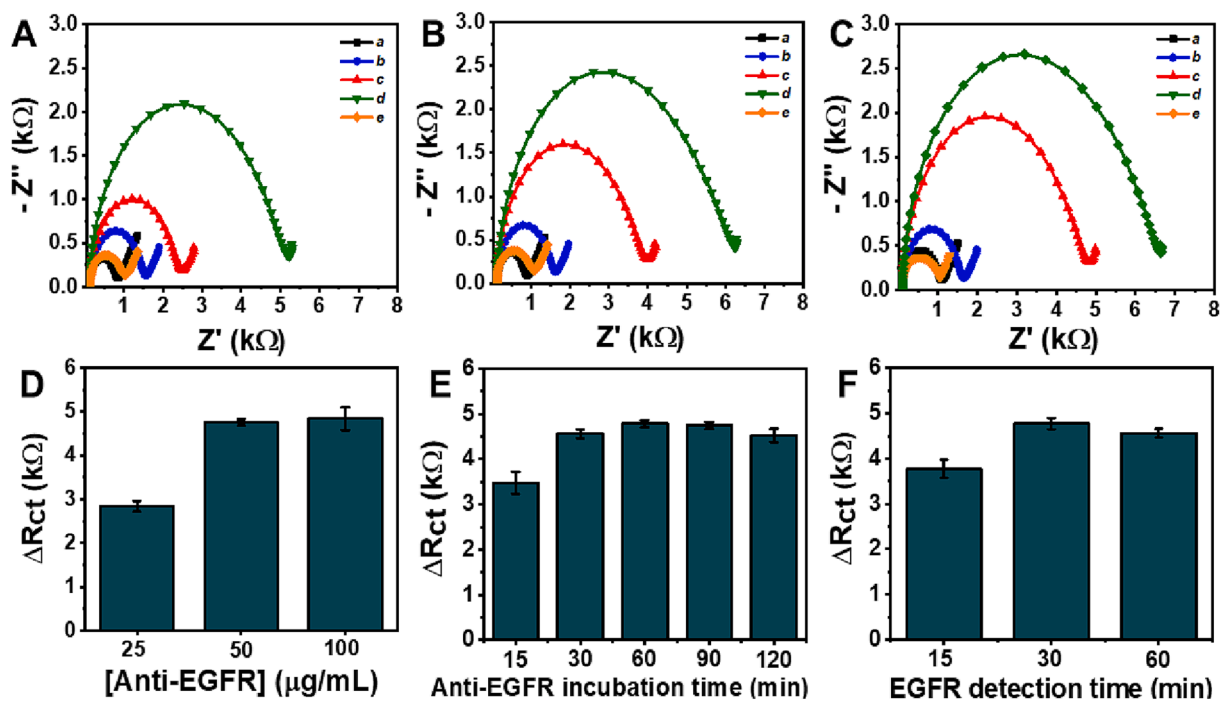


Fig. 2. Optimization of the anti-EGFR nanobody concentration on the NiO-based biosensor: a) bare SPCE, b) NiO NPs, c) anti-EGFR Nb, d) BSA, and e) EGFR for A) 25, B) 50, and C) 100 $\mu\text{g mL}^{-1}$. The histograms show D) the summary and quantification of the ΔR_{ct} for the anti-EGFR concentration experiment, E) the anti-EGFR incubation time, and F) the EGFR incubation time. Error bars indicate the standard deviation of duplicate measurements.

the Ni salt (Fig. S2A) by the “H₂ coevolution method”, i.e., the reduced Ni on the graphitic surface of the SPCE serves to catalyze the evolution of H₂ at the applied reduction potential, producing visible bubbles that act like a blockage in the growth stages of Ni NPs [37]. NiO NPs were obtained by electrochemical oxidation of Ni in phosphate buffer (10X PB, pH 7.4) by CV, as shown in Fig. S2B. We can notice two pronounced oxidation and reduction peaks characteristic of Ni oxidation at pH 7.4, which decreased with the number of cycles [38]. The electrochemical oxidation was stopped after 40 CV cycles since almost stable response curves were obtained. The concentration of NiCl₂ was tested from 5 to 15 mM. However, 10 mM NiCl₂ was selected as the optimal concentration in agreement with previous works [37] since the electrochemical response by CV and EIS (Fig. S2C and D) was very similar in all concentrations. Therefore, this effect corroborated the controlled electrodeposition of Ni by using H₂ bubbles as blocking agents [37]. The morphology and elemental composition of the nanostructured NiO and PTAA platforms were characterized by FE-SEM and EDS. Fig. S3A and S3B show the FE-SEM images of electrodeposited NiO NPs on SPCE. Image analysis with the ImageJ software revealed that the NPs had a size of 56 ± 7 nm ($n = 60$), and the surface coverage was 0.57 %. The EDS analysis was performed at various points on the surface of the working electrode and confirmed the presence of nickel (26 %) and oxygen (74 %), associated with the NiO NPs formation.

The architecture of the PTAA-based nanobiosensor is shown in Scheme 1B. The PTAA film was electrosynthesized on SPCE in the presence of the perchlorate (ClO₄⁻) counterion to compensate for the monomer-positive charges. Electropolymerization of TAA monomer was carried out at a fixed potential of + 1.1 V to generate the radical, cationic species TAA^{•+} involved in the nucleation and growth processes of the PTAA polymer chain [39]. Different values of electric charge involved in the potentiostatic polymerization of the PTAA layer were evaluated to achieve an interface with a high density of carboxylic acid groups, as shown in Figs. S4 and S5. The synthesis of PTAA up to an electrical charge of 600 μC was selected to form a stable film with a high density of carboxyl groups, ideal for bioconjugation processes and without causing damage by overoxidation as occurred with polymerization carried out

up to 1200 μC.

3.4. Assembly and characterization of the biosensing interface

The investigation of electrochemical interfacial properties of NiO- or PTAA-based platforms and assembly of the detection assay using anti-EGFR Nb coupled to the nanostructures was performed by CV and EIS, as shown in Fig. 1A-B and S6A-B. Each SPCE modification step was followed by the electroactive area (A_e) calculated with the Randles-Sevcik equation shown in SI-Eq 1 and summarized in Table S1 and S2. The cyclic voltammograms in Fig. 1A show quasi-reversible peaks with constant anodic and cathodic peak separations at all stages of biosensor assembly.

First, the successful electrodeposition of NiO NPs was corroborated by the decreased A_e of the NiO interface (10.3 mm²) compared to the bare SPCE (13.2 mm²) due to the semiconducting properties of the NiO NPs [40]. After immobilizing the anti-EGFR Nb on the NiO NPs, the A_e decreased to 5.1 mm², demonstrating the effective coupling between the 6xHis tag of the Nb and the NiO NPs. The Nb-metal ions affinity interaction was generated through the coordination of the Ni²⁺ cations of NiO with the free nitrogen electrons of the imidazole ring in His to orient the Nb. Remarkably, at pH values < 6.0, the imidazole groups of histidine involved in the coordination bond can be protonated and prevent the union of Nb with NiO NPs [41]. Therefore, electrochemical measurements were performed in 1X PBS pH 7.4 solution containing 5 mM [Fe(CN)₆]^{3-/4-}. The A_e decreased to 4.0 mm² due to the insulating nature of bovine serum albumin (BSA) used as a blocking agent to prevent non-specific adsorption in the detection steps. The CV results demonstrated the customized assembly of an engineered Nb-based bio-interface using a simple and fast methodology without additional bioconjugation steps compared to the PTAA-based platform, which requires activation of carboxylic acid groups with EDC/NHS chemistry, as discussed in the SI. Finally, the effective immunoreaction between EGFR and the BSA/anti-EGFR/NiO/SPCE-based nanobiosensor showed an increase in A_e up to 11.3 mm² due to the high amount of N-glycosylation in the EGFR structure. N-glycosylation contributes up to 50 kDa to the total

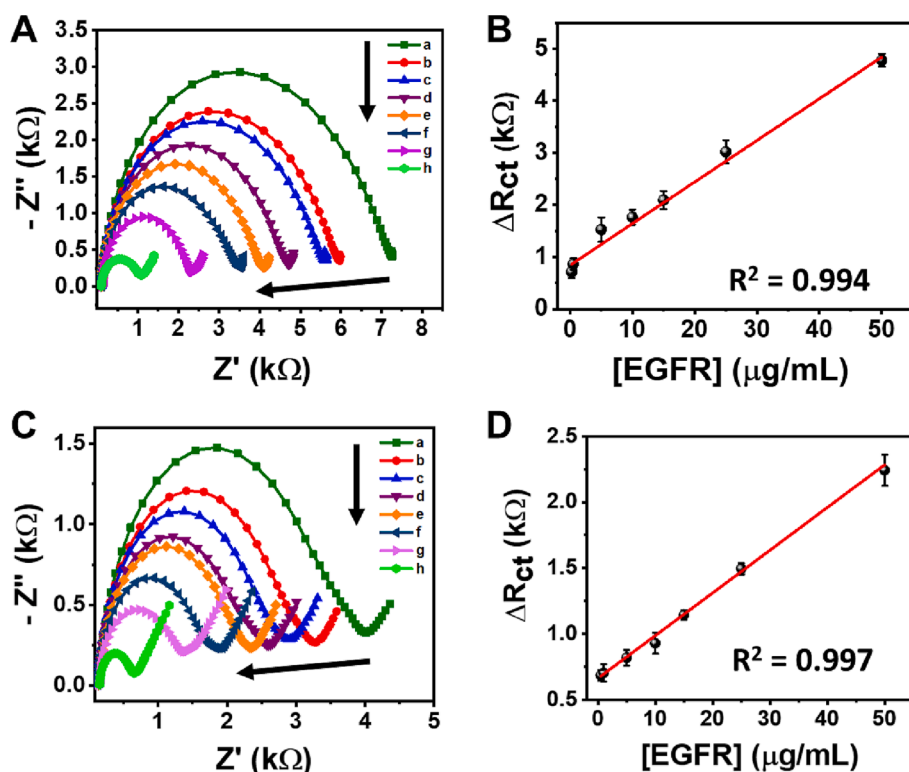


Fig. 3. A) EIS signals acquired from the label-free electrochemical NiO-based biosensor upon different EGFR concentrations, i.e., (a-h) 0, 0.25, 0.5, 5, 10, 15, 25, and 50 μg mL⁻¹ EGFR. B) Resultant linear regression curve of ΔR_{ct} upon different concentrations of EGFR. C) EIS signals acquired from the label-free electrochemical PTAA-based biosensor upon different EGFR concentrations, i.e., (a-h) 0, 0.5, 1, 5, 10, 15, 25, and 50 μg mL⁻¹ EGFR. D) Resultant linear regression curve of ΔR_{ct} upon different concentrations of EGFR.

molecular weight of the extracellular domain of the EGFR (~110 kDa) [42]. Furthermore, in the molecular probe used here, the extracellular domain of the EGFR is fused to an antibody Fc fragment, which contributes two additional N-glycosylation sites. Therefore, the partially neutral charge of the target enhanced the diffusion of the redox probe towards the electrode surface, and the detection was correlated with the A_e increase by CV.

The biosensors' effective architecture and target detection were confirmed by EIS, monitoring the resistance to electron transfer in the NiO- and PTAA-based platforms. Fig. 1B and S6C-D show the Nyquist diagrams derived from EIS, where the impedance data was presented in a complex plane with the real part (Z') plotted on the x-axis and the imaginary part ($-Z''$) plotted on the y-axis [43]. The EIS spectra were fitted using Randles equivalent circuit for electron transfer reactions with mass transfer control at low frequencies (ω), inserted in Fig. 1B. The equivalent circuit consists of a solution resistance (R_s), a charge transfer resistance (R_{ct}), and a constant phase element (CPE). $CPE = -1/(i\omega C)^n$ for a non-ideal capacitor, where n is the exponent of the CPE (1 for a pure capacitor and 0.5 for non-uniform and rough surfaces). Z_w represents the Warburg impedance for diffusion-controlled processes of the species in solution and corresponds to a straight line in the complex plane plots [43].

Table S2 summarizes the calculated data from the EIS analysis. The R_{ct} of NiO NP-modified SPCE increased to $1526.8 \pm 113.4 \Omega$ compared to bare SPCE ($R_{ct} = 743.8 \pm 76.2 \Omega$), supporting the CV results for efficient NiO electrosynthesis. Immobilization of anti-EGFR Nb on the NiO NPs was verified from an increased semicircle in the Nyquist plot with an R_{ct} of $4374.9 \pm 57.9 \Omega$. Such an increase is due to hindered electron transfer from the redox probe at the Nb-coated platform. The free sites not covered with Nb were blocked with BSA, and the insulating nature of this biomolecule produced an increase in R_{ct} equal to $6262.4 \pm 74.2 \Omega$. These results confirmed the simple and fast assembly process of the synthetic Nb-based nanobiosensor on NiO NPs like the CV analysis. The significant decrease in R_{ct} confirmed the immunocomplex formation to $773.4 \pm 15.4 \Omega$. This result corroborated the successful molecular biorecognition event since the glycosylated EGFR decreased the difficulty of the redox probe to diffuse toward the electrode surface. The PTAA-based biosensor assembly described in the SI showed similar electrochemical responses to the NiO-based platform and the EGFR target biosensing with decreased R_{ct} . In this way, the activity of the anti-EGFR Nb synthesized *in vitro* for binding with EGFR was demonstrated electrochemically, considering the chemical properties of each biomolecule.

In addition, XPS analysis was used to study the mechanism of surface nanostructuring and anti-EGFR Nb binding in the assembly of NiO-NPs and PTAA-based biosensors. XPS analysis of the PTAA-based biosensor assembly was detailed in Figs. S7A-H. The survey spectra in Fig. 1C show the evolution of signals for C1s, O1s, and Ni2p in the NiO NP-modified SPCE. Besides, the emergence of signals for N1s and S2p after Nb immobilization. Fig. 1D shows the high-resolution spectra of the Ni2p core level corresponding to the electrochemically synthesized NiO NPs on SPCE. The Ni2p spectral line showed a multiplet division with two key components at 855.2 eV and 872.9 eV with satellite peaks at 862.6 eV and 880.0 eV corresponding to Ni2p_{3/2} and Ni2p_{1/2}, respectively. The splitting peak separation (ΔE) was 17.7 eV. Since the peak position of Ni2p line cannot be assigned to a single chemical state, the range of energies of each component is associated with Ni²⁺ in NiO or Ni(OH)₂ [44]. This result was supported by the analysis of the core level spectrum of O1s shown in Fig. S8A, which presents a component at 531.6 eV assigned to lattice oxygen in NiO. Likewise, the components at high binding energies are attributed to OH groups, possibly due to the spontaneous hydroxylation of the Ni surface and carboxylates present in SPCE [44]. The components in the O1s spectrum at 532.4 and 533.5 eV and in the C1s spectrum (Fig. S8B) at 284.5, 286.2, and 289.0 eV for C-(C,H), C-O and (C = O)-OH bonds, respectively, were associated with the graphitic carbon of the NiO NPs uncoated working electrode, as

evidenced in the FE-SEM images in Fig. S2. The effective immobilization of anti-EGFR Nb on NiO NPs was clearly evidenced by the decrease in intensity of the Ni2p spectral line shown in Fig. 1D. The emerging peaks in the high-resolution spectra of O1s, C1s, N1s, and S2p (Figs. S8C-F) show the typical signals of the peptide bond and the amino acid residues present in the primary structure of the Nb attached to the NiO NPs. Thus, the components at 532.7 eV in O1s, 588.3 eV in C1s, and 400.2 eV in N1s were attributed to the amide bond ((C = O) - NH) [45]. C - S bond in the cysteine and methionine residues of Nb was observed at 286.5 eV in the C1s spectrum, and the new doublet peaks of the S2p spectrum at 163.9 and 165.4 eV. A small component of 534.8 eV in O1s was related to OH groups in the protein chain.

The biofunctionalization of NiO or PTAA nanostructures with anti-EGFR Nb were differentiated in the N1s spectra of both platforms. For example, the N1s spectrum (Fig. S8E) of Nb coupled to the NiO platform shows a small component at 402.2 eV corresponding to terminal amines (C - NH₃⁺) of free lysines, which were protonated under the vacuum conditions of the XPS analysis [44]. In contrast, Fig. S7E shows the N1s core level spectrum of the Nb-PTAA-based platform with a component at 398.4 eV related to the C=N bond of free imidazole ring and a signal at 402.4 eV, probably from the free protonated imidazole ring (C=NH⁺-) in the 6xHis tag. Therefore, XPS analysis corroborated the effective bioengineering of the synthetic Nb for proper bioconjugated chemistry in biosensor development.

3.5. Optimization of experimental parameters involved in EGFR detection

To compare how the moieties generated at the nanobody and the two approaches to immobilize them at the SPCE through the 6x-his-tag or Lys residues at the C-terminal tail impact the analytical performance of the nanocomposite biosensing interfaces, we first optimized the binding conditions. For example, we studied the optimal concentration of anti-EGFR Nb and incubation time on the NiO and PTAA nanostructures and the optimal incubation time for the EGFR glycoprotein. A higher ΔR_{ct} value between $R_{ct}(BSA)$ and $R_{ct}(EGFR)$ containing $50 \mu\text{g mL}^{-1}$ of EGFR was taken as a criterion to select the optimal values in both the NiO-based and PTAA-based platforms described in the S.I. First, 25, 50, and $100 \mu\text{g mL}^{-1}$ of anti-EGFR Nb were incubated on the surface of NiO-NPs-modified SPCE for 90 min to obtain the optimal concentration for EGFR detection (Fig. 2A-D). Immobilization of 50 and $100 \mu\text{g mL}^{-1}$ of anti-EGFR Nb resulted in an ΔR_{ct} of $4745.7 \pm 75.9 \Omega$ and $4830.1 \pm 255.9 \Omega$, respectively, compared to the lowest ΔR_{ct} value for $25 \mu\text{g mL}^{-1}$ ($2835.8 \pm 125.4 \Omega$). Therefore, a concentration of $50 \mu\text{g mL}^{-1}$ provided a sufficiently dense surface of Nbs to maximize interaction with EGFR.

Anti-EGFR Nb immobilization for 15, 30, 60, 90, and 120 min were evaluated (Fig. S9). Immobilization of anti-EGFR Nb for 15 min ($3475.8 \pm 246.9 \Omega$) was insufficient. However, 30 ($4566.1 \pm 99.6 \Omega$), 60 ($4783.6 \pm 84.4 \Omega$), 90 ($4745.7 \pm 75.9 \Omega$), and 120 min ($4523.1 \pm 147.9 \Omega$) were not statistically significantly different (Fig. 2E). Therefore, 30 min was optimal for the 6xHis-tag/Ni²⁺ coordinated bond formation. Finally, optimization of the interaction times of EGFR with the assembled biosensors is shown in Fig. 2F and S10. Immune complex formation on the electrode surface was insufficient in only 15 min of reaction ($3775.9 \pm 201.3 \Omega$) compared to 30 and 60 min, with ΔR_{ct} values of $4778.1 \pm 122.6 \Omega$ and $4566.1 \pm 99.6 \Omega$, respectively. Whereby 30 min was chosen as the optimal EGFR detection time to evaluate the analytical performance of the biosensor. In the same sense, the optimal conditions to detect EGFR on the PTAA-based biosensor required immobilizing $50 \mu\text{g mL}^{-1}$ for 60 min of anti-EGFR Nb on the activated carboxylic acids of the PTAA interface, as shown sequentially in the Figs. S11-13. Likewise, the EGFR biosensing time took 60 min, possibly because a fraction of the anti-EGFR Nb may have bound to PTAA through the amino group in the N-terminal residue, causing the antigen-Nb affinity interaction to be slightly delayed in comparison with the highly oriented NiO NPs-based biosensor.

3.6. Analytical performance

We evaluated the analytical performance of both biosensor platforms under optimized conditions by EIS in 1X PBS containing 5 mM [Fe(CN)₆]^{3-/4-}. The detection with increasing concentrations of EGFR generated decreased R_{ct} due to the partially neutral charge of the immunocomplex, which promotes the diffusion of the redox probe toward the electrode interface, as explained above. Fig. 3 shows the calibration curves of NiO NPs and PTAA-based biosensor platforms by estimating the ΔR_{ct} for the different solutions with known EGFR concentrations. The linear correlation between ΔR_{ct} and the EGFR glycoprotein concentration of the NiO NP-based platform in a range of 0.25 to 50 $\mu\text{g mL}^{-1}$ exhibited a linear regression equation expressed as $\Delta R_{ct} = 79.89[\text{EGFR}] + 842.47$ with a correlation coefficient $R^2 = 0.994$ (Fig. 3B). Meanwhile, Fig. 3D shows the detection of EGFR on the PTAA-based platform in a linear range between 0.5 and 50 $\mu\text{g mL}^{-1}$ with an equation described as $\Delta R_{ct} = 32.39[\text{EGFR}] + 663.72$ and an $R^2 = 0.997$. The limit of detection (LOD = 3SD/slope), the limit of quantification (LOQ = 10SD/slope), and sensitivity ($S = \text{slope}/A_e$) were calculated taking into account the standard deviation (SD) for R_{ct} (BSA), the slope of the calibration curves and the A_e for each assembled platform. The LOD, LOQ, and sensitivity of the NiO NPs-based platform were 0.46 $\mu\text{g mL}^{-1}$, 1.55 $\mu\text{g mL}^{-1}$, and 19.97 $\Omega \mu\text{g}^{-1} \text{mL mm}^{-2}$, respectively, using an SD of 12.41 Ω ($n = 10$) for measurements in the absence of EGFR protein. Similarly, the PTAA-based platform presented analytical performance with a LOD, LOQ, and sensitivity of 1.14 $\mu\text{g mL}^{-1}$, 3.87 $\mu\text{g mL}^{-1}$, and 5.68 $\Omega \mu\text{g}^{-1} \text{mL mm}^{-2}$, respectively, with an SD of the blank signal of 12.32 Ω ($n = 10$). LOD and LOQ of the NiO-NPs platform were lower than those from PTAA. This could be explained by the conformational freedom of the immobilized Nb through the 6xHis-tag that adopts a more upright, end-on orientation with better flexibility and provides closer packing, resulting in a higher surface area accessible to the target [46], compared to covalent immobilization of Nbs via the Lys-tag, which may reduce bioreceptor flexibility on the surface that hampers interaction with EGFR. The methods were reproducible with a relative standard deviation (RSD) below 5% for EGFR detection using three replicate assays for all concentrations tested. Additionally, Fig. S14 shows the Nyquist spectra with high inter-device reproducibility assembled on the SPCEs at optimal conditions with RSD of 1.6 and 2.3 % for the NiO NPs and PTAA-based platforms, respectively.

In the same fashion, we constructed an enzyme-linked immunosorbent assay (ELISA) adsorbing different known concentrations of EGFR onto a 96-well plate and using an anti-SV5 antibody (anti-SV5 Ab) coupled with horseradish peroxidase (HRP) to support the impedimetric results and test the SV5 tag (SV5tag) in the C-terminal region of the Nb. Fig. S15 shows the ELISA with a linear regression equation expressed as Absorbance = 0.78[EGFR] + 0.10 and an $R^2 = 0.984$, with a blank SD equal to 0.003 ($n = 10$). The LOD and LOQ of the ELISA were 10 ng mL^{-1} and 40 ng mL^{-1} , respectively. Including an SV5 or equivalent tag as part of a C-terminal tail is a useful feature that may be implemented in engineered nanobody-based biosensors. In this context, bioengineering of the 6xHis-, Lys-, and SV5- tags added to the C-terminal part of the engineered Nb was confirmed.

Table S3 compares the analytical performance of nanostructured platforms based on the engineered Nb with the ELISA assay and other biosensors described for EGFR detection. Although the LODs achieved in the nanostructured platforms are not as low as those reported by other authors or the ELISA, the platforms based on NiO-NPs and PTAA offered adequate sensitivity for detecting tumor cells with surface-expressed EGFR, without any further purification, as demonstrated below. Other inherent advantages of the NiO NP-based platform developed with the engineered Nb were the time required to prepare the biosensor (1 h) and the assay time of 30 min required for effective target interaction. Overall, the on-demand engineered Nb demonstrated a versatile approach to orient these bioreceptors at the surface of nanoarchitectures with a similar working linear range. The NiO-based nanobiocomposite

had a 2.5-fold lower LOD concerning the PTAA-based interface due to a possible better orientation when coupling through NiO NPs. In addition, it highlights the benefits of the unique assembly from on-demand designed Nbs. On the other hand, natural Nb-based approaches using signaling systems such as Förster resonance energy transfer (FRET) or fluorescent signaling systems take > 1 h to detect the target [47,48]. In this way, the simple, fast, and portable detection on the SPCE decorated with the nanobiocomposite proved suitable for developing miniaturized systems compatible with the point-of-care concept.

3.7. Specificity and selectivity

The specificity and selectivity of the nano-biosensors were tested with different biomolecules that could interfere with the EGFR protein determination. Therefore, we evaluated the potential cross-reactivity of the EGFR protein to carcinoembryonic antigen (CEA), p53 antigen, and IgG antibody (IgG). Notably, the IgG antibody contains the same type of Fc moiety in the fusion EGFR-Fc protein used here as the probe.

The interfering species were measured ten times more concentrated than the target to corroborate the reliability of the assay. Fig. 4 shows the impedimetric response assays for the two platforms in the presence of the three possible interferents at 5 $\mu\text{g mL}^{-1}$, the mix of them, and the mix with 0.5 $\mu\text{g mL}^{-1}$ target. Fig. 4A and 4C show the Nyquist plot from EIS measurements and the corresponding ΔR_{ct} . The results in Fig. 4B and 4D show that the ΔR_{ct} expressed in Ω was higher for the EGFR protein (861.85 \pm 110.45 and 685.89 \pm 40.76 Ω) and EGFR protein and the mix (853.17 \pm 111.56 and 771.33 \pm 39.83 Ω) compared to CEA (56.81 \pm 53.03 and 115.17 \pm 18.98 Ω), p53 (105.17 \pm 35.63 and 132.58 \pm 18.57 Ω), IgG (57.85 \pm 76.44 and 112.85 \pm 17.89 Ω) and the mix (85.52 \pm 49.26 and 163.23 \pm 52.57 Ω), for the NiO- and PTAA-based platforms, respectively. In addition, the ΔR_{ct} signal for the EGFR protein showed significant statistical differences when compared with the blank and the other proteins tested individually or mixed, with a level of statistical significance of 95% ($p < 0.05$). These results indicate that the biosensor was highly selective and specific for EGFR protein detection.

3.8. EGFR detection in the whole cancer cell membrane

As proof of concept, both platforms were tested with cell lines expressing different levels of EGFR in the membrane. Fig. 5A and 5C show the Nyquist diagrams of the biosensors incubated with each cell line (1×10^6 cell mL^{-1}). The impedimetric signals show a clear differentiation and hierarchy among cell lines in both platforms, with a decrease in the R_{ct} signal caused by the glycosylations on the cell surface. Fig. 5B and 5D show the adjustment value for the ΔR_{ct} of the different cell lines. A higher level of EGFR expression was evidenced in A431 cells, followed by the SW480, SW620, and the HEK293 cell line used as control. This result agrees with previous reports since the A431 cell line, isolated from an epidermoid carcinoma, expresses abnormally high levels of EGFR and is a standard positive control for EGFR expression [49]. Likewise, the SW480 and SW620 cell lines derived from a colon adenocarcinoma and a lymph node metastasis showed a higher ΔR_{ct} than the normal HEK293 cells used as non-neoplastic control [50–52]. This effect is consistent with previous reports [53], in which EGFR overexpression is found in CRC cell lines, particularly in SW480 (stage II) cell lines where membrane receptors are crucial for abnormal cell proliferation.

4. Conclusions

We successfully developed two nanostructured platforms based on NiO NPs and PTAA for the specific binding of an engineered anti-EGFR nanobody as a molecular recognition element in label-free impedimetric detection of the EGFR glycoprotein. The amino acid sequence of the Nb was engineered to provide a 6xHis-tag and a Lys dual functionality to link it to the nanosensing platform by complexing to metal chelates or

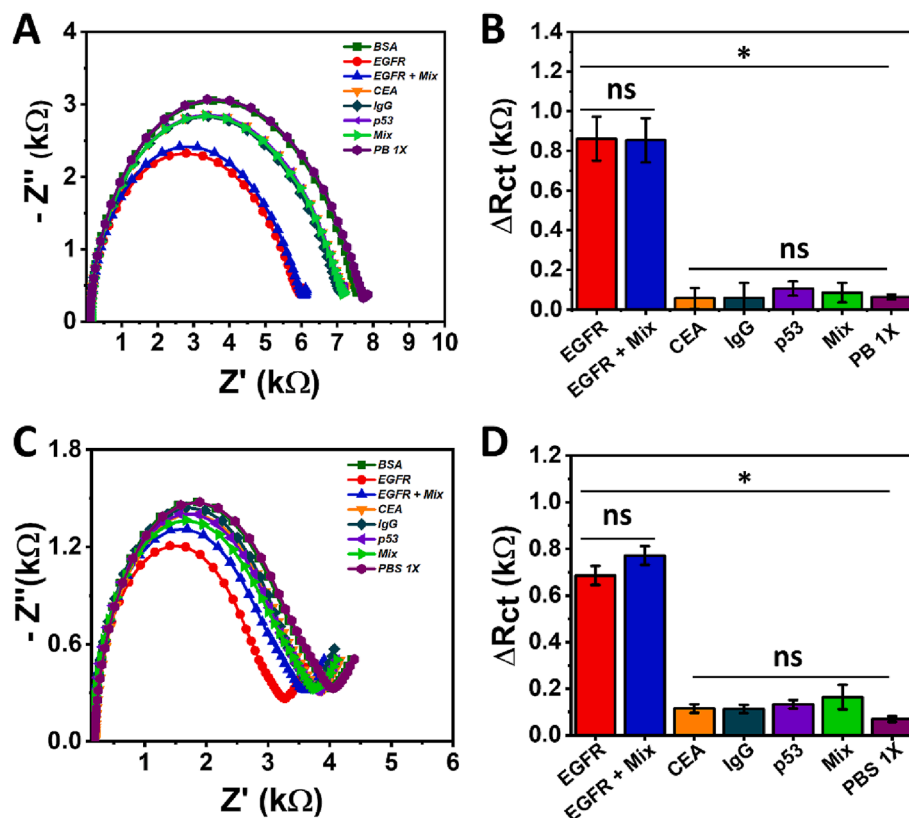


Fig. 4. Nyquist plot for $0.5 \mu\text{g mL}^{-1}$ EGFR and 10-fold ($5 \mu\text{g mL}^{-1}$) interfering species and the mixture of all proteins and antibodies, respectively, in a 1X PBS pH 7.4 solution for A) NiO- and C) PTAA-based biosensor. The difference in the ΔR_{ct} for each sample in B) NiO- and D) PTAA-based biosensor. * Indicates significant differences with $p < 0.05$ and ns denotes no significant differences ($p < 0.05$).

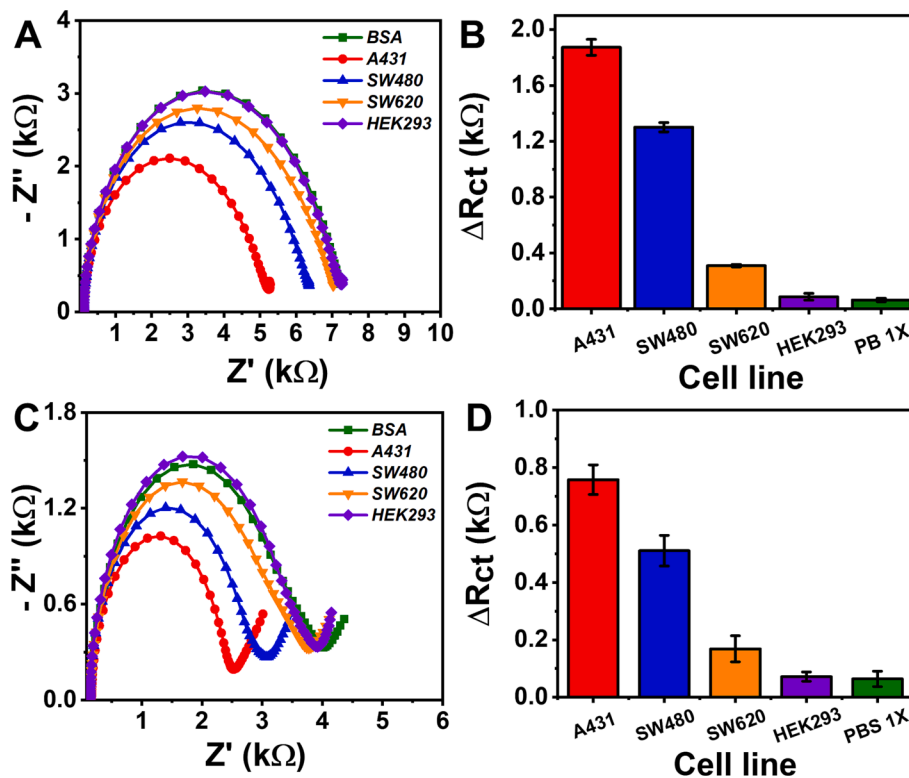


Fig. 5. Change in EIS response of the biosensor of different cell lines for A) NiO- and C) PTAA-based biosensor. The difference in the ΔR_{ct} for each sample in B) NiO- and D) PTAA-based biosensor. Error bars indicate the standard deviation of duplicate measurements.

covalently coupling to the interface, respectively. Electropolymerization and potentiostatic electrodeposition were robust techniques for obtaining highly reproducible NiO NPs and PTAA thin films. Electrochemical techniques, XPS, and other physicochemical analyses characterized the successful assembly of the biosensor platforms. The obtained nanobiosensors monitored the EGFR glycoprotein using EIS and discriminated cancer cells with different levels of EGFR expression with high specificity and reproducibility. In addition, the functionality of engineered anti-EGFR Nb was compared on both platforms assembled in parallel, demonstrating the reliability of coordination interaction between Ni²⁺ of NiO NPs with the 6xHis-tag and the covalent bond between the carboxyl groups of PTAA and the Lys-tag of Nbs. Although both proposed platforms had adequate performance, bioengineering Nbs with end-Lys tags may improve the more upright orientation of the bioreceptor with high coverage on functional polymer-based substrates to detect targets in a few minutes, like the His-tag strategy proposed. Overall, engineered Nb-based platforms hold promise for developing robust, low-cost, and easily miniaturized detection devices for cancer-related biomarker detection.

CRedit authorship contribution statement

Andrés F. Cruz-Pacheco: Conceptualization, Methodology, Formal analysis, Investigation, Data curation, Writing – original draft. **Yeison Monsalve:** Conceptualization, Methodology, Formal analysis, Investigation, Data curation, Writing – original draft. **Yunier Serrano-Rivero:** Methodology, Formal analysis, Investigation, Writing – original draft. **Julietta Salazar-Uribe:** Methodology, Formal analysis, Investigation. **Ernesto Moreno:** Methodology, Formal analysis, Investigation. **Jahir Orozco:** Conceptualization, Formal analysis, Writing – review & editing, Supervision, Project administration, Funding acquisition.

Declaration of Competing Interest

The authors declare that they have no known competing financial interests or personal relationships that could have appeared to influence the work reported in this paper.

Data availability

The authors are unable or have chosen not to specify which data has been used.

Acknowledgments

The work has been funded by Minciencias, MinEducación, Mincit, and ICETEX through the Program Ecosistema Científico Cod. FP44842-211-2018, project numbers 58536 and 58676. J.O. thanks support from The University of Antioquia and the Max Planck Society through the cooperation agreement 566-1, 2014. E.M., thanks for the support from the University of Medellín. We thank EPM and The Ruta N complex for hosting the Max Planck Tandem Groups.

Appendix A. Supplementary data

Supplementary data to this article can be found online at <https://doi.org/10.1016/j.cej.2023.142941>.

References

- C. Hamers-Casterman, T. Atarhouch, S. Muyldermans, G. Robinson, C. Hammers, E. B. Songa, N. Bendahman, R. Hammers, Naturally occurring antibodies devoid of light chains, *Nature*. 363 (1993) 446–448, <https://doi.org/10.1038/363446a0>.
- B. Li, X. Qin, L.-Z. Mi, Nanobodies: from structure to applications in non-injectable and bispecific biotherapeutic development, *Nanoscale*. 14 (2022) 7110–7122.
- S. Muyldermans, Nanobodies: Natural single-domain antibodies, *Annu. Rev. Biochem.* 82 (2013) 775–797, <https://doi.org/10.1146/annurev-biochem-063011-092449>.
- M.S. Valdés-Tresanco, A. Molina-Zapata, A.G. Pose, E. Moreno, Structural Insights into the Design of Synthetic Nanobody Libraries, *Molecules*. 27 (2022) 1–18, <https://doi.org/10.3390/molecules27072198>.
- T. De Meyer, S. Muyldermans, A. Depicker, Nanobody-based products as research and diagnostic tools, *Trends Biotechnol.* 32 (2014) 263–270, <https://doi.org/10.1016/j.tibtech.2014.03.001>.
- Q. Zhou, G. Li, K. Chen, H. Yang, M. Yang, Y. Zhang, Y. Wan, Y. Shen, Y. Zhang, Simultaneous unlocking optoelectronic and interfacial properties of c60 for ultrasensitive immunosensing by coupling to metal-organic framework, *Anal. Chem.* 92 (2020) 983–990, <https://doi.org/10.1021/acs.analchem.9b03915>.
- D. Pan, G. Li, H. Hu, H. Xue, M. Zhang, M. Zhu, X. Gong, Y. Zhang, Y. Wan, Y. Shen, Direct Immunoassay for Facile and Sensitive Detection of Small Molecule Aflatoxin B1 based on Nanobody, *Chem. - A Eur. J.* 24 (2018) 9869–9876, <https://doi.org/10.1002/chem.201801202>.
- Q. Zhou, G. Li, Y. Zhang, M. Zhu, Y. Wan, Y. Shen, Highly Selective and Sensitive Electrochemical Immunoassay of Cry1C Using Nanobody and π - π Stacked Graphene Oxide/Thionine Assembly, *Anal. Chem.* 88 (2016) 9830–9836, <https://doi.org/10.1021/acs.analchem.6b02945>.
- B. Kovalchuk, A.S. Berghoff, M.A. Karreman, K. Frey, M. Piechutta, M. Fischer, J. Grosch, S. Heiland, M.O. Breckwoldt, F. Hilberg, W. Wick, F. Winkler, Nintedanib and a bi-specific anti-VEGF/Ang2 nanobody selectively prevent brain metastases of lung adenocarcinoma cells, *Clin. Exp. Metastasis*. 37 (2020) 637–648, <https://doi.org/10.1007/s10585-020-10055-x>.
- J. Liu, Y. Jiang, X. Chen, L. Chen, X. Zhang, D. Cui, Y. Li, Z. Liu, Q. Zhao, A. Diao, Development of active affibody aggregates induced by a self-assembling peptide for high sensitive detection of alpha-fetoprotein, *Chem. Eng. J.* 436 (2022), 135208, <https://doi.org/10.1016/j.cej.2022.135208>.
- S. Spinelli, L.G.J. Frenken, P. Hermans, T. Verrips, K. Brown, M. Tegoni, C. Cambillau, M. Biologiques, C.J. Aiguier, Camelid Heavy-Chain Variable Domains Provide Efficient Combining Sites to, *Biochemistry*. 1217–1222 (2000).
- A. Ganji, M. Islami, M. Ejtehadi, E. Zarei-Mehrvarz, M. Darvish, Nanobody and aptamer as targeting moiety against bacterial toxins: Therapeutic and diagnostic applications, *Rev. Res. Med. Microbiol.* 30 (2019) 183–190, <https://doi.org/10.1097/MRM.0000000000000175>.
- N. An, Y.N. Hou, Q.X. Zhang, T. Li, Q.L. Zhang, C. Fang, H. Chen, H.C. Lee, Y. J. Zhao, X. Du, Anti-Multiple Myeloma Activity of Nanobody-Based Anti-CD38 Chimeric Antigen Receptor T Cells, *Mol. Pharm.* 15 (2018) 4577–4588, <https://doi.org/10.1021/acs.molpharmaceut.8b00584>.
- M. Shu, Y. Xu, D. Wang, X. Liu, Y. Li, Q. He, Z. Tu, Y. Qiu, Y. Ji, X. Wang, Anti-idiotypic nanobody: A strategy for development of sensitive and green immunoassay for Fumonisin B1, *Talanta*. 143 (2015) 388–393, <https://doi.org/10.1016/j.talanta.2015.05.010>.
- D. Schumacher, J. Helma, A.F.L. Schneider, H. Leonhardt, C.P.R. Hackenberger, Nanobodies: Chemical Functionalization Strategies and Intracellular Applications, *Angew. Chemie - Int. Ed.* 57 (2018) 2314–2333, <https://doi.org/10.1002/anie.201708459>.
- L. Wang, Y. Ding, N. Li, Y. Chai, Q. Li, Y. Du, Z. Hong, L. Ou, Nanobody-based polyvinyl alcohol beads as antifouling adsorbents for selective removal of tumor necrosis factor- α , *Chinese Chem. Lett.* 33 (2022) 2512–2516, <https://doi.org/10.1016/j.ccl.2021.12.087>.
- W. Wu, L. Shi, Y. Duan, S. Xu, L. Shen, T. Zhu, L. Hou, X. Meng, B. Liu, Nanobody modified high-performance AIE photosensitizer nanoparticles for precise photodynamic oral cancer therapy of patient-derived tumor xenograft, *Biomaterials*. 274 (2021), 120870, <https://doi.org/10.1016/j.biomaterials.2021.120870>.
- D. Echeverri, A.F. Cruz-Pacheco, J. Orozco, Capacitive nanobiosensing of β -1,4-galactosyltransferase-V colorectal cancer biomarker, *Sensors Actuators: B. Chemical*. 374 (2023) 132784.
- S. Cajigas, D. Alzate, J. Orozco, Gold/DNA-based nanobioconjugate for electrochemical detection of zika virus, *Microchimica Acta* 187 (594) (2020).
- A.F. Cruz-Pacheco, J. Quinchia, J. Orozco, Nanostructured poly(thiophene acetic acid)/Au/poly(methylene blue) interface for electrochemical immunosensing of p53 protein, *Sensors Actuators: B. Chemical*. 190 (2023) 136.
- A.F. Cruz-Pacheco, J. Quinchia, J. Orozco, Cerium oxide-doped PEDOT nanocomposite for label-free electrochemical immunosensing of anti-p53 autoantibodies, *Microchimica Acta* 189 (2022) 228.
- J. Quinchia, D. Echeverri, A.F. Cruz-Pacheco, M.E. Maldonado, J.A. Orozco, Electrochemical biosensors for determination of colorectal tumor biomarkers, *Micromachines*. 11 (2020) 1–46, <https://doi.org/10.3390/M11040411>.
- A. Mashkooi, A. Mostafavi, T. Shamspur, M. Torzadeh-Mahani, Electrochemical enzyme-based blood uric acid biosensor: new insight into the enzyme immobilization on the surface of electrode via poly-histidine tag, *Microchim. Acta*. 189 (2022), <https://doi.org/10.1007/s00604-022-05408-0>.
- C.L. Meyerkord, H. Fu, Protein-protein interactions: Methods and applications: Second edition, *Protein-Protein Interact. Methods Appl. Second Ed.* 1278 (2015) 1–613. doi: 10.1007/978-1-4939-2425-7.
- N. Aydemir, J. Malmström, J. Travas-Sejdic, Conducting polymer based electrochemical biosensors, *Phys. Chem. Phys.* 18 (2016) 8264–8277, <https://doi.org/10.1039/c5cp06830d>.
- P. Wee, Z. Wang, Epidermal Growth Factor Receptor Cell Proliferation Signaling Pathways, *Cancers (Basel)* (2017) 1–45, <https://doi.org/10.3390/cancers9050052>.

- [27] M.W. Saif, Colorectal cancer in review: The role of the EGFR pathway, *Expert Opin. Investig. Drugs*. 19 (2010) 357–369, <https://doi.org/10.1517/13543781003593962>.
- [28] S.L. Grant, A. Hammacher, A.M. Douglas, G.A. Goss, R.K. Mansfield, J.K. Heath, C. G. Begley, An unexpected biochemical and functional interaction between gp130 and the EGF receptor family in breast cancer cells, *Oncogene*. 21 (2002) 460–474, <https://doi.org/10.1038/sj.onc.1205100>.
- [29] O.M. Fischer, S. Hart, A. Gschwind, A. Ullrich, EGFR signal transactivation in cancer cells, *Biochem. Soc. Trans.* 31 (2003) 1203–1208, <https://doi.org/10.1042/bst0311203>.
- [30] G. Lin, X.J. Sun, Q.B. Han, Z. Wang, Y.P. Xu, J.L. Gu, W. Wu, G. Zhang, J.L. Hu, W. Y. Sun, W.M. Mao, Epidermal growth factor receptor protein overexpression and gene amplification are associated with aggressive biological behaviors of esophageal squamous cell carcinoma, *Oncol. Lett.* 10 (2015) 901–906, <https://doi.org/10.3892/ol.2015.3277>.
- [31] J.A. McKay, L.J. Murray, S. Curran, V.G. Ross, C. Clark, G.I. Murray, J. Cassidy, H. L. McLeod, Evaluation of the epidermal growth factor receptor (EGFR) in colorectal tumours and lymph node metastases, *Eur. J. Cancer*. 38 (2002) 2258–2264, [https://doi.org/10.1016/S0959-8049\(02\)00234-4](https://doi.org/10.1016/S0959-8049(02)00234-4).
- [32] R.C. Roovers, M.J.W.D. Vosjan, T. Laeremans, R. El Khoulati, R.C.G. De Bruin, K. M. Ferguson, A.J. Verkleij, G.A.M.S. Van Dongen, P.m.p., Van Bergen En Henegouwen, A biparatopic anti-EGFR nanobody efficiently inhibits solid tumour growth, *Int. J. Cancer*. 129 (2011) 2013–2024, <https://doi.org/10.1002/ijc.26145>.
- [33] K.R. Schmitz, A. Bagchi, R.C. Roovers, P.M.P. Van Bergen En, K.M.F. Henegouwen, Structural evaluation of EGFR inhibition mechanisms for nanobodies/VHH domains, *Structure*. 21 (2013) 1214–1224, <https://doi.org/10.1016/j.str.2013.05.008>.
- [34] A. Noor, G. Walsler, M. Wesseling, P. Giron, A.-M. Laffra, F. Haddouchi, J. De Grève, P. Kronenberger, Production of a mono-biotinylated EGFR nanobody in the *E. coli* periplasm using the pET22b vector, *BMC Res Notes* 11 (1) (2018).
- [35] J.Z. Kaczmarek, P.D. Skottrup, Selection and characterization of camelid nanobodies towards urokinase-type plasminogen activator, *Mol. Immunol.* 65 (2015) 384–390, <https://doi.org/10.1016/j.molimm.2015.02.011>.
- [36] A. González Pose, R. Montesino Seguí, R. Maura Pérez, F. Hugues Salazar, I. Cabezas Ávila, C. Altamirano Gómez, O. Sánchez Ramos, J. Roberto Toledo, Characterisation of a new molecule based on two E2 sequences from bovine viral diarrhoea-mucosal disease virus fused to the human immunoglobulin Fc fragment, *J. Vet. Res.* 65 (2021) 27–37, <https://doi.org/10.2478/jvetres-2021-0006>.
- [37] M.P. Zach, R.M. Penner, Nanocrystalline nickel nanoparticles, *Adv. Mater.* 12 (2000) 878–883, [https://doi.org/10.1002/1521-4095\(200006\)12:12<878::AID-ADMA878>3.0.CO;2-X](https://doi.org/10.1002/1521-4095(200006)12:12<878::AID-ADMA878>3.0.CO;2-X).
- [38] L.-F. Huang, M.J. Hutchison, R.J. Santucci, J.R. Scully, J.M. Rondinelli, Improved Electrochemical Phase Diagrams from Theory and Experiment: The Ni-Water System and Its Complex Compounds, *J. Phys. Chem. C*. 121 (18) (2017) 9782–9789.
- [39] P.N. Bartlett, D.H. Dawson, Electrochemistry of poly(3-thiopheneacetic acid) in aqueous solution: Evidence for an intramolecular chemical reaction, *J. Mater. Chem.* 4 (1994) 1805–1810, <https://doi.org/10.1039/JM9940401805>.
- [40] A. Noorbakhsh, A. Salimi, Development of DNA electrochemical biosensor based on immobilization of ssDNA on the surface of nickel oxide nanoparticles modified glassy carbon electrode, *Biosens. Bioelectron.* 30 (2011) 188–196, <https://doi.org/10.1016/j.bios.2011.09.010>.
- [41] M. Ganesana, G. Istarboulie, J.L. Marty, T. Noguer, S. Andreescu, Site-specific immobilization of a (His)₆-tagged acetylcholinesterase on nickel nanoparticles for highly sensitive toxicity biosensors, *Biosens. Bioelectron.* 30 (2011) 43–48, <https://doi.org/10.1016/j.bios.2011.08.024>.
- [42] K. Kaszuba, M. Grzybek, A. Orłowski, R. Danne, T. Róg, K. Simons, Ü. Coskun, I. Vattulainen, N-Glycosylation as determinant of epidermal growth factor receptor conformation in membranes, *Proc. Natl. Acad. Sci. U. S. A.* 112 (2015) 4334–4339, <https://doi.org/10.1073/pnas.1503262112>.
- [43] C.M.A. Brett, *Electrochemical Impedance Spectroscopy in the Electrochemical Sensors and Biosensors*, *Molecules*. 27 (2022) 1497.
- [44] N. Weidler, J. Schuch, F. Knaus, P. Stenner, S. Hoch, A. Maljusch, R. Schäfer, B. Kaiser, W. Jaegermann, X-ray Photoelectron Spectroscopic Investigation of Plasma-Enhanced Chemical Vapor Deposited NiOx, NiOx(OH)y, and CoNiOx(OH)y: Influence of the Chemical Composition on the Catalytic Activity for the Oxygen Evolution Reaction, *J. Phys. Chem. C*. 121 (2017) 6455–6463, <https://doi.org/10.1021/acs.jpcc.6b12652>.
- [45] D.M. Eby, K. Artyushkova, A.K. Paravastu, G.R. Johnson, Probing the molecular structure of antimicrobial peptide-mediated silica condensation using X-ray photoelectron spectroscopy, *J. Mater. Chem.* 22 (2012) 9875–9883, <https://doi.org/10.1039/c2jm30837a>.
- [46] D. Wasserberg, J. Cabanas-Danés, J. Prangmsa, S. O'Mahony, P.A. Cazade, E. Tromp, C. Blum, D. Thompson, J. Huskens, V. Subramaniam, P. Jonkheijm, Controlling Protein Surface Orientation by Strategic Placement of Oligo-Histidine Tags, *ACS Nano*. 11 (2017) 9068–9083, <https://doi.org/10.1021/acsnano.7b03717>.
- [47] X. Qiu, K.D. Wegner, Y.T. Wu, P.M.P. Van Bergen En, T.L. Henegouwen, N. H. Jennings, Nanobodies and antibodies for duplexed EGFR/HER2 immunoassays using terbium-to-quantum dot FRET, *Chem. Mater.* 28 (2016) 8256–8267, <https://doi.org/10.1021/acs.chemmater.6b03198>.
- [48] K.D. Wegner, S. Lindén, Z. Jin, T.L. Jennings, R. El Khoulati, P.M.P. Van Bergen En, N.H. Henegouwen, Nanobodies and nanocrystals: Highly sensitive quantum dot-based homogeneous FRET immunoassay for serum-based EGFR detection, *Small*. 10 (2014) 734–740, <https://doi.org/10.1002/sml.201302383>.
- [49] R.K. Schmidt-Ullrich, R.B. Mikkelsen, P. Dent, D.G. Todd, K. Valerie, B. D. Kavanagh, J.N. Contessa, W.K. Rorrer, P.B. Chen, Radiation-induced proliferation of the human A431 squamous carcinoma cells is dependent on EGFR tyrosine phosphorylation, *Oncogene*. 15 (1997) 1191–1197, <https://doi.org/10.1038/sj.onc.1201275>.
- [50] Z. Wang, X. Zhang, Z. Yang, H. Du, Z. Wu, J. Gong, J. Yan, Q. Zheng, MiR-145 regulates PAK4 via the MAPK pathway and exhibits an antitumor effect in human colon cells, *Biochem. Biophys. Res. Commun.* 427 (2012) 444–449, <https://doi.org/10.1016/j.bbrc.2012.06.123>.
- [51] Y. Xu, P. Soo, F. Walker, H.H. Zhang, N. Redpath, C.W. Tan, N.A. Nicola, T. E. Adams, T.P. Garrett, J.G. Zhang, A.W. Burgess, LRIG1 extracellular domain: Structure and function analysis, *J. Mol. Biol.* 427 (2015) 1934–1948, <https://doi.org/10.1016/j.jmb.2015.03.001>.
- [52] Y. Li, Z. Sun, B. Liu, Y. Shan, L. Zhao, L.I. Jia, Tumor-suppressive miR-26A and miR-26B inhibit cell aggressiveness by regulating fut4 in colorectal cancer, *Cell Death Dis.* 8 (6) (2017) e2892–e.
- [53] T. Holbro, R.R. Beerli, F. Maurer, M. Koziczak, C.F. Barbas, N.E. Hynes, The ErbB2/ErbB3 heterodimer functions as an oncogenic unit: ErbB2 requires ErbB3 to drive breast tumor cell proliferation, *Proc. Natl. Acad. Sci. U.S.A.* 100 (15) (2003) 8933–8938.